Mathematical and numerical methods for modeling and computing the cyclic steady states in non-linear mechanics

Ustim Khristenko

université PARIS-SACLAY

NNT : 2018SACLX001

Méthodes mathématiques et numériques pour la modélisation et le calcul des états établis cycliques en mécanique non-linéaire

Thèse de doctorat de l'Université Paris-Saclay
préparée à l'École Polytechnique

École doctorale n°579 Sciences mécaniques et énergétiques, matériaux et géosciences (SMEMAG)
Spécialité de doctorat: Mécanique des solides

Thèse présentée et soutenue à Palaiseau, le 17/01/2018, par

Ustim Khristenko

Composition du Jury :

Philippe Moireau Directeur de Recherche, Inria	Président
André Fortin Professeur, Université Laval Québec	Rapporteur
Stéphane Pagano Directeur de Recherche, Université de Montpellier	Rapporteur
Jean-François Deldon Ingénieur de Recherche, Michelin	Examinateur
Barbara Wohlmuth Professeur, Technische Universität München	Examinatrice
Patrick Le Tallec Professeur, École Polytechnique	Directeur de thèse

Thèse de doctorat

Mathematical and numerical methods for modeling and computing the cyclic steady states in non-linear mechanics

Ph.D. thesis

Ustim Khristenko

Remerciements

Tout d'abord je remercie le directeur de ma thèse Patrick Le Tallec, un enseignant exceptionnel, de m'avoir guidé et donné un soutien fiable durant toute ma thèse. Sa persistance solide dans la résolution de problèmes posés ainsi que sa sensibilisation dans tous les domaines de mécaniques et mathématiques sont toujours pour moi un exemple à suivre.

Je souhaite remercier le chef de projet excellent et dynamique Jean-François Deldon pour son aide et son soutien pendant ma thèse, surtout dans la réalisation industrielle des méthodes élaborées.

Je souhaite remercier mes deux rapporteurs, Stéphane Pagano et André Fortin, pour leurs remarques et questions qui m'ont permis améliorer mon manuscrit, ainsi que tous les jurys de ma thèse, en particulier, Barbara Wohlmuth et le président de la comité Philippe Moireau pour leurs questions de fond. De plus, je souhaite remercier Philippe pour le modèle numérique du cœur, ce qui m'a résulté le dernier chapitre, ainsi que pour l'idée du contrôle en forme prédicteur-correcteur.

Je souhaite aussi remercier toute l'équipe de simulation numérique Michelin, en particulier Thomas Homolle et le chef d'équipe Ramzi Bousseta, pour l'accueil chaleureux au sein du centre technologique Michelin à Ladoux, ainsi que pour leur aide et soutien à mon travail. Je souhaite surtout remercier Patrice Hauret de m'avoir proposé le sujet de thèse si intéressant et passionnant.

Mes grands remerciements à l'excellent secrétariat du LMS en la personne d'Alexandra Joly et Anna Johnsson. Je remercie mon comité de suivi: Dominique Chapelle, Andrei Constantinescu et Martin Genet. Je tiens à remercier tous mes collègues et mes amis au LMS et M3disim pour le temps agréable passé ensemble et pour toute la contribution directe ou indirecte apportée dans ma thèse et dans ma vie, surtout ceux qui ont passé ces années à côté de moi, notamment, Blandine, Florent, Federica, François, Arthur. Finalement, je remercie ma chère Nadia pour son soutien quotidien qui est difficile à surestimer.

Résumé

Ce travail a pour objet l'étude des techniques rapides pour calculer l'état cyclique établi des problèmes d'évolution en mécanique non-linéaire avec des conditions de périodicité en espace-temps. Un exemple typique est le roulage stationnaire d'un pneu présentant des sculptures périodiques, où l'état en chaque point est le même que l'état observé au point correspondant de la sculpture suivante une période en temps auparavant.

L'application de solveurs directs pour la solution de tels problèmes est impossible car ils exigent l'inversion des matrices gigantesques. Pour résoudre ce genre de problèmes, les logiciels de calcul utilisés dans l'industrie recherchent une telle solution cyclique comme la limite asymptotique d'un problème à valeur initiale avec des données initiales arbitraires. Cependant, quand le temps de relaxation du problème physique est élevé, la vitesse de convergence vers le cycle limite peut devenir trop lente. Comme on ne s'intéresse pas à la solution transitoire et que seul importe d'avoir un accès rapide au cycle limite, le développement des méthodes qui accélèrent la convergence vers le cycle limite sont d'un grand intérêt. Ce travail développe, étudie et compare deux techniques d'analyse et de calcul rapide de la solution périodique en espace-temps.

La première est la méthode de Newton-Krylov, qui considère l'état initial comme l'inconnue du problème à calculer à partir de la condition de périodicité. Le problème résultant est résolu par l'algorithme de Newton-Raphson. Comme le Jacobien associé ne s'exprime pas explicitement mais uniquement implicitement à travers son action par multiplication, il est nécessaire d'introduire des solveurs itératifs de type Krylov. Par réutilisation optimale de l'information obtenue sur le Jacobien pendant le calcul du résidu, la résolution du système linéaire par algorithme de Krylov devient très rapide et de faible coût par rapport au calcul de l'erreur de périodicité. Cette technique de calcul peut être vue comme une méthode de tir. Mais nous l'écrivons ici par changement de variables sous la forme

d'une méthode de type observateur-contrôleur, qui corrige la solution transitoire après chaque cycle et accélère ainsi la convergence vers la limite cyclique.

La deuxième méthode de calcul et d'analyse proposée dans ce travail met en œuvre une modification du problème d'évolution initial en y introduisant un terme de contrôle rétroactif, basé sur l'erreur de périodicité. Le contrôle rétroactif est un outil bien connu et puissant dans le cadre de la stabilisation des orbites périodiques instables des processus chaotiques. Dans le cadre de ce travail, il est appliqué à un système initialement stable pour accélérer la convergence vers la limite cyclique. De plus, le terme de contrôle inclut les décalages en temps ainsi qu'en espace, ce qui complique son analyse. L'enjeu est ici de construire l'opérateur de gain à appliquer à l'erreur de périodicité dans le terme de contrôle. Dans un cadre linéaire très général, après décomposition spectrale et introduction des fonctions de Lambert, nous pouvons analyser explicitement l'existence et la convergence de solutions en temps, et construire la forme optimale du gain qui assure la convergence la plus rapide vers la solution cyclique. L'efficacité de la méthode proposée croit avec le temps de relaxation du problème. L'algorithme est présenté sous la forme d'un schéma prédicteur-correcteur en temps, où l'étape de correction est explicite et de très faible coût numérique. Sous cette forme, le contrôle proposé a été adapté et testé sur des problèmes non-linéaires.

Les deux méthodes ont été appliquées sur diverses applications académiques et comparées à la méthode asymptotique classique. Enfin, elles ont été intégrées et mises en œuvre dans le code industriel de Michelin pour application au roulage stationnaire d'un pneu complet avec sculptures périodiques en présence de forces de contact au sol en régime de frottement adhérant-glissant.

Abstract

This work is focused on fast techniques for computing the steady cyclic states of evolution problems in non-linear mechanics with space and time periodicity conditions. This kind of problems can be faced, for instance, in the beating heart modeling. Another example concerns the rolling of a tyre with periodic sculptures, where the cyclic state satisfies "rolling" periodicity condition, including shifts both in time and space. More precisely, the state at any point is the same that at the corresponding point observed at the next sculpture one time period ago.

Direct solvers for such problems are not very convenient, since they require the inversion of very large matrices. In industrial applications, in order to avoid this, such a cyclic solution is usually computed as an asymptotic limit of the associated initial value problem with arbitrary initial data. However, when the relaxation time is high, convergence to the limit cycle can be very slow. In such cases nonetheless, one is not interested in the transient solution, but only in a fast access to the limit cycle. Thus, developing methods accelerating convergence to this limit is of high interest. This work is devoted to study and comparison of two techniques for fast calculation of the space-time periodic solution.

The first is the well-known Newton-Krylov shooting method, looking for the initial state, which provides the space-time periodic solution. It considers the space-time periodicity condition as a non-linear equation on the unknown initial state, which is solved using Newton-Raphson technique. Since the associated Jacobian can not be expressed explicitly, the method uses one of the matrix-free Krylov iterative solvers. Using information stored while computing the residual to solve the linear system makes its calculation time negligible with respect to the residual calculation time. On the one hand, the algorithm is a shooting method, on the other side, it can be considered as an observer-controller method, correcting the transient solution after each cycle and accelerating convergence to the space-time periodic state.

The second method, considered in this work, is an observer-controller type modification of the standard evolution to the limit cycle by introducing a feedback control term, based on the periodicity error. The time-delayed feedback control is a well-known powerful tool widely used for stabilization of unstable periodic orbits in deterministic chaotic systems. In this work the time-delayed feedback technique is applied to an a priori stable system in order to accelerate its convergence to the limit cycle. Moreover, given the space-time periodicity, along with the time-delay, the feedback term includes also a shift in space. One must then construct the gain operator, applied to the periodicity error in the control term. Our main result is to propose and to construct the optimal form of the gain operator for a very general class of linear evolution problems, providing the fastest convergence to the cyclic solution. The associated control term can be mechanically interpreted. Efficiency of the method increases with the problem's relaxation time. The method is presented in a simple predictor-corrector form, where correction is explicit and numerically cheap. In this later form, the feedback control has been also adapted and tested for a nonlinear problem.

The discussed methods have been studied using academic applications and they also have been implemented into the Michelin industrial code, applied to a full 3D tyre model with periodic sculptures in presence of slip-stick frictional contact with the soil, and then compared to the standard asymptotic convergence.

Contents

List of Figures

List of Tables

Introduction

Motivation

Mechanics of nonlinear continua has been the topic of many developments. Nowadays, these problems are faced with new challenges, such as handling large memory and diffusion effects or solving time dependent coupled problems on multi-scale geometries with space and time periodicity conditions. This kind of problems can be faced, for instance, in the beating heart modeling [Moireau 2009, Imperiale 2013, Caruel et al. 2014]. Another example concerns the steady rolling of a viscoelastic tyre [Le Tallec and Rahier 1994, Govindjee et al. 2014] with a periodic sculpture. In this case, the periodic steady state satisfies a "rolling" periodicity condition, including shifts both in time and space, i.e. the state $\underline{u}(t, \underline{X})$ at any point $\underline{X}$ is the same that at the corresponding point observed at the next sculpture one time period T ago:

$$\underline{u}(t, \underline{X}) = \underline{u}(t - T, \underline{\underline{R}}_{\omega T} \underline{X}).$$

Here, $\underline{\underline{R}}_{\omega T}$ denotes the rotation of angle ωT and ω is the rotation speed. Typical illustrations of space-time periodic problems are presented in Chapter 1.

In industrial applications, in order to avoid the inversion of very large matrices, time periodic states are often computed as the asymptotic limit solution of an initial value boundary value problem with arbitrarily chosen initial data. Calculating such initial value problems until the asymptotic limit may take a lot of time for "viscous" problems, when memory effects are very large. In such cases nonetheless, one is not interested in the evolution history of the transient solution, but only in a fast access to the asymptotic limit cycle. Thus, developing methods accelerating convergence to this limit is of high interest, and is the topic of the current work.

Issues and state of the art

Let us consider the class of evolution problems, where the current state of the system depends on time as well as on the previous evolution history. Such a time dependence in mechanics occurs through different phenomena:

- Diffusion (heat propagation in solids, for example).
- Viscoelasticity [Le Tallec and Rahier 1994, Reese and Govindjee 1997, Christensen 2012].
- Friction [Wriggers 2006, Laursen 2003, Alart and Curnier 1991, Hüeber et al. 2007].
- Dynamics (for example, beating heart [Moireau et al. 2009, Imperiale 2013, Caruel et al. 2014]).

In this context, we distinguish a well-studied class of initial value problems, where the evolution is defined by the initial state. Numerical methods, searching for its solution, are based on the consecutive time integration from the given initial state. Given a natural damping of the mechanical system, solution of a well-posed initial value problem converges to a certain asymptotic limit, independent of the initial state. In particular, the steady state (time independent) and time periodic state are examples of such a limit solution. More complicated case is a cyclic steady state, which is periodic in space-time (rolling structure [Govindjee et al. 2014], for example). The class of problems, where we are interested only in such cyclic state, and not in the evolution leading to it, is less explored, and more sophisticated. The possible techniques, solving such periodic problems, include:

- **Direct solvers.** They are looking for the space-time periodic solution as an element in the space-time. That is, its numerical solution is given by a large generalized vector of dimension $N_{space} \times N_{time}$, where N_{space} and N_{time} are respectively spacial and temporal degrees of freedom of the fully discretized problem. Thus, it solves a linear or non-linear algebraic system, requiring inversion of $N_{space} \times N_{time}$ matrices. So, for very fine discretizations, when N_{space} and N_{time} are large, this method is of very high numerical cost.
- **Asymptotic limit.** This method comes naturally from the discussion above. Indeed, if the problem is well-posed, from any admissible initial state, its solution converges in time to the desired cyclic steady state. Thus, the space-time periodic solution can be found as the asymptotic limit of the associated initial value problem with arbitrary initial data. However, the final computational time is defined by the convergence rate of the initial value problem solution. When the memory effects are too strong, the convergence time can be unacceptably long. It happens, for example, in presence of strong diffusion effects (see Section 1.2).

- **Shooting methods** constitute a typical class of iterative solvers for two points boundary value problems. In this context, a periodic problem is treated as a two points boundary value problem in time. The technique consists to solve iteratively an initial value problem over one time period, with the initial state obtained from the previous iteration, in order to evaluate the state in the end of the period and compare it to the initial one. Then the initial state for the next iteration is corrected in a way to better approach the periodicity condition. Thus, on each iteration until periodicity error convergence, given a predicted initial state, the solution is integrated to the end of the period to compute the periodicity error, which is then used to correct the initial state. Examples of shooting technique for periodic problems include the adjoint-based optimal control methods as in [Bristeau et al. 1998, Ambrose and Wilkening 2010], and the Newton-Krylov shooting algorithm [Govindjee et al. 2014, Brandstetter and Govindjee 2017]. The Newton-Krylov shooting method is the subject of Chapter 2 of this work and will be discussed in more details further.

- **Delayed feedback control method** is a modification of the asymptotic limit technique, where an additional control term, based on the periodicity error, is introduced in order to accelerate the convergence to the limit cycle. This observer-controller technique has been inspired by filtering techniques, like Kalman filter [Kalman and Bucy 1961] and others [Moireau et al. 2009]. The method is similar to the feedback control methods, stabilizing unstable periodic orbits, proposed first by [Pyragas 1992]. Theoretical analysis and application of this method is the topic of Chapter 3.

This work is therefore devoted to two techniques for fast calculation of the space-time periodic solution: Newton-Krylov shooting algorithm, discussed in Chapter 2, and Delayed Feedback Control method, proposed in Chapters 3 and 4.

The first technique is based on the Newton-Krylov method [Chan and Jackson 1984, Telichevesky et al. 1995, Knoll and Keyes 2004], considered as a shooting method for space-time periodic problem [Govindjee et al. 2014, Brandstetter and Govindjee 2017]. The main idea consists in considering the periodicity condition as an equation for the unknown initial state, corresponding to the periodic solution. Indeed, once we have found the true initial state, the periodic solution is obtained solving the associated initial value problem during only one time period. The equation on the unknown initial state includes an evolution function, requiring to solve the non-linear initial value problem during one time period. The periodicity condition, comparing the resulting state after one time period to the initial one, provides a non-linear equation to solve, whose unknown is the initial state. So, it is natural to solve this non-linear equation by a classical Newton-Raphson technique. The most challenging is to construct the global tangent matrix (Jacobian), which can not be expressed explicitly. We propose a way to construct it, using the tangent matrices of the evolution problem, stored after each time step. In practice, this

global tangent matrix is never assembled, but defined implicitly through its action by multiplication. Because of this, we can apply one of the matrix-free Krylov solvers (GMRES, for example) [Saad 2003, Saad and Schultz 1986, Balay et al. 2016] to solve the linear system, appearing at each global Newton step. This leads to the Jacobian-free Newton-Krylov method [Knoll and Keyes 2004]. Application of this technique, as a shooting method, searching for the initial state of the space-time periodic solution (cyclic steady state), to a steady rolling threaded wheel is already proposed and discussed in [Govindjee et al. 2014]. In our work, we propose another point of view on this method, namely, to consider it as a correction after each time period of the classical transient solution, which simplifies its implementation. Moreover, the discussed algorithm has been implemented in Michelin industrial code, applied to a full 3D tyre model and compared to the standard asymptotic convergence.

Another technique considered in this work (Chapters 3-4) is the delayed feedback control method [Pyragas 1992]. This is an observer-controller type modification of the asymptotic limit technique. Even if the asymptotic limit is periodic, the evolution solution of the initial value problem is not. The lack of periodicity of the calculated solution is then an extra information (observation) on which one can apply control techniques. In other words, we modify the initial value problem by introducing a closed loop feedback control term, based on this observation (periodicity error). So, the state shifted in space as well as in time (hence delayed feedback) is present in the modified equation. When solution of the modified initial value problem converges to the limit cycle, the control term vanishes, and the modified and original problems have thus the same asymptotic limit. The main issue here is to construct the factor operator (or gain operator), applied to the periodicity error in the control term. We do that by finding the optimal gain operator providing the fastest convergence of the modified problem solution to the limit cyclic steady state.

The time-delayed feedback control (or time-delay autosynchronization), first proposed in [Pyragas 1992] and further extended by [Socolar et al. 1994], is a powerful tool widely used for stabilization of unstable periodic orbits in deterministic chaotic systems [Kittel et al. 1995, Pyragas 1995, 2002, Bleich and Socolar 1996] and unstable steady states [Hövel and Schöll 2005, Yanchuk et al. 2006]. Detailed overview on the time-delayed feedback control can be also found in [Pyragas 2012] and in [Hövel 2010].

In this work the time-delayed feedback technique is applied to an initially stable system in order to accelerate its convergence to the limit cycle (space-time periodic solution). Moreover, given the space-time periodicity, along with the time-delay the feedback term includes also a shift in space. Our main result in this framework is to propose and to analyze the optimal form of the gain operator in the feedback term for a very general class of linear evolution problems, providing the fastest convergence to the steady cyclic solution. This form of the feedback control has

been also adapted and tested for nonlinear problems.

Outline of the work

Chapter 1 presents some reference periodic problems, used for illustration of the context. Besides, they will serve as model problems on which to test the accelerating methods proposed and discussed in this work. First, in Section 1.1, we consider the steady rolling of a tyre with periodic sculptures in presence of stick-slip frictional contact. This is the problem that has originally inspired this work. Then, Section 1.2 introduces an academic linear problem, where a planar disk is heated with a source periodically moving along a circular path, which may be a simple model problem for additive manufacturing or for representing the heating of a rolling tyre by localized energy dissipation sources. Section 1.3 describes a beating heart model, which is an example of time periodicity for second order problems in time, where the space shift is given by identity operator.

Chapter 2 is devoted to the application of the Newton-Krylov algorithm to the space-time periodic problems. In particular, Section 2.3 describes first the classical Newton-Krylov shooting algorithm, looking for the "correct" initial state, which provides the space-time periodic steady state. On each global Newton iteration, given an initial state (starting with an arbitrary guess), it solves the non-linear initial value problem during the first period, and computes the periodicity error, which is used as right hand side of the Newton linear system to correct the initial state for the next step. In this formulation, it can be considered as a shooting method: starting with an arbitrary left boundary value, we go through one period evolution to obtain the right boundary value and use it for correction of the left boundary value and so on.

Section 2.6 proposes an alternative implementation of the same algorithm, where after a change of variable, we approximate the initial state of the current time period instead of the initial state of the first period. Then the method turns out to be a modification of a standard time evolution, introducing a correction of solution after each time period (which corresponds to the current global Newton step). In this way, the method can be easily derived from the classic time evolution by adding the correction step in the end of each period. Indeed, it may be treated as an observer-controller process, where correction, performed in the end of each period, is based on the observation during this period.

Sections 2.8 and 2.9 are devoted to implementation of the proposed technique, applied to the model problems described in Chapter 1. First, the method has been applied to the linear 2D heat problem from Section 1.2. For such a linear problem, solution is obtained after the first global iteration. After, we have tested the method on a tyre rolling model, described in Section 1.1.4. This problem is three dimensional and non-linear. The alternative formulation of the present method has been implemented along with the classical non-modified time evolution, in order to

compare the rates of convergence to the asymptotic space-time periodic solution. Finally, we present the results of integration of the Newton-Krylov method to the Michelin industrial code.

Chapter 3 is dedicated to construction and validation of the optimal delayed feedback control, minimizing the convergence time of the initial value problem solution to the asymptotic limit cyclic steady state.

First, we present an analytical analysis of an abstract linear evolution problem, modified by introducing a feedback control term. The feedback term includes both shifts in space and in time (time-delay). We are able to perform a spectral decomposition of the problem in space and then the modified (controlled) problem leads to a delayed differential system [Bellman and Cooke 1963, Yi et al. 2010, Asl and Ulsoy 2003], whose explicit solution uses the Lambert W function [Corless et al. 1996, 1997, Valluri et al. 2000, Shinozaki 2007, Shinozaki and Mori 2006]. This calculation provides an existence and time convergence result for both the non-controlled and the controlled problems. Having studied the influence of the control term on the convergence rate, we propose then the optimal gain operator, by optimizing the spectrum in time (Floquet exponents) of the controlled transient solution and minimizing thus the convergence time. We also study the influence of the magnitude of the memory effects on the efficiency of the method. Then, we propose and analyze a simplified modification of the optimal control, which is numerically cheaper while preserving the efficiency. Moreover, a predictor-corrector form of the proposed feedback control is introduced, which is quite easy in implementation. In this form, the present control technique has been extended and adapted to the non-linear case.

To confirm the theoretical results, in Sections 3.4 and 3.5 the feedback control technique has been applied to the same problems as those treated in Chapter 2 by the Newton-Krylov method. The problems have been numerically solved applying the feedback control, which has been compared to the non-controlled convergence as well as to the Newton-Krylov results of Chapter 2. We have also studied the sensitivity of the method to the variation of relaxation time of the problem. Finally, the presented feedback control method in the predictor-corrector form has been integrated into Michelin industrial code.

In Chapter 4, the proposed delayed feedback control technique is adapted for the dynamical problems – differential systems of second order in time. A linear 3D beating heart model is considered, where the feedback control has been applied only to the several principal modes in the spectral decomposition of the solution.

CHAPTER 1

Reference problems

Summary

1.1 Rolling tyre

A typical example of a space-time periodic problem, which motivated the study of this subject, is the problem of the steady rolling of a tyre [Le Tallec and Rahier 1994] with space periodic sculptures (Figure 1.1), in presence of frictional contact with the soil. Indeed, given the periodic geometry and the constant rotation, for the established (asymptotic limit) rolling, the state at any material point will be the same as at the corresponding point of the next sculpture but one time period ago.

Figure 1.1: A car tyre with periodic sculpture (images from media-aevent.michelin.com).

1.1.1 Mechanical model

Let us consider a 3D tyre with periodic sculptures, each period covering a section of angle θ along the tyre circumference. The steady rolling configuration is defined by two parameters: the constant linear velocity of the wheel axle $\underline{v}_{ax}$ and the constant angular velocity ω of the rigid rim Γ_0 (Figure 1.2), rotating around the axle. There is a load applied to the tyre axle, defined by the constant distance r_{load} (loaded radius) between the tyre axle and the ground. So a part of tyre boundary Γ_c is in contact with the ground.

The non-linear mechanics of a rolling tyre is described in the frame of the finite strain theory [Le Tallec et al. 1994, Le Tallec 2009, Ciarlet 1988, Le Tallec and Rahier 1994]. Let us introduce the deformation gradient:

$$\underline{\underline{\mathcal{F}}} = \mathrm{Id} + \frac{\partial \underline{u}}{\partial \underline{X}}, \tag{1.1}$$

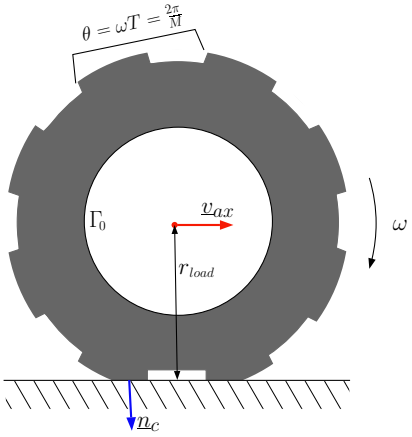

Figure 1.2: Rolling tyre scheme. The tyre with periodic sculptures of size θ is rolling with angular velocity ω around its axle, moving with linear velocity $\underline{v}_{ax}$. The contact zone with the outer unit normal $\underline{n}_c$ is defined by the constant distance r_{load} between the tyre axle and the ground.

where the displacement field is $\underline{u} = \underline{x} - \underline{X}$, and $\underline{x}$ and $\underline{X}$ are respectively the Euler and Lagrange coordinates in $\mathbb{R}^3$. Here and further, Id denotes the identity operator. The (right) Cauchy-Green strain tensor is

$$\underline{\underline{\mathcal{C}}} = \underline{\underline{\mathcal{F}}}^t \underline{\underline{\mathcal{F}}} = \left(\mathrm{Id} + \frac{\partial \underline{u}}{\partial \underline{X}}\right)^t \left(\mathrm{Id} + \frac{\partial \underline{u}}{\partial \underline{X}}\right).$$

The superscribe $(\,)^t$ denotes transposed tensor. The second Piola-Kirchhoff stress tensor is defined as

$$\underline{\underline{\Sigma}} = \frac{\partial W_e}{\partial \underline{\underline{\mathcal{C}}}}(\underline{X}, \underline{\underline{\mathcal{C}}}, A) - p\,\underline{\underline{\mathcal{C}}}^{-1}, \tag{1.2}$$

where the Lagrange multiplier p, representing the hydrostatic pressure, is introduced to handle the incompressibility constraint at places where the material is taken as truly incompressible. Above, W_e denotes the hyper-elastic potential, or the free energy density per unit volume in the reference configuration, and A stands for any internal variable (like temperature, irreversible strain, etc.). The potential W_e of an elastic isotropic material depends only on the invariants of the Cauchy-Green strain tensor [Le Tallec et al. 1994, Le Tallec 2009]:

$$I_1 = \mathrm{tr}\,\underline{\underline{\mathcal{C}}}, \qquad I_2 = \frac{1}{2}\left(\mathrm{tr}^2\,\underline{\underline{\mathcal{C}}} - \mathrm{tr}\,\underline{\underline{\mathcal{C}}}^2\right), \qquad I_3 = \det \underline{\underline{\mathcal{C}}}.$$

Notations tr and det are used respectively for the trace and determinant of a tensor. The expression for $W_e(I_1, I_2, I_3)$ is given by a constitutive law, reflecting material properties. See [Le Tallec et al. 1994, Le Tallec 2009, Ciarlet 1988] for the examples. A typical example of elastic isotropic constitutive law is proposed

in [Ciarlet and Geymonat 1982, Ciarlet 1988]:

$$W_e(I_1, I_2, I_3) = c_1(I_1 - 3) + c_2(I_2 - 3) + c_3(I_3 - 1) - (c_1 + 2c_2 + c_3) \ln I_3,$$

where coefficients c_1, c_2, c_3 are defined by the material. In particular, in the incompressible case, when $I_3 = 1$, it gives the Mooney-Rivlin constitutive law:

$$W_e(I_1, I_2) = c_1(I_1 - 3) + c_2(I_2 - 3).$$

Let Ω be the interior of the tyre domain (in Lagrangian configuration) with Γ_0 the boundary associated to the rim, and Γ_c the surface contacting with the ground with the outer unit normal $\underline{n}_c$. Then, the contact force density $\underline{p}_c$ can be represented as a sum

$$\underline{p}_c = p_N \, \underline{n}_c + \underline{p}_\tau$$

of the normal contact pressure p_N and the friction force density $\underline{p}_\tau$, tangent to the contact surface, i.e. $\underline{p}_\tau \cdot \underline{n}_c = 0$.

The normal contact pressure $p_N = p_N(\underline{X} + \underline{u})$ is a non-linear and non-smooth function of the displacement. To define it, let us introduce a normal gap

$$g_N = r_{load} - (\underline{X} + \underline{u}) \cdot \underline{n}_c.$$

Then the contact is defined by the non-penetration condition [Wriggers 2006, Laursen 2003, Alart and Curnier 1991]. The gap can not be negative (no penetration). There is no contact force, if the gap is positive. When the contact takes place, the gap is zero, and a normal pressure is then applied (Figure 1.3, left):

$$g_N \geq 0, \quad p_N \leq 0, \quad p_N \cdot g_N = 0.$$

In the model, we use a regularized contact law (Figure 1.3, right):

$$p_N = \begin{cases} \epsilon_N \, g_N, & \text{if } g_N \leq 0, \\ 0, & \text{if } g_N > 0, \end{cases} \tag{1.3}$$

with a large penalty coefficient $\epsilon_N > 0$.

The tangent contact pressure $\underline{p}_\tau$ is represented by a stick-slip friction, defined by the Coulomb law [Wriggers 2006, Laursen 2003, Alart and Curnier 1991, Hüeber et al. 2007]. It acts in two regimes: adherence and sliding. In the adherent mode, the contacting material point is stuck to the ground, that is $\dot{\underline{u}} = 0$. When the adherent friction force reaches a threshold, which depends on the normal pressure p_N, the material points enters to the sliding regime and starts to slip by the ground with no further increase of the friction force. Let us introduce a relative slip velocity $\dot{\underline{s}}$ defined on the contact surface through

$$\dot{\underline{s}} = \dot{\underline{u}} - (\dot{\underline{u}} \cdot \underline{n}_c)\underline{n}_c.$$

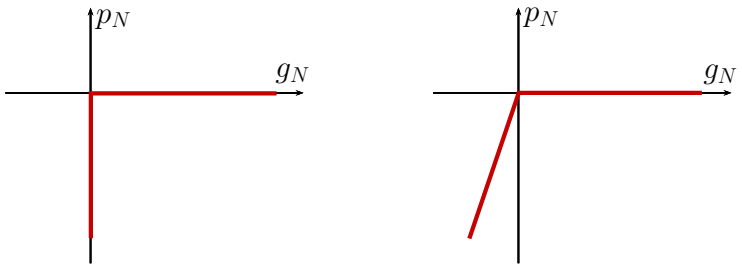

Figure 1.3: Contact law (left) and its regularized version (right).

In terms of the relative slip, in the adherent regime $\dot{\underline{s}} = 0$ and the friction force density is less than a specified threshold. When it reaches the threshold, there is no more friction force growth, but instead the slipping regime starts, so the slip velocity becomes different from zero (Figure 1.4, left):

$$\begin{aligned} &|\dot{\underline{s}}| = 0, \qquad |\underline{p}_\tau| < \mu |p_N| \qquad (\textit{adherence}),\\ &|\dot{\underline{s}}| \neq 0, \qquad \underline{p}_\tau = -\mu\,|p_N|\,\frac{\dot{\underline{s}}}{|\dot{\underline{s}}|} \qquad (\textit{sliding}). \end{aligned}$$

Above μ denotes the Coulomb friction coefficient. In the model, we use a regularized Coulomb law (Figure 1.4, right):

$$\underline{p}_\tau = \begin{cases} -\epsilon_\tau \dot{\underline{s}}, & \text{if } \epsilon_\tau |\dot{\underline{s}}| < \mu |p_N| \qquad (\textit{adherence}),\\ -\mu\,|p_N|\,\dfrac{\dot{\underline{s}}}{|\dot{\underline{s}}|}, & \text{if } \epsilon_\tau |\dot{\underline{s}}| \geq \mu |p_N| \qquad (\textit{sliding}), \end{cases} \tag{1.4}$$

using a large penalty coefficient ϵ_τ. Note a non-linear dependency of $\underline{p}_\tau$ on $\dot{\underline{u}}$ and $\underline{u}$, together with an important memory effect in the friction force definition with characteristic time $\epsilon_\tau r_1/E$, where E stands for a reference Young's modulus and r_1 denotes the tyre radius.

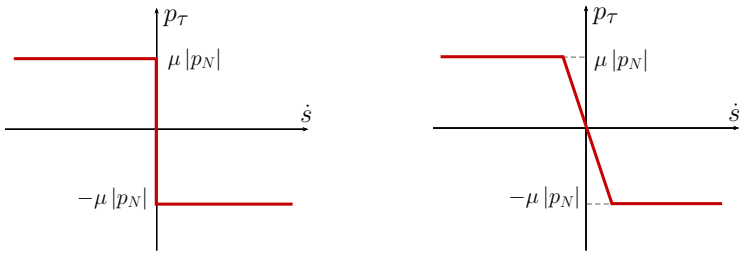

Figure 1.4: Coulomb friction law (left) and its regularized version (right).

The absolute displacement $\underline{u}$ can be decomposed into a rigid body motion and a wheel related displacement:

$$\underline{u} = \underline{u}_{rig} + \tilde{\underline{u}},$$

where $\underline{\tilde{u}}$ denotes the wheel related displacement, and the rigid body displacement $\underline{u_{rig}}$ is a given function of t and $\underline{X}$:

$$\underline{u_{rig}} = \underline{\underline{R}}_{\omega t}\underline{X} - \underline{X} + \underline{v}_{ax}t.$$

Here and further, $\underline{\underline{R}}_{\omega t}$ denotes rotation in $\mathbb{R}^3$ of angle ωt around the tyre axle in the $\underline{v}_{ax} \times \underline{n}_c$ plane. If there is no internal variables, the system configuration is entirely defined by the displacement. And we are going to use the material displacement $\underline{\tilde{u}}$ as the only unknown state variable, instead of $\underline{u}$.

In terms of $\underline{\tilde{u}}$, Euler coordinates, the normal gap and the absolute velocity respectively write:

$$\begin{aligned}
\underline{x} &= \underline{X} + \underline{u} = \underline{X} + \underline{u_{rig}} + \underline{\tilde{u}} = \underline{\underline{R}}_{\omega t}\underline{X} + \underline{v}_{ax}t + \underline{\tilde{u}},\\
g_N &= r_{load} - (\underline{\tilde{u}} + \underline{\underline{R}}_{\omega t}\underline{X} + \underline{v}_{ax}t)\cdot\underline{n}_c = r_{load} - (\underline{\underline{R}}_{\omega t}\underline{X} + \underline{\tilde{u}})\cdot\underline{n}_c,\\
\underline{\dot{u}} &= \underline{\dot{u}_{rig}} + \underline{\dot{\tilde{u}}} = (\partial_t\underline{\underline{R}}_{\omega t})\underline{X} + \underline{v}_{ax} + \underline{\dot{\tilde{u}}} = \omega\underline{\underline{\Pi}}\,(\underline{\underline{R}}_{\omega t}\underline{X}) + \underline{v}_{ax} + \underline{\dot{\tilde{u}}}, \qquad (1.5)
\end{aligned}$$

where $\underline{\underline{\Pi}} = (-\underline{v}_{ax}\otimes\underline{n}_c + \underline{n}_c\otimes\underline{v}_{ax})/|\underline{v}_{ax}|$. Then the deformation gradient and the second Piola-Kirchhoff stress tensor respectively write

$$\begin{aligned}
\underline{\underline{\mathcal{F}}} &= \frac{\partial(\underline{\underline{R}}_{\omega t}\underline{X} + \underline{\tilde{u}})}{\partial\underline{X}},\\
\underline{\underline{\Sigma}} &= \underline{\underline{\Sigma}}\,(\underline{X}, \underline{\underline{R}}_{\omega t}\underline{X} + \underline{\tilde{u}}).
\end{aligned}$$

And from (1.3) and (1.4), given $\underline{v}_{ax}\cdot\underline{n}_c = 0$, we conclude that the contact pressure is in the form

$$\underline{p}_c(t, \underline{X}, \underline{\tilde{u}}, \underline{\dot{\tilde{u}}}) = p_N(\underline{\underline{R}}_{\omega t}\underline{X}, \underline{\tilde{u}})\,\underline{n}_c + \underline{p}_\tau(\underline{\underline{R}}_{\omega t}\underline{X}, \underline{\tilde{u}}, \underline{\dot{\tilde{u}}}).$$

Let us introduce a Hilbert space $V_0 = \{\,\underline{v} \in H^1(\Omega)^3 \mid \underline{v}|_{\Gamma_0} = 0\}$. Then, if $\underline{\tilde{u}} \in V_0$, and if we only keep the centrifugal part of the inertia forces, which are dominant in such situations [Le Tallec and Rahier 1994], at any time t, the principle of conservation of linear momentum takes the variational form:

$$\int_\Omega \underline{\underline{\mathcal{F}}}\,\underline{\underline{\Sigma}} : \frac{\partial\underline{v}}{\partial\underline{X}}\,\mathrm{d}\Omega = \int_{\Gamma_c}\underline{p}_c\cdot\underline{v}\,\mathrm{d}\Gamma_c + \int_\Omega \rho\omega^2(\underline{\underline{R}}_{\omega t}\underline{X} + \underline{\tilde{u}})\cdot\underline{v}\,\mathrm{d}\Omega, \qquad \forall\underline{v} \in V_0,$$

where ρ stands for the mass density. We introduce then a non-linear function $F(t, \underline{X}, \underline{\tilde{u}}, \underline{\dot{\tilde{u}}})$ by

$$\begin{aligned}
\langle F(t, \underline{X}, \underline{\tilde{u}}, \underline{\dot{\tilde{u}}}),\ \underline{v}\rangle = &\int_\Omega \frac{\partial(\underline{\underline{R}}_{\omega t}\underline{X} + \underline{\tilde{u}})}{\partial\underline{X}}\cdot\underline{\underline{\Sigma}}\,(\underline{X}, \underline{\underline{R}}_{\omega t}\underline{X} + \underline{\tilde{u}}) : \left(\frac{\partial\underline{v}}{\partial\underline{X}}\right)^t \mathrm{d}\Omega\\
&- \int_{\Gamma_c}\underline{p}_c(\underline{\underline{R}}_{\omega t}\underline{X}, \underline{\tilde{u}}, \underline{\dot{\tilde{u}}})\cdot\underline{v}\,\mathrm{d}\Gamma_c - \int_\Omega \rho\omega^2(\underline{\underline{R}}_{\omega t}\underline{X} + \underline{\tilde{u}})\cdot\underline{v}\,\mathrm{d}\Omega,
\end{aligned}$$

where $\langle\cdot,\cdot\rangle$ denotes the inner product in $L^2(\Omega)^3$. Thus, the wheel related displacement $\underline{\tilde{u}} : \mathbb{R} \to V_0$ at any time $t \in \mathbb{R}$ satisfies

$$\langle F(t, \underline{X}, \underline{\tilde{u}}, \underline{\dot{\tilde{u}}}),\ \underline{v}\rangle = 0, \quad \forall\underline{v} \in V_0. \qquad (1.6)$$

1.1.2 Space-time periodic solution (cyclic steady state)

We are interested in a "rolling" space-time periodic state. That is, the state is the same at any material point as at the corresponding point of the next sculpture but one time period $T = \theta/\omega$ ago. In the ground frame of reference, this writes as the following space-time periodicity condition:

$$\underline{X} + \underline{u}(t, \underline{X}) = \underline{\underline{R}}_\theta \, \underline{X} + \underline{u}(t - T, \underline{\underline{R}}_\theta \, \underline{X}) + \underline{v}_{ax} T, \tag{1.7}$$

where $\underline{\underline{R}}_\theta$ denotes the rotation of angle θ (sculpture size).

Let us denote the space shift operator by S:

$$\forall \underline{v} \quad S : \underline{v}(\underline{X}) \mapsto \underline{v}(\underline{\underline{R}}_\theta \underline{X}). \tag{1.8}$$

As it was mentioned, we use the material displacement $\underline{\tilde{u}}$ as the unknown state variable. Space-time periodicity condition (1.7) in term of $\underline{\tilde{u}}$ writes

$$\begin{aligned}
\underline{\tilde{u}}(t) &= \underline{u}(t) - \underline{u}_{rig}(t) \\
&= \underline{u}(t) + \underline{X} - \underline{\underline{R}}_{\omega t} \underline{X} - \underline{v}_{ax} t \\
&= S(\underline{u}(t - T) + \underline{X}) + \underline{v}_{ax} T - \underline{\underline{R}}_{\omega t} \underline{X} - \underline{v}_{ax} t \\
&= S\underline{u}(t - T) + \underline{\underline{R}}_\theta \underline{X} - \underline{\underline{R}}_{\omega(t-T)} \underline{\underline{R}}_\theta \underline{X} - \underline{v}_{ax}(t - T) \\
&= S(\underline{u}(t - T) - \underline{u}_{rig}(t - T)) \\
&= S\underline{\tilde{u}}(t - T),
\end{aligned}$$

that is,

$$\underline{\tilde{u}}(t) = S\underline{\tilde{u}}(t - T). \tag{1.9}$$

So, we are looking for $\underline{\tilde{u}}(t, \underline{X})$, the space-time periodic solution of (1.6), which satisfies the space-time periodicity condition (1.9). Thus, in the Hilbert space $V_0 = \{ \underline{v} \in H^1(\Omega)^3 \mid \underline{v}|_{\Gamma_0} = 0 \}$, the problem writes:

$$\begin{gathered}
\text{Find } \underline{\tilde{u}} : \mathbb{R} \to V_0, \text{ such that } \forall \underline{v} \in V_0 \text{ and } \forall t \in \mathbb{R} : \\
\langle F(t, \underline{\tilde{u}}, \dot{\underline{\tilde{u}}}), \, \underline{v} \rangle = 0, \\
\underline{\tilde{u}}(t) = S\underline{\tilde{u}}(t - T),
\end{gathered} \tag{1.10}$$

where the non-linear operator F is defined for all $\underline{v} \in V_0$ by

$$\begin{aligned}
\langle F(t, \underline{\tilde{u}}, \dot{\underline{\tilde{u}}}), \, \underline{v} \rangle = &\int_\Omega \underline{\underline{\mathcal{F}}}\,(\underline{X}, \underline{\underline{R}}_{\omega t} \underline{X} + \underline{\tilde{u}}) \cdot \underline{\underline{\Sigma}}\,(\underline{X}, \underline{\underline{R}}_{\omega t} \underline{X} + \underline{\tilde{u}}) : \left(\frac{\partial \underline{v}}{\partial \underline{X}} \right)^t \mathrm{d}\Omega \\
&- \int_{\Gamma_c} \underline{p}_c(\underline{\underline{R}}_{\omega t} \underline{X}, \underline{\tilde{u}}, \dot{\underline{\tilde{u}}}) \cdot \underline{v} \, \mathrm{d}\Gamma_c - \int_\Omega \rho \omega^2 \, (\underline{\underline{R}}_{\omega t} \underline{X} + \underline{\tilde{u}}) \cdot \underline{v} \, \mathrm{d}\Omega,
\end{aligned} \tag{1.11}$$

with the deformation gradient $\underline{\underline{\mathcal{F}}}$ and the second Piola-Kirchhoff stress tensor $\underline{\underline{\Sigma}}$ respectively given by (1.1) and (1.2). As for the contact force, it writes

$$\underline{p}_c(\underline{\underline{R}}_{\omega t} \underline{X}, \underline{\tilde{u}}, \dot{\underline{\tilde{u}}}) = p_N(\underline{\underline{R}}_{\omega t} \underline{X}, \underline{\tilde{u}}) \, \underline{n}_c + \underline{p}_\tau(\underline{\underline{R}}_{\omega t} \underline{X}, \underline{\tilde{u}}, \dot{\underline{\tilde{u}}}),$$

where the normal contact pressure p_N and the friction force density $\underline{p}_\tau$ are respectively defined by (1.3) and (1.4).

1.1.3 Rotational invariance of the problem

Let us now prove that the formulation (1.10) is invariant under the combined action of the time shift $t \to t+T$ and of the functional space shift $\underline{\tilde{u}} \to S\underline{\tilde{u}}$.

Proposition 1. *Let us define for any domain $\Omega \in \mathbb{R}^3$ its rotation of angle θ by $\Omega_\theta = \{\underline{\underline{R}}_\theta \underline{X} \mid \underline{X} \in \Omega\}$. Then if $\Omega = \Omega_\theta$, it holds for any function $f : \mathbb{R}^3 \to \mathbb{R}$*

$$\int_\Omega f(\underline{\underline{R}}_\theta \underline{X})\,\mathrm{d}\Omega = \int_{\Omega_\theta} f(\underline{\underline{R}}_\theta \underline{X})\,\mathrm{d}\Omega_\theta = \int_\Omega f(\underline{X})\,\mathrm{d}\Omega, \tag{1.12}$$

where we have used change of integration variable $\underline{X} \to \underline{\underline{R}}_\theta \underline{X}$.

Corollary 1. *The shift S given by (1.8) is a unitary operator on $H^1(\Omega)^3$, i.e. $\langle Su,\ Sv\rangle_{\mathcal{H}^1(\Omega)^3} = \langle u,\ v\rangle_{\mathcal{H}^1(\Omega)^3}$ for any $u,\ v \in \mathcal{H}^1(\Omega)^3$.*

Proof. It follows from the direct writing of the integrals using the change of integration variable (1.12):

$$\begin{aligned}
\int_\Omega S\underline{u} \cdot S\underline{v}\,\mathrm{d}\Omega &= \int_\Omega \underline{u} \cdot \underline{v}(\underline{\underline{R}}_\theta \underline{X})\,\mathrm{d}\Omega \\
&= \int_\Omega \underline{u} \cdot \underline{v}\,\mathrm{d}\Omega \\
\int_\Omega \frac{\partial(S\underline{u})}{\partial \underline{X}} : \frac{\partial(S\underline{v})}{\partial \underline{X}}\,\mathrm{d}\Omega &= \int_\Omega \frac{\partial \underline{u}(\underline{\underline{R}}_\theta \underline{X})}{\partial \underline{X}} : \frac{\partial \underline{v}(\underline{\underline{R}}_\theta \underline{X})}{\partial \underline{X}}\,\mathrm{d}\Omega \\
&= \int_\Omega \left(\underline{\underline{R}}_\theta^{-1} \frac{\partial \underline{u}}{\partial \underline{X}}(\underline{\underline{R}}_\theta \underline{X})\right) : \left(\underline{\underline{R}}_\theta^{-1} \frac{\partial \underline{v}}{\partial \underline{X}}(\underline{\underline{R}}_\theta \underline{X})\right)\mathrm{d}\Omega \\
&= \int_\Omega \frac{\partial \underline{u}}{\partial \underline{X}}(\underline{\underline{R}}_\theta \underline{X}) : \frac{\partial \underline{v}}{\partial \underline{X}}(\underline{\underline{R}}_\theta \underline{X})\,\mathrm{d}\Omega \\
&= \int_\Omega \frac{\partial \underline{u}}{\partial \underline{X}} : \frac{\partial \underline{v}}{\partial \underline{X}}\,\mathrm{d}\Omega
\end{aligned}$$

for any $u,\ v \in \mathcal{H}^1(\Omega)^3$. □

Lemma 1. *Operator F defined by (1.11) satisfies for all $u, w, v \in H^1(\Omega)$*

$$\langle F(t+T, S\underline{u}, S\underline{w}),\ S\underline{v}\rangle = \langle F(t, \underline{u}, \underline{w}),\ \underline{v}\rangle,$$

where the space shift S is given by (1.8).

Proof. First, note that $\underline{\underline{R}}_{\omega(t+T)}\underline{X} = \underline{\underline{R}}_{\omega t}\underline{\underline{R}}_\theta \underline{X}$. Then, by construction of the shift operator S, the contact pressure satisfies

$$\underline{p}_c(\underline{\underline{R}}_{\omega(t+T)}\underline{X}, S\underline{\tilde{u}}, S\dot{\underline{\tilde{u}}}) = \underline{p}_c(\underline{\underline{R}}_{\omega t}\underline{\underline{R}}_\theta \underline{X}, \underline{\tilde{u}}(\underline{\underline{R}}_\theta \underline{X}), \dot{\underline{\tilde{u}}}(\underline{\underline{R}}_\theta \underline{X})).$$

Let us study now the stress term $\underline{\underline{\mathcal{F}}} \cdot \underline{\underline{\Sigma}} : \left(\frac{\partial \underline{v}}{\partial \underline{X}}\right)^t$. For this purpose, for any second order tensor $\underline{\underline{L}}(\underline{X})$ involved in this expression, the notation $\underline{\underline{L}}_\theta$ would be

the tensor which would be obtained at point $\underline{\underline{R}}_\theta \underline{X}$ by applying locally the same geometrical transformation but after a rotation $\underline{\underline{R}}_\theta$ of the frame of reference. Under this notation, we will have

$$\begin{aligned}
\underline{\underline{\mathcal{F}}}\left(t+T, \underline{X}, S\underline{\tilde{u}}\right) &= \frac{\partial(\underline{\underline{R}}_{\omega(t+T)}\underline{X} + S\underline{\tilde{u}})}{\partial \underline{X}} \\
&= \frac{\partial(\underline{\underline{R}}_{\omega t}\underline{\underline{R}}_\theta \underline{X} + \underline{\tilde{u}}(\underline{\underline{R}}_\theta \underline{X}))}{\partial \underline{\underline{R}}_\theta \underline{X}} \cdot \frac{\partial \underline{\underline{R}}_\theta \underline{X}}{\partial \underline{X}} \\
&= \underline{\underline{\mathcal{F}}}\,(t, \underline{\underline{R}}_\theta \underline{X}, \underline{\tilde{u}}(\underline{\underline{R}}_\theta \underline{X})) \cdot \underline{\underline{R}}_\theta \\
&= \underline{\underline{\mathcal{F}}}_\theta \cdot \underline{\underline{R}}_\theta,
\end{aligned}$$

$$\begin{aligned}
\underline{\underline{\mathcal{C}}}\left(t+T, \underline{X}, S\underline{\tilde{u}}\right) &= \left(\underline{\underline{\mathcal{F}}}^t \cdot \underline{\underline{\mathcal{F}}}\right)\left(t+T, \underline{X}, S\underline{\tilde{u}}\right) \\
&= \underline{\underline{R}}_\theta^t \cdot \underline{\underline{\mathcal{F}}}_\theta^t \cdot \underline{\underline{\mathcal{F}}}_\theta \cdot \underline{\underline{R}}_\theta \\
&= \underline{\underline{R}}_\theta^t \cdot \underline{\underline{\mathcal{C}}}_\theta \cdot \underline{\underline{R}}_\theta.
\end{aligned}$$

But the tyre is mechanically invariant under the rotation $\underline{\underline{R}}_\theta$. This means that in term of free energy W_e we have

$$W_e(\underline{\underline{R}}_\theta \underline{X}, \underline{\underline{\mathcal{C}}}_\theta) = W_e(\underline{X}, \underline{\underline{\mathcal{C}}}),$$

or equivalently after differentiation along any elastic evolution $d\underline{\underline{\mathcal{C}}}$

$$\underline{\underline{\Sigma}} : d\underline{\underline{\mathcal{C}}} = dW = \underline{\underline{\Sigma}}_\theta : d\underline{\underline{\mathcal{C}}}_\theta = \underline{\underline{\Sigma}}_\theta : \underline{\underline{R}}_\theta \cdot d\underline{\underline{\mathcal{C}}} \cdot \underline{\underline{R}}_\theta^t = \underline{\underline{R}}_\theta^t \cdot \underline{\underline{\Sigma}}_\theta \cdot \underline{\underline{R}}_\theta : d\underline{\underline{\mathcal{C}}}\,.$$

That leads to the mechanical rotational invariance property

$$\underline{\underline{\Sigma}}\left(t+T, \underline{X}, S\underline{\tilde{u}}\right) = \underline{\underline{R}}_\theta^t \cdot \underline{\underline{\Sigma}}_\theta \cdot \underline{\underline{R}}_\theta.$$

Altogether, we finally get

$$\begin{aligned}
\left(\underline{\underline{\mathcal{F}}} \cdot \underline{\underline{\Sigma}}\right)\left(t+T, \underline{X}, S\underline{\tilde{u}}\right) : \left(\frac{\partial S\underline{v}}{\partial \underline{X}}\right)^t &= \underline{\underline{\mathcal{F}}}_\theta \cdot \underline{\underline{R}}_\theta \cdot \underline{\underline{R}}_\theta^t \cdot \underline{\underline{\Sigma}}_\theta \cdot \underline{\underline{R}}_\theta : \left(\frac{\partial S\underline{v}}{\partial \underline{\underline{R}}_\theta \underline{X}} \cdot \underline{\underline{R}}_\theta\right)^t \\
&= \underline{\underline{\mathcal{F}}}_\theta \cdot \underline{\underline{\Sigma}}_\theta : \left(\frac{\partial S\underline{v}}{\partial \underline{\underline{R}}_\theta \underline{X}}\right)^t.
\end{aligned}$$

Note that the tyre domain Ω is invariant to rotation by one sculpture angle θ. Then, by putting all the above results in the variational form (1.11) and after the change of integration variable (1.12) in the resulting integral, we finally prove the statement

$$\langle F(t+T, S\underline{u}, S\underline{w}),\ S\underline{v}\rangle = \langle F(t, \underline{u}, \underline{w}),\ \underline{v}\rangle, \tag{1.13}$$

satisfied for any test function $\underline{v}$, any velocity field $\underline{w}$ and any displacement field $\underline{u}$. □

Remark 1. *If (1.13) holds, it is then obvious to prove that if* $\underline{\tilde{u}}$ *and* $\dot{\underline{\tilde{u}}}$ *are solution of the time evolution problem on the first period* $[0, T]$*, then* $S\underline{\tilde{u}}$ *and* $S\dot{\underline{\tilde{u}}}$ *will be solution on the second period* $[T, 2T]$ *and so on. In particular, this proves that if we have* $\underline{\tilde{u}}(T) = S\underline{\tilde{u}}(0)$ *on the first period, then we have a solution for all times later on. Thus, the propriety (1.13) is a necessary condition for existence of the space-time periodic state (1.9).*

1.1.4 Simplified academic model

In this paragraph, let us present a simplification of the tyre model, described above, with less non-linearity and more time dependence. This new model will give more flexibility in the possible tests. In contrast to the previous paragraph, we make the following simplifications and additions:

- **Simple geometry.** Tyre is modeled simply by a 3D ring (Figure 1.5, left). Periodicity of the sculptures is represented not by a modification of the geometry but by a modification of material parameters (Young's modulus, etc.), which are periodic functions of the angle, almost vanishing in the sculpture voids (see Figure 1.5, right).

- **Rotating frame of reference.** We choose the rotating frame of reference, associated to the wheel, i.e. the coordinate system with the origin on the tyre axle and rotating with the tyre rim. In this framework, the ground surface turns around the origin with angular velocity ω, remaining at the constant distance r_{load} from it. In other words, the unit normal $\underline{n_c}$ is now a functions of time: $\underline{n_c}(t) = \underline{\underline{R}}_{\omega t}^{-1}\underline{n_c}(0)$. Besides, the contact surface is shifting with the linear velocity $\underline{v}_{soil}(t) = -\underline{\underline{R}}_{\omega t}^{-1}\underline{v}_{ax}$, orthogonal to $\underline{n_c}(t)$.

  Displacements and velocity in the ground and the wheel frames of reference are related as follows

$$(\underline{X} + \underline{u})_{ground} = \underline{\underline{R}}_{\omega t}(\underline{X} + \underline{u})_{wheel} + \underline{v}_{ax}t$$

  and

$$\dot{\underline{u}}_{ground} = \underline{\underline{R}}_{\omega t}\,\dot{\underline{u}}_{wheel} + \omega\underline{\underline{\Pi}}\,\underline{\underline{R}}_{\omega t}(\underline{X} + \underline{u})_{wheel} + \underline{v}_{ax},$$

  where $\underline{\underline{\Pi}}$ is defined as in (1.5). In what follows we use $\underline{u}$ for $\underline{u}_{wheel}$. Then, given the time period $T = \theta/\omega$, the space-time periodicity condition writes

$$\underline{u}(t) = S\underline{u}(t - T),$$

  where the space shift operator S is redefined in the rotating frame of reference as

$$\forall \underline{v} \qquad S : \underline{v}(\underline{X}) \mapsto \underline{\underline{R}}_{\theta}^{-1}\,\underline{v}(\underline{\underline{R}}_{\theta}\underline{X}). \tag{1.14}$$

- **Small strains and quasi-static assumptions.** For the sake of simplicity, we assume that we are in small strains. That is, the Cauchy-Green stain tensor is linearized in the rotating frame of reference as

$$\underline{\underline{\mathcal{C}}} \approx \mathrm{Id} + \frac{\partial \underline{u}}{\partial \underline{X}} + \left(\frac{\partial \underline{u}}{\partial \underline{X}}\right)^t.$$

  In addition, we will neglect all inertia forces.

- **Viscoelasticity.** To have an additional source of memory effects, we assume the material to be viscoelastic. We use a Kelvin-Voigt viscoelasticity model, represented by an elastic spring and a dashpot connected in parallel [Chawla and Meyers 1999, Christensen 2012]. So, the Cauchy stress tensor $\underline{\underline{\sigma}}$ is defined in the rotating frame of reference by a time-dependent constitutive law:

$$\underline{\underline{\sigma}}\,(t, \underline{X}) = \eta(\underline{X})\, \partial_t \underline{\underline{e}}\,(t, \underline{X}) + \underline{\underline{\underline{\underline{K}}}}(\underline{X})\, \underline{\underline{e}}\,(t, \underline{X}),$$

  where $\underline{\underline{e}}$ is the linearized Green-Lagrange strain tensor

$$\underline{\underline{e}} = \frac{1}{2}\left(\underline{\underline{\mathcal{C}}} - \mathrm{Id}\right) \approx \frac{1}{2}\left(\nabla \underline{u} + (\nabla \underline{u})^t\right) = \nabla_s \underline{u},$$

  η is a scalar viscosity coefficient and $\underline{\underline{\underline{\underline{K}}}}$ is the fourth-order isotropic elasticity tensor:

$$\underline{\underline{\underline{\underline{K}}}} : \quad \underline{\underline{e}} \quad \mapsto \quad \lambda \operatorname{tr} \underline{\underline{e}} \cdot \mathrm{Id} + 2\mu\, \underline{\underline{e}}\,.$$

  Here, λ and μ (not to confuse with the Coulomb friction coefficient) are the Lamé coefficients:

$$\lambda = \frac{E\nu}{(1+\nu)(1-2\nu)}, \qquad \mu = \frac{E}{2(1+\nu)}, \tag{1.15}$$

  where E and ν are Young's modulus and Poisson's ratio respectively. As mentioned above, the periodic structure of the wheel is taken into account by imposing an angular periodicity of the Young's modulus $E(\underline{X})$ and viscosity coefficient $\eta(\underline{X})$:

$$E(\underline{X}) = E(\underline{\underline{R}}_\theta \underline{X}), \qquad \eta(\underline{X}) = \eta(\underline{\underline{R}}_\theta \underline{X}).$$

  Herein, we use piece-wise constant coefficients, repeating on M motives:

$$E(\underline{X}), \eta(\underline{X}) = \begin{cases} \approx 0 & \text{if } \cos(M \cdot \arg \underline{X}) < 0 \text{ and } |\underline{X}| > r_{sculpture}, \\ E_0, \eta_0 & \text{otherwise,} \end{cases} \tag{1.16}$$

  where E_0 and η_0 are respectively the constant reference Young's modulus and viscosity coefficient of the constitutive material. Note that Young's modulus and viscosity coefficient are never exactly zeros. Moreover, the viscosity-stiffness ratio has to be very small in the empty spaces, in order not to have memory effects in these regions.

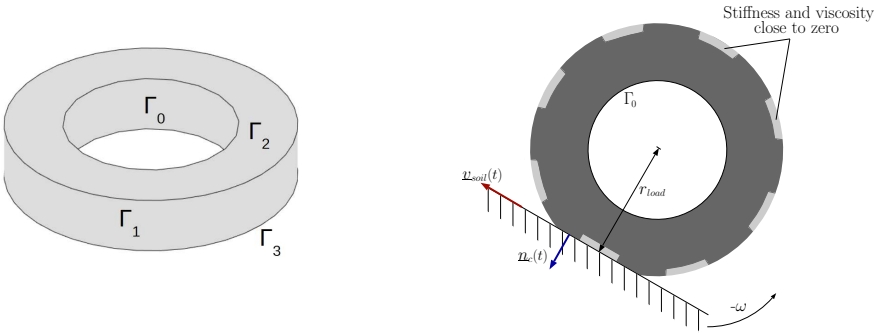

Figure 1.5: Rolling tyre scheme (simplified academic model). The tyre is represented by a 3D ring (left), where the periodic sculpture is represented by periodicity of material parameters (right), instead of geometric periodicity. In the wheel frame of reference, the ground surface turns around the origin with angular velocity ω, remaining at the constant distance r_{load} from it and shifting with the linear velocity $\underline{v}_{soil}(t) = -\underline{\underline{R}}_{\omega t}^{-1}\underline{v}_{ax}$. The unit normal to the contact surface is thus a functions of time $\underline{n}_c(t) = \underline{\underline{R}}_{\omega t}^{-1}\underline{n}_c(0)$.

- **Inexact incompressibility.** We consider just nearly incompressible material with a uniform Poisson's ratio $\nu = 0.48$.

Under the above assumptions, in the absence of inertia forces, the momentum conservation law writes as $\nabla \cdot \underline{\underline{\sigma}}(\underline{u}) = 0$ in Ω. Thus, in the Hilbert space $V_0 = \{\, \underline{v} \in H^1(\Omega)^3 \mid \underline{v}|_{\Gamma_0} = 0\}$, the problem writes in variational form:

$$\begin{aligned} &\text{Find } \underline{u} : \mathbb{R} \mapsto V_0, \text{ such that } \forall \underline{v} \in V_0 \text{ and } \forall t \in \mathbb{R} \\ &\qquad \langle F(t, \underline{u}, \dot{\underline{u}}),\ \underline{v} \rangle = 0, \\ &\qquad \underline{u}(t) = S\underline{u}(t - T), \end{aligned} \tag{1.17}$$

where the non-linear operator F is defined by

$$\langle F(t, \underline{u}, \dot{\underline{u}}),\ \underline{v} \rangle = \int_\Omega \left(\eta\, \nabla_s \dot{\underline{u}} + \underline{\underline{\underline{\underline{K}}}}\, \nabla_s \underline{u} \right) : \nabla \underline{v}\ \mathrm{d}\Omega - \int_{\Gamma_1} \underline{p}_c(t, \underline{u}, \dot{\underline{u}}) \cdot \underline{v}\ \mathrm{d}\Gamma. \tag{1.18}$$

Above, the space shift operator S is defined by (1.14). The contact force density $\underline{p}_c$ is given by

$$\underline{p}_c(t, \underline{u}, \dot{\underline{u}}) = p_N(t, \underline{u})\, \underline{n}_c(t) + \underline{p}_\tau(t, \underline{u}, \dot{\underline{u}}),$$

where the normal contact pressure p_N and the friction density $\underline{p}_\tau$ are defined respectively by (1.3) and (1.4) through the normal gap and the slip velocity, which

in the rotating frame of reference have the form

$$g_N(t,\underline{u}) = r_{load} - (\underline{X}+\underline{u})\cdot\underline{n}_c(t),$$
$$\dot{\underline{s}}(t,\underline{u},\dot{\underline{u}}) = \big(\mathrm{Id} - \underline{n}_c(t)\otimes\underline{n}_c(t)\big)\big(\dot{\underline{u}} + \omega\underline{\underline{\Pi}}\,(t)\underline{u} + \underline{v}_{rel}(t)\big).$$

Here, $\underline{v}_{rel}(t) = \underline{v}_{soil}(t) + \omega\underline{\underline{\Pi}}\,(t)\underline{X}$ is the relative velocity of the moving contact surface with respect to contacting material points of the tyre, and $\underline{\underline{\Pi}}\,(t) = (-\underline{v}_{soil}(t)\otimes\underline{n}_c(t)+\underline{n}_c(t)\otimes\underline{v}_{soil}(t))/|\underline{v}_{ax}|$. The following lemma proves that the above formulation (1.18) is invariant under the space-time shift $t\to t+T,\ u\to Su$.

Lemma 2. *Operator F defined by (1.18) satisfies for all $u,w,v\in H^1(\Omega)$*

$$\langle F(t+T,S\underline{u},S\underline{w}),\ S\underline{v}\rangle = \langle F(t,\underline{u},\underline{w}),\ \underline{v}\rangle,$$

where the space shift S is given by (1.14).

Proof. First, recall that the simplified tyre domain Ω is simply a 3D ring and is thus invariant to any rotation, in particular to $\underline{\underline{R}}_\theta$. Then the Proposition 1 holds.

Due to the contact surface motion, the contact unit normal and the ground velocity vector satisfy

$$\underline{n}_c(t+T) = \underline{\underline{R}}_{\omega T}^{-1}\underline{n}_c(t) = \underline{\underline{R}}_\theta^{-1}\underline{n}_c(t), \qquad \underline{v}_{soil}(t+T) = \underline{\underline{R}}_{\omega T}^{-1}\underline{v}_{soil}(t) = \underline{\underline{R}}_\theta^{-1}\underline{v}_{soil}(t).$$

Then the shifted normal gap writes

$$\begin{aligned} g_N(t+T,S\underline{u}) &= r_{load} - (\underline{X}+S\underline{u})\cdot\underline{n}_c(t+T),\\ &= r_{load} - \Big(\underline{\underline{R}}_\theta^{-1}(\underline{\underline{R}}_\theta\underline{X}) + \underline{\underline{R}}_\theta^{-1}\underline{u}(\underline{\underline{R}}_\theta\underline{X})\Big)\cdot\Big(\underline{\underline{R}}_{\omega T}^{-1}\underline{n}_c(t)\Big)\\ &= r_{load} - (\underline{\underline{R}}_\theta\underline{X} + \underline{u}(\underline{\underline{R}}_\theta\underline{X}))\cdot\underline{n}_c(t), \end{aligned}$$

which leads by (1.3) to

$$p_N(t+T,S\underline{u})\,\underline{n}_c(t+T) = S\big(p_N(t,\underline{u})\underline{n}_c(t)\big). \tag{1.19}$$

Further, from the fact that $\underline{\underline{\Pi}}\,(t+T) = \underline{\underline{R}}_\theta^{-1}\underline{\underline{\Pi}}\,(t)\underline{\underline{R}}_\theta$ we have that

$$\begin{aligned} \underline{v}_{rel}(t+T) &= \underline{v}_{soil}(t+T) + \omega\underline{\underline{\Pi}}\,(t+T)\underline{X}\\ &= \underline{\underline{R}}_\theta^{-1}\underline{v}_{soil}(t) + \underline{\underline{R}}_\theta^{-1}\omega\underline{\underline{\Pi}}\,(t)\underline{\underline{R}}_\theta\underline{X}\\ &= \underline{\underline{R}}_\theta^{-1}\big(\underline{v}_{soil}(t) + \omega\underline{\underline{\Pi}}\,(t)\underline{\underline{R}}_\theta\underline{X}\big)\\ &= S\underline{v}_{rel}(t) \end{aligned}$$

and that for any $\underline{u}$ and $\underline{w}$

$$\begin{aligned} S\underline{w} + \omega\underline{\underline{\Pi}}\,(t+T)S\underline{u} &= \underline{\underline{R}}_\theta^{-1}\underline{w}(\underline{\underline{R}}_\theta\underline{X}) + \omega\underline{\underline{R}}_\theta^{-1}\underline{\underline{\Pi}}\,(t)\underline{\underline{R}}_\theta\Big(\underline{\underline{R}}_\theta^{-1}\underline{u}(\underline{\underline{R}}_\theta\underline{X})\Big)\\ &= \underline{\underline{R}}_\theta^{-1}\big(\underline{w}(\underline{\underline{R}}_\theta\underline{X}) + \omega\underline{\underline{\Pi}}\,(t)\,\underline{u}(\underline{\underline{R}}_\theta\underline{X})\big)\\ &= S\big(\underline{w} + \omega\underline{\underline{\Pi}}\,(t)\,\underline{u}\big). \end{aligned}$$

Hence, we obtain for the slip velocity that

$$\begin{aligned}\dot{\underline{s}}(t+T, S\underline{u}, S\underline{w}) &= \big(\mathrm{Id} - \underline{n}_c(t+T)\otimes\underline{n}_c(t+T)\big)\cdot \\ &\qquad\qquad \cdot\big(S\underline{w} + \omega\underline{\underline{\Pi}}\,(t+T)S\underline{u} + \underline{v}_{rel}(t+T)\big) \\ &= \underline{\underline{R}}_\theta^{-1}\big(\mathrm{Id} - \underline{n}_c(t)\otimes\underline{n}_c(t)\big)\underline{\underline{R}}_\theta\; S\big(\underline{w} + \omega\underline{\underline{\Pi}}\,(t)\,\underline{u} + \underline{v}_{rel}(t)\big) \\ &= S\dot{\underline{s}}(t, \underline{u}, \underline{w}).\end{aligned}$$

This and (1.19) lead by (1.4) to

$$\underline{p}_\tau(t+T, S\underline{u}, S\underline{w}) = S\underline{p}_\tau(t, \underline{u}, \underline{w}). \tag{1.20}$$

Together (1.19) and (1.20) prove the space-time periodicity of the contact forces:

$$\underline{p}_c(t+T, S\underline{u}, S\underline{w}) = S\underline{p}_c(t, \underline{u}, \underline{w}).$$

Hence, given the invariance of the outer boundary Γ_1 to rotation, we use the change of integration variable (1.12) in Proposition 1 to write the integral

$$\int_{\Gamma_1} \underline{p}_c(t+T, S\underline{u}, S\underline{w})\cdot S\underline{v}\;\mathrm{d}\Gamma = \int_{\Gamma_1} S\underline{p}_c(t, \underline{u}, \underline{w})\cdot S\underline{v}\;\mathrm{d}\Gamma = \int_{\Gamma_1} \underline{p}_c(t, \underline{u}, \underline{w})\cdot \underline{v}\;\mathrm{d}\Gamma. \tag{1.21}$$

Let us study now the first term in (1.18). For any $\underline{u}\in H^1(\Omega)^3$ it holds

$$\begin{aligned}\nabla(S\underline{u}) &= \frac{\partial\big(\underline{\underline{R}}_\theta^{-1}\underline{u}(\underline{\underline{R}}_\theta\underline{X})\big)}{\partial\underline{X}} \\ &= \underline{\underline{R}}_\theta^{-1}\frac{\partial\underline{u}(\underline{\underline{R}}_\theta\underline{X})}{\partial(\underline{\underline{R}}_\theta\underline{X})}\cdot\frac{\partial(\underline{\underline{R}}_\theta\underline{X})}{\partial\underline{X}} \\ &= \underline{\underline{R}}_\theta^{-1}\frac{\partial\underline{u}}{\partial\underline{X}}(\underline{\underline{R}}_\theta\underline{X})\,\underline{\underline{R}}_\theta\end{aligned}$$

Then for any $\underline{u},\underline{v}\in H^1(\Omega)^3$ and any θ-periodic scalar function $\alpha(\underline{X}) = \alpha(\underline{\underline{R}}_\theta\underline{X})$ the shift S satisfies

$$\begin{aligned}\int_\Omega \alpha\,\nabla(S\underline{u}) : \nabla(S\underline{v})\;\mathrm{d}\Omega &= \int_\Omega \alpha(\underline{X})\left(\underline{\underline{R}}_\theta^{-1}\frac{\partial\underline{u}}{\partial\underline{X}}(\underline{\underline{R}}_\theta\underline{X})\,\underline{\underline{R}}_\theta\right) : \left(\underline{\underline{R}}_\theta^{-1}\frac{\partial\underline{v}}{\partial\underline{X}}(\underline{\underline{R}}_\theta\underline{X})\,\underline{\underline{R}}_\theta\right)\mathrm{d}\Omega \\ &= \int_\Omega \alpha(\underline{\underline{R}}_\theta\underline{X})\,\frac{\partial\underline{u}}{\partial\underline{X}}(\underline{\underline{R}}_\theta\underline{X}) : \frac{\partial\underline{v}}{\partial\underline{X}}(\underline{\underline{R}}_\theta\underline{X})\;\mathrm{d}\Omega \\ &= \int_\Omega \alpha\,\nabla\underline{u} : \nabla\underline{v}\;\mathrm{d}\Omega,\end{aligned} \tag{1.22}$$

where we have used again the change of integration variable (1.12). In addition, this demonstrates that the shift S given by (1.14) is a unitary operator on $H^1(\Omega)^3$.

Similarly, given the orthogonality of rotation $\underline{\underline{R}}_\theta^t = \underline{\underline{R}}_\theta^{-1}$, we can obtain the same result for the transposed and thus for the symmetric gradient:

$$\begin{aligned}\int_\Omega \alpha\;(\nabla(S\underline{u}))^t : \nabla(S\underline{v})\;\mathrm{d}\Omega &= \int_\Omega \alpha\;(\nabla\underline{u})^t : \nabla\underline{v}\;\mathrm{d}\Omega, \\ \int_\Omega \alpha\,\nabla_s(S\underline{u}) : \nabla(S\underline{v})\;\mathrm{d}\Omega &= \int_\Omega \alpha\,\nabla_s\underline{u} : \nabla\underline{v}\;\mathrm{d}\Omega.\end{aligned}$$

Let us remind the form of the elastic term:

$$\underline{\underline{\underline{\underline{K}}}}\ \nabla_s \underline{u} = \lambda \operatorname{tr} \nabla_s \underline{u} \cdot \mathrm{Id} + 2\mu\, \nabla_s \underline{u},$$

where Lamé coefficients λ and μ are defined by (1.15) through the θ-periodic Young modulus (1.16). Therefore, we have $\lambda(\underline{X}) = \lambda(\underline{\underline{R}}_\theta \underline{X})$ and $\mu(\underline{X}) = \mu(\underline{\underline{R}}_\theta \underline{X})$. As for the divergence term, it holds

$$\begin{aligned}
\operatorname{tr} \nabla_s(S\underline{u}) &= \nabla(S\underline{u}) : \mathrm{Id} \\
&= \left(\underline{\underline{R}}_\theta^{-1} \frac{\partial \underline{u}}{\partial \underline{X}} (\underline{\underline{R}}_\theta \underline{X})\, \underline{\underline{R}}_\theta \right) : \mathrm{Id} \\
&= \frac{\partial \underline{u}}{\partial \underline{X}} (\underline{\underline{R}}_\theta \underline{X}) : \mathrm{Id},
\end{aligned}$$

which gives

$$\begin{aligned}
\int_\Omega \lambda\ \operatorname{tr} \nabla_s(S\underline{u})\, \mathrm{Id} : \nabla(S\underline{v})\ \mathrm{d}\Omega &= \int_\Omega \lambda\ \operatorname{tr} \nabla(S\underline{u}) \cdot \operatorname{tr} \nabla(S\underline{v})\ \mathrm{d}\Omega \\
&= \int_\Omega \lambda(\underline{\underline{R}}_\theta \underline{X})\ \operatorname{tr} \frac{\partial \underline{u}}{\partial \underline{X}} (\underline{\underline{R}}_\theta \underline{X}) \cdot \operatorname{tr} \frac{\partial \underline{v}}{\partial \underline{X}} (\underline{\underline{R}}_\theta \underline{X})\ \mathrm{d}\Omega \\
&= \int_\Omega \lambda\ \operatorname{tr} \nabla \underline{u} \cdot \operatorname{tr} \nabla \underline{v}\ \mathrm{d}\Omega \\
&= \int_\Omega (\lambda\ \operatorname{tr} \nabla_s \underline{u} \cdot \mathrm{Id}) : \nabla \underline{v}\ \mathrm{d}\Omega.
\end{aligned}$$

By this and (1.22), given θ-periodicity of the viscosity coefficient η (1.16), we finally have

$$\int_\Omega \left(\eta\, \nabla_s(S\dot{\underline{u}}) + \underline{\underline{\underline{\underline{K}}}}\ \nabla_s(S\underline{u}) \right) : \nabla(S\underline{v})\ \mathrm{d}\Omega = \int_\Omega \left(\eta\, \nabla_s \dot{\underline{u}} + \underline{\underline{\underline{\underline{K}}}}\ \nabla_s \underline{u} \right) : \nabla \underline{v}\ \mathrm{d}\Omega. \quad (1.23)$$

Combination of (1.21) and (1.23) proves the statement of the lemma. □

1.2 Linear 2D heat problem

The same "rolling" type space-time periodic solution can be illustrated by a simpler but possibly more diffusive example. Here we present a linear 2D model. It considers a planar disk heated with a source periodically moving along a circular path (see Figure 1.6), which may be a simple model problem for additive manufacturing or for a rolling tyre heated by localized energy dissipation sources. The source can take one of M positions on a circle inside the disk. After having heated one spot during a time period T, it moves to the next position, i.e. rotates to the angle $\theta = 2\pi/M$. All material parameters are supposed to be θ-periodic with respect to the angle.

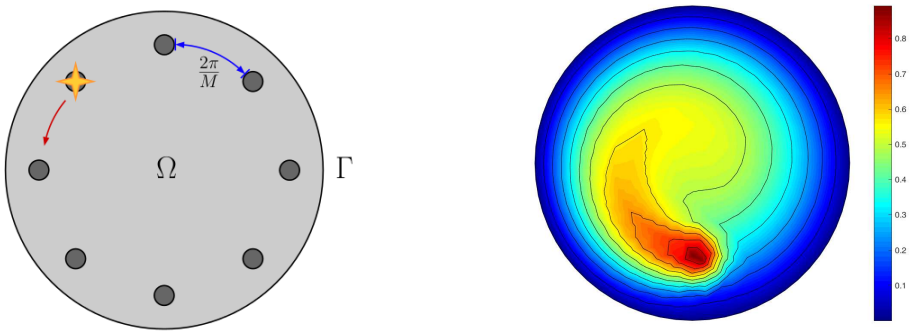

Figure 1.6: Planar disk heated with a periodically moving source: geometry, loading (left) and finite elements solution (right).

In more details, let us consider a planar disk of radius R with the interior Ω and the boundary Γ (Figure 1.6). The state is characterized by the unknown temperature u, which satisfies the heat equation in Ω and a Robin boundary condition on Γ:

$$c\,\dot{u} - \nabla \cdot [\kappa\,\nabla u] = q \qquad in\ \Omega,$$

$$\kappa\,\nabla u \cdot \underline{n} + a\,(u - u_0) = 0 \qquad on\ \Gamma,$$

where c, κ and a are the heat capacity, heat conductivity and heat transfer coefficients respectively, and u_0 is the reference ambient temperature. The vector $\underline{n}$ denotes the outer unit normal to the boundary Γ and q represents a moving heat source defined by

$$q(t,\underline{x}) = q_0 \cdot \mathbf{1}_C\left(\underline{\underline{R}}^{-1}_{\varphi(t)}\,\underline{x}\right), \quad \text{where} \quad \varphi(t) = \theta \cdot ceil(t/T).$$

Above, q_0 represents the amount of provided heat, $\mathbf{1}_C$ is the characteristic function of the local circular heated spot at initial time, and the operator $\underline{\underline{R}}_\varphi$ denotes rotation of angle φ. The function *ceil* provides the smallest integer greater than the argument. Note that the source term $q(t,\underline{x})$ is space-time periodic, i.e. it satisfies the "rolling" periodicity condition:

$$q(t,\underline{x}) = q(t - T,\, \underline{\underline{R}}^{-1}_{\theta}\,\underline{x}).$$

In numbers, the heat source density is $q = 10^7\ W/m^3$, it successively heats one of $M = 30$ circular spots of radius $0.1\,R$ along a circle path of radius $0.6\,R$ during a time interval of $T = 0.1\ s$.

All material parameters are supposed to be θ-periodic in space:

$$\begin{aligned} c(\underline{x}) = c(\underline{\underline{R}}_\theta\,\underline{x}), \quad \kappa(\underline{x}) &= \kappa(\underline{\underline{R}}_\theta\,\underline{x}) \qquad \forall \underline{x} \in \Omega; \\ a(\underline{x}) &= a(\underline{\underline{R}}_\theta\,\underline{x}) \qquad \forall \underline{x} \in \Gamma. \end{aligned}$$

More precisely, in polar coordinates (r, φ) it writes

$$c(r,\varphi) = \rho\bar{c}_p \cdot (1 + 0.5\cos M\varphi), \quad \kappa(r,\varphi) = \bar{\kappa} \cdot (1 + 0.5\cos M\varphi) \qquad \forall r \in [0, R],$$
$$a(\varphi) = \bar{a} \cdot (1 + 0.5\cos M\varphi).$$

The average coefficients are those associated to lithium which is one of the most "viscous" materials (large memory effects) in the sense that it has very low diffusivity:

$$\rho = 534\ kg/m^3, \qquad \bar{c}_p = 3.58 \cdot 10^3\ J/(kg \cdot K), \qquad \bar{\kappa} = 84.8\ W/(m \cdot K).$$

We also use a very large value of the average boundary heat transfer coefficient $\bar{a} = 10^4\ W/(m^2 \cdot K)$ in order to have a good control of the boundary temperature.

We are looking for a "rolling" periodic solution, i.e. a solution satisfying the following space-time periodicity condition:

$$u(t, \underline{x}) = u(t - T, \underline{\underline{R}}_\theta^{-1}\, \underline{x}).$$

In other words, the state at any point is the same that at the previously heated point one time period ago. Let us therefore define the space shift operator S by

$$\forall u \quad S : u(\underline{x}) \mapsto u(\underline{\underline{R}}_\theta^{-1}\, \underline{x}). \tag{1.24}$$

Thus, our model problem writes:

Find $u : \mathbb{R}_+ \mapsto H^1(\Omega)$, such that $\forall v \in H^1(\Omega)$ and $\forall t \in \mathbb{R}_+$
$$\langle F(t, u, \dot{u}),\ v\rangle = 0,$$
$$u(t) = Su(t - T),$$

where $\langle \cdot,\ \cdot \rangle$ denotes the inner product in $L^2(\Omega)$, and the linear operator F is defined by

$$\langle F(t,u,\dot{u}),\ v\rangle = \int_\Omega c\,\dot{u}\,v\,\mathrm{d}\Omega + \int_\Omega \kappa\,\nabla u \cdot \nabla v\,\mathrm{d}\Omega + \int_\Gamma a \cdot (u - u_0)\,v\ \mathrm{d}\Gamma - \int_\Omega qv\,\mathrm{d}\Omega. \tag{1.25}$$

The associated finite element solution is represented on Figure 1.6 (right). The following lemma proves that this formulation is invariant under the space-time shift $t \to t + T,\ u \to Su$.

Lemma 3. *Operator F defined by (1.25) satisfies for all $u, w, v \in H^1(\Omega)$*

$$\langle F(t + T, Su, Sw),\ Sv\rangle = \langle F(t, u, w),\ v\rangle, \tag{1.26}$$

where the space shift S is given by (1.24).

Proof. First, let us note that, since the disk domain Ω is invariant to rotation, the shift S is a unitary operator on $L^2(\Omega)$, i.e. for any $u, v \in L^2(\Omega)$

$$\begin{aligned}\int_\Omega Su \cdot Sv \,\mathrm{d}\Omega &= \int_\Omega u(\underline{\underline{R}}_\theta^{-1}\underline{x}) \cdot v(\underline{\underline{R}}_\theta^{-1}\underline{x}) \,\mathrm{d}\Omega \\ &= \int_0^R \int_0^{2\pi} u(r, \varphi - \theta) \cdot v(r, \varphi - \theta) \,\mathrm{d}\varphi \,\mathrm{d}r \\ &= \int_0^R \int_0^{2\pi} u(r, \varphi) \cdot v(r, \varphi) \,\mathrm{d}\varphi \,\mathrm{d}r \\ &= \int_\Omega u \cdot v \,\mathrm{d}\Omega,\end{aligned}$$

where we have used change of integration variable $\underline{x} \to \underline{\underline{R}}_\theta^{-1}\underline{x}$, expressed in the polar coordinates (r, φ).

Thus, given the space-time periodicity of the heat source $q(t+T, \underline{x}) = q(t, \underline{\underline{R}}_\theta^{-1}\underline{x})$, we have

$$\int_\Omega q(t+T) \cdot Sv \,\mathrm{d}\Omega = \int_\Omega Sq(t) \cdot Sv \,\mathrm{d}\Omega = \int_\Omega q(t) \cdot v \,\mathrm{d}\Omega.$$

Recall the periodicity of the coefficients $c(\underline{x}) = c(\underline{\underline{R}}_\theta^{-1}\underline{x})$, $\kappa(\underline{x}) = \kappa(\underline{\underline{R}}_\theta^{-1}\underline{x})$, $a(\underline{x}) = a(\underline{\underline{R}}_\theta^{-1}\underline{x})$. Then, we can write

$$\begin{aligned}\int_\Omega c \cdot Sw \cdot Sv \,\mathrm{d}\Omega &= \int_\Omega c(\underline{\underline{R}}_\theta^{-1}\underline{x}) \cdot w(\underline{\underline{R}}_\theta^{-1}\underline{x}) \cdot v(\underline{\underline{R}}_\theta^{-1}\underline{x}) \,\mathrm{d}\Omega \\ &= \int_\Omega S(cw) \cdot Sv \,\mathrm{d}\Omega \\ &= \int_\Omega c\, w\, v \,\mathrm{d}\Omega.\end{aligned}$$

Similarly, using the same change of integration variables $\underline{x} \to \underline{\underline{R}}_\theta^{-1}\underline{x}$, we obtain

$$\begin{aligned}\int_\Gamma a \cdot (Su - u_0) \cdot Sv \;\mathrm{d}\Gamma &= \int_\Gamma a(\underline{\underline{R}}_\theta^{-1}\underline{x}) \cdot \big(u(\underline{\underline{R}}_\theta^{-1}\underline{x}) - u_0\big) \cdot v(\underline{\underline{R}}_\theta^{-1}\underline{x}) \;\mathrm{d}\Gamma \\ &= \int_\Gamma a \cdot (u - u_0)\, v \;\mathrm{d}\Gamma.\end{aligned}$$

Finally, let us consider the diffusion term. From the fact that for any $u \in H^1(\Omega)$

$$\nabla(Su) = \frac{\partial u(\underline{\underline{R}}_\theta^{-1}\underline{x})}{\partial \underline{x}} = \frac{\partial u(\underline{\underline{R}}_\theta^{-1}\underline{x})}{\partial(\underline{\underline{R}}_\theta^{-1}\underline{x})} \cdot \frac{\partial(\underline{\underline{R}}_\theta^{-1}\underline{x})}{\partial \underline{x}} = \underline{\underline{R}}_\theta \, \frac{\partial u}{\partial \underline{x}}(\underline{\underline{R}}_\theta^{-1}\underline{x}) = \underline{\underline{R}}_\theta \, S(\nabla u)$$

and from the invariance of Ω to rotation, we obtain with the same change of

integration variable $\underline{x} \to \underline{\underline{R}}_\theta^{-1}\underline{x}$ that

$$\begin{aligned}\int_\Omega \kappa\,\nabla(Su)\cdot\nabla(Sv)\,\mathrm{d}\Omega &= \int_\Omega \big(\kappa\,\underline{\underline{R}}_\theta\; S(\nabla u)\big)\cdot\big(\underline{\underline{R}}_\theta\; S(\nabla v)\big)\,\mathrm{d}\Omega\\ &= \int_\Omega \kappa\, S(\nabla u)\cdot S(\nabla v)\,\mathrm{d}\Omega\\ &= \int_\Omega \kappa(\underline{\underline{R}}_\theta^{-1}\underline{x})\;\frac{\partial u}{\partial \underline{x}}(\underline{\underline{R}}_\theta^{-1}\underline{x})\cdot\frac{\partial v}{\partial \underline{x}}(\underline{\underline{R}}_\theta^{-1}\underline{x})\,\mathrm{d}\Omega\\ &= \int_\Omega \kappa\,\nabla u\cdot\nabla v\,\mathrm{d}\Omega,\end{aligned}$$

which in addition demonstrates that S is a unitary operator on $H^1(\Omega)$. Combining all above results proves the statement (1.26). □

1.3 Cardiac model

Let us consider finally a particular case of space-time periodicity, that is periodicity in time, defined for some period $T > 0$ as

$$u(t) = u(t - T),$$

where the shift in space is simply the identity operator $S \equiv \mathrm{Id}$. We will also introduce second order derivatives in time through a full consideration of the inertia forces. To illustrate such a periodic problem, let us consider in this section a beating heart model, presented in [Caruel et al. 2014, Imperiale 2013].

1.3.1 General bio-mechanical model

Like in the tyre mechanics model above, we recall the elements of the finite strain theory. The deformation gradient, the Cauchy-Green and Green-Lagrange strain tensors respectively are

$$\underline{\underline{\mathcal{F}}} = \mathrm{Id} + \frac{\partial \underline{u}}{\partial \underline{X}}, \qquad \underline{\underline{\mathcal{C}}} = \left(\mathrm{Id} + \frac{\partial \underline{u}}{\partial \underline{X}}\right)^t \left(\mathrm{Id} + \frac{\partial \underline{u}}{\partial \underline{X}}\right), \qquad \underline{\underline{e}} = \frac{1}{2}\left(\underline{\underline{\mathcal{C}}} - \mathrm{Id}\right),$$

where the displacement field is $\underline{u} = \underline{x} - \underline{X}$, and where $\underline{x}$ and $\underline{X}$ are respectively the Euler and Lagrange coordinates. The second Piola-Kirchhoff stress tensor $\underline{\underline{\Sigma}}$ consists of the passive part $\underline{\underline{\Sigma}}_p$ (without fiber activation) and the active one-dimensional component $\sigma_{1\mathrm{D}}$, acting in the fiber direction given by the field $\underline{\tau}_{fib}$:

$$\underline{\underline{\Sigma}} = \underline{\underline{\Sigma}}_p + \underbrace{\sigma_{1\mathrm{D}}\,(\underline{\tau}_{fib}\otimes\underline{\tau}_{fib})}_{\text{active stress}}.$$

The passive stress $\underline{\underline{\Sigma}}_p$ is defined through a hyper-elastic potential W_e and a viscous pseudo-potential W_v:

$$\underline{\underline{\Sigma}}_p = \frac{\partial W_e}{\partial \underline{\underline{e}}}(\underline{\underline{e}}) + \frac{\partial W_v}{\partial \dot{\underline{\underline{e}}}}(\dot{\underline{\underline{e}}}, \underline{\underline{e}}) - p\,\underline{\underline{C}}^{-1},$$

where the Lagrange multiplier p (hydrostatic pressure) is introduced to ensure the incompressibility.

Let us denote the one-dimensional fiber-directed strain $e_{1\mathrm{D}} = \underline{\tau}_{fib} \cdot \underline{\underline{e}} \cdot \underline{\tau}_{fib}$. Following [Sainte-Marie et al. 2006, Chapelle et al. 2012, Caruel et al. 2014, Imperiale 2013], we define the active stress $\sigma_{1\mathrm{D}}$, using a Hill-Maxwell rheological model:

$$\sigma_{1\mathrm{D}} = E_s \frac{e_{1\mathrm{D}} - e_c}{(1+2e_c)^2},$$
$$\mu \dot{e}_c + \tau_c = E_s \frac{(e_{1\mathrm{D}} - e_c)(1+2e_{1\mathrm{D}})}{(1+2e_c)^3},$$

where E_s is the stiffness of the Z disks, μ is a damping parameter of the viscous component in the sarcomere, e_c is the strain in the sarcomere, and τ_c is the stress, associated to the myosin "springs" in the sarcomere, defined along with the sarcomere stiffness k_c through a time dependent relation

$$\begin{bmatrix} \dot{\tau}_c \\ \dot{k}_c \end{bmatrix} = f(\dot{e}_c, \tau_c, k_c).$$

This relation models the activation part of the sarcomere. For the sake of simplicity, we leave this relation in the general form. The reader can refer to [Chapelle et al. 2012, Caruel et al. 2014, Imperiale 2013] for the explicit form of the function $f(\dot{e}_c, \tau_c, k_c)$.

Let Ω be the heart tissue domain (Lagrangian configuration) with the internal boundary Γ_c (endocardium surface or cavity boundary), and $\underline{u} \in \mathcal{V}$, the space of all kinematically admissible displacements. Then the momentum conservation writes in variational form:

$$\int_\Omega \rho \underline{\ddot{u}}\, \underline{v}\, \mathrm{d}\Omega + \int_\Omega \underline{\underline{\mathcal{F}}}\, \underline{\underline{\Sigma}} : \frac{\partial \underline{v}}{\partial \underline{X}}\, \mathrm{d}\Omega = -\int_{\Gamma_c} P_v\, \underline{n}_c \cdot \underline{\underline{\mathcal{F}}}^{-1} \underline{v}\, \mathrm{d}\Gamma_c, \qquad \forall \underline{v} \in \mathcal{V}.$$

Here the load, applied to the internal boundary with outward unit normal vector field $\underline{n}_c$, is defined by the internal ventricular blood pressure P_v, which is also coupled to the ejected blood flow Q through the cavity valves. The state of the valves (open/close) is defined by the internal and external pressure balance. This balance equation governs the evolution of the blood flux Q entering or leaving the cavity through a constitutive law given by

$$Q = q(P_v, P_{ar}, P_{at}),$$

where along with the ventricle pressure P_v, we denote by P_{ar} and P_{at} the pressure in the artery (aorta) and in the atrium respectively. According to [Sainte-Marie et al. 2006], the regularized valve function q is given by

$$q(P_v, P_{ar}, P_{at}) = \begin{cases} K_{at}(P_v - P_{at}), & \text{if } P_v \leq P_{at}, \\ K_{iso}(P_v - P_{at}), & \text{if } P_{at} \leq P_v \leq P_{ar}, \\ K_{ar}(P_v - P_{ar}) + K_{iso}(P_{ar} - Pat), & \text{if } P_v \geq P_{ar}, \end{cases} \tag{1.27}$$

where the regularizing constants K_{at}, K_{iso} and K_{ar} must be chosen such that K_{iso} is much smaller than K_{at} and K_{ar} to ensure that the flow is negligible in isovolumic phases. On the other hand, the outflow Q is equal to the rate of change of volume:

$$Q = \int_{\Gamma_c} \underline{\underline{\mathcal{F}}}^{-1} \underline{\dot{u}} \cdot \underline{n_c} \, \mathrm{d}\Gamma_c.$$

The overall valve law reduces therefore to the scalar differential equation in time

$$C_v \dot{P}_v + \int_{\Gamma_c} \underline{\underline{\mathcal{F}}}^{-1} \underline{\dot{u}} \cdot \underline{n_c} \, \mathrm{d}\Gamma_c = q(P_v, P_{ar}, P_{at}).$$

The external circulation is defined by the Windkessel model [Westerhof et al. 2009, Imperiale 2013], which governs the time evolution of the aorta pressure:

$$\begin{aligned} C_p \dot{P}_{ar} + (P_{ar} - P_d)/R_d &= Q, \\ C_d \dot{P}_d + (P_d - P_{ar})/R_p &= (P_{vs} - P_d)/R_d, \end{aligned}$$

where coefficients C_p, R_p, C_d and R_d denote capacitances and resistances of the proximal and distal circulations, the distal pressure P_d is an additional variable, and the venous system pressure P_{vs} is a given constant.

Thus, the overall governing system writes:

$$\begin{aligned} &\int_\Omega \rho \underline{\ddot{u}} \, \underline{v} \, \mathrm{d}\Omega + \int_\Omega \underline{\underline{\mathcal{F}}} \, \underline{\underline{\Sigma}} : \frac{\partial \underline{v}}{\partial \underline{X}} \, \mathrm{d}\Omega = - \int_{\Gamma_c} P_v \, \underline{n_c} \cdot \underline{\underline{\mathcal{F}}}^{-1} \underline{v} \, \mathrm{d}\Gamma_c, \qquad \forall \underline{v} \in \mathcal{V}, \\ &\qquad \underline{\underline{\Sigma}} = \sigma_{1\mathrm{D}} \left(\underline{\tau}_{fib} \otimes \underline{\tau}_{fib} \right) + \frac{\partial W_e}{\partial \underline{\underline{e}}}(\underline{\underline{e}}) + \frac{\partial W_v}{\partial \underline{\underline{\dot{e}}}}(\underline{\underline{\dot{e}}}, \underline{\underline{e}}), \\ &\qquad \sigma_{1\mathrm{D}} = E_s \frac{e_{1\mathrm{D}} - e_c}{(1 + 2e_c)^2}, \qquad e_{1\mathrm{D}} = \underline{\tau}_{fib} \cdot \underline{\underline{e}} \cdot \underline{\tau}_{fib} \\ &\mu \dot{e}_c = E_s \frac{(e_{1\mathrm{D}} - e_c)(1 + 2e_{1\mathrm{D}})}{(1 + 2e_c)^3} - \tau_c, \qquad \begin{bmatrix} \dot{\tau}_c \\ \dot{k}_c \end{bmatrix} = f(\dot{e}_c, \tau_c, k_c), \\ &C_v \dot{P}_v + \int_{\Gamma_c} \underline{\underline{\mathcal{F}}}^{-1} \underline{\dot{u}} \cdot \underline{n_c} \, \mathrm{d}\Gamma_c = q(P_v, P_{ar}, P_{at}), \\ &C_p \dot{P}_{ar} + (P_{ar} - P_d)/R_d = q(P_v, P_{ar}, P_{at}), \\ &C_d \dot{P}_d \ + (P_d - P_{ar})/R_p = (P_{vs} - P_d)/R_d, \end{aligned} \tag{1.28}$$

where the valve function q is given by (1.27).

1.3.2 Linearized mechanical model

Let us introduce a linearized heart beating problem. We consider only mechanical part, that is the first equation of system (1.28):

$$\int_\Omega \rho\ddot{\underline{u}}\cdot\underline{v}\,\mathrm{d}\Omega+\int_\Omega \underline{\underline{\mathcal{F}}}\,\underline{\underline{\Sigma}}\,(\dot{\underline{u}},\underline{u}):\frac{\partial\underline{v}}{\partial\underline{X}}\,\mathrm{d}\Omega=\mathcal{P}^{ext},\qquad\forall\underline{v}\in\mathcal{V},\tag{1.29}$$

where $\mathcal{P}^{ext}$ stands for the external forces [Moireau et al. 2008, 2009, Moireau 2009]. The system's state is only described by the displacement field $u\in\mathcal{V}$, where $\mathcal{V}$ denotes the space of all kinematically admissible displacements. We are looking for the time-periodic solution $u\in\mathcal{V}$ defined by the time-periodicity condition with period T

$$\underline{u}(t)=\underline{u}(t-T)\qquad\forall t\in\mathbb{R}.$$

Let us consider an isotropic viscoelastic material, using Saint-Venant-Kirchhoff model with proportional damping. Then, under the small strain assumption, we have

$$\underline{\underline{\mathcal{F}}}\,\underline{\underline{\Sigma}}\approx\underline{\underline{\sigma}}=\lambda\,\mathrm{tr}(\eta\dot{\underline{\underline{e}}}+\underline{\underline{e}})\,\mathrm{Id}+2\mu(\eta\dot{\underline{\underline{e}}}+\underline{\underline{e}}),$$

where λ and μ are the Lamé coefficients, $\underline{\underline{\sigma}}$ denotes the Cauchy stress, and the linearized Green-Lagrange strain tensor is

$$\underline{\underline{e}}=\frac{1}{2}\left(\underline{\underline{\mathcal{C}}}-\mathrm{Id}\right)\approx\frac{1}{2}\left(\nabla\underline{u}+(\nabla\underline{u})^t\right)=\nabla_s\underline{u}.$$

Let us introduce the fourth-order isotropic elasticity tensor $\underline{\underline{\underline{\underline{K}}}}$, defined for any second-order tensor $\underline{\underline{t}}$ by $\underline{\underline{\underline{\underline{K}}}}\,\underline{\underline{t}}=\lambda\,\mathrm{tr}(\underline{\underline{t}})\,\mathrm{Id}+2\mu\,\underline{\underline{t}}$. Then the problem writes in variational form as

Find $\underline{u}:\mathbb{R}\mapsto\mathcal{V}$, such that $\forall\underline{v}\in\mathcal{V}$ and $\forall t\in\mathbb{R}$

$$\int_\Omega\rho\ddot{\underline{u}}\cdot\underline{v}\,\mathrm{d}\Omega+\int_\Omega\underline{\underline{\underline{\underline{K}}}}\,(\eta\nabla_s\dot{\underline{u}}+\nabla_s\underline{u}):\nabla\underline{v}\,\mathrm{d}\Omega=\mathcal{P}^{ext},$$
$$\underline{u}(t)=\underline{u}(t-T).\tag{1.30}$$

CHAPTER 2

Newton-Krylov method for computing the space-time periodic solution of non-linear problems

Summary

2.1 Introduction

In industrial applications, in order to avoid the inversion of very large matrices, time periodic states are often computed as the asymptotic limit solution of an initial value boundary value problem with arbitrarily chosen initial data. This kind of problems can be faced, for instance, in the cardiac contractions modeling. Another example concerns the steady rolling of a viscoelastic tyre [Le Tallec and Rahier 1994, Govindjee et al. 2014] with a periodic sculpture. In this case, the steady state satisfies a "rolling" periodicity condition (cyclic steady state [Govindjee et al. 2014]), including shifts both in time and space: the state $\underline{u}(t, \underline{X})$ at any point $\underline{X}$ is the same that at the corresponding point observed at the next sculpture one time period T ago

$$\underline{u}(t, \underline{X}) = \underline{u}(t - T, \underline{\underline{R}}_{\omega T} \underline{X}).$$

Above, $\underline{\underline{R}}_{\omega T}$ denotes the rotation of angle ωT, and ω is the rotation speed. So, the angle ωT is the size of one sculpture.

In this chapter, we consider the Newton-Krylov method [Chan and Jackson 1984, Telichevesky et al. 1995, Knoll and Keyes 2004], considered as a shooting method for calculating the space-time periodic solution (steady cyclic state) of evolution problems [Govindjee et al. 2014, Brandstetter and Govindjee 2017]. The main idea consists in considering the periodicity condition as an equation for the unknown initial state, which would lead to the periodic solution. Indeed, once we have found the true initial state, the periodic solution is obtained solving the associated initial value problem during only one time period. The equation on the unknown initial state includes an evolution function, requiring to solve the non-linear initial value problem during one time period. The periodicity condition, comparing the resulting state after one time period to the initial one, provides a non-linear equation to solve. So, it is natural to solve this non-linear equation by a classical Newton-Raphson technique. The most challenging part is to construct the global Jacobian. We propose a way to construct it using the tangent matrices of the evolution problem, calculated and stored during each time step of the forward time integration of the problem. Then, the global Jacobian matrix is never assembled in practice, but defined implicitly by its action during multiplication operation. With that in hand, one of the matrix-free Krylov methods [Saad 2003, Balay et al. 2016] (we use GMRES [Saad and Schultz 1986]) can be applied to solve the linear system, which appears at each global Newton step. This leads to the Jacobian-free Newton-Krylov method [Knoll and Keyes 2004]. Application of this technique, as a shooting method searching for the initial state of the space-time periodic solution (cyclic steady state), to a steady rolling threaded wheel is already proposed and discussed in [Govindjee et al. 2014]. In our work, we propose another point of view on this method, namely, to consider it as a correction after each time period of a standard rolling solution. This modified algorithm has been implemented in Michelin industrial code, applied to a full 3D tyre model and compared to the standard asymptotic convergence.

The organization of the chapter is as follows. The classical Newton-Krylov algorithm is described in Section 2.3. It looks for the "correct" initial state, which provides the periodic solution. On each global Newton iteration, given an initial state (starting with an arbitrary guess), it solves the non-linear initial value problem during the first period, computing the periodicity error, which is used as right hand side of the Newton linear system to correct the initial state for the next step. In this formulation, Newton algorithm is reminiscent to shooting methods.

Section 2.6 is dedicated to an alternative point of view of the same Newton algorithm, where a change of variable leads to the convenient way to implement the method. The working variable will now be the initial state of the current time period instead of the initial state of the first period. In this way, the method can be easily derived from the classic time evolution by adding the correction step in the end of each period. Therefore, it can be compared with the methods, which look for the periodic state as an asymptotic limit of the solution, in particular those accelerating convergence to the limit state, like Delayed Feedback Control method (see the next chapter). Indeed, it may be considered as an observer-controller process, where correction, performed in the end of each period, is based on the observation during this period.

Sections 2.8 and 2.9 are devoted to implementation of the proposed technique, applied to the model problems, described in Chapter 1. First, the method has been tested on the linear 2D heat problem from Section 1.2, where a planar disk is heated with a source periodically moving along a circular path. As expected, the method only requires one Newton iteration to converge, but does need several Krylov iterations to solve the linear system. Finally, the method has been applied to our main model problem, that is the rolling 3D tyre in presence of stick-slip frictional contact with the soil (Section 1.1.1). This problem is three dimensional and non-linear. The Newton-Krylov method has been implemented along with the non-modified time evolution, in order to compare the rates of convergence to the limit space-time periodic solution. We study first a simplified model using MatLab R2016b. Then, we present results of implementation of the Newton-Krylov shooting method into the Michelin industrial code.

2.2 Abstract problem formulation

2.2.1 Time continuous problem

Let $\mathcal{H}$ be a Hilbert space and let us consider a nonlinear evolution problem (2.1) on $u : \mathbb{R} \to \mathcal{H}$ with the space-time periodicity condition (2.2):

$$F(t, u(t), \dot{u}(t)) = 0 \quad \forall t \in \mathbb{R}, \tag{2.1}$$

$$u(t + T) = Su(t), \tag{2.2}$$

where $\dot{u} = \partial_t u$ denotes the time derivative of the state variable u, $T > 0$ is the time period, and the space shift S is a unitary linear operator on $\mathcal{H}$ (isometry).

A typical example of such problem is the rolling tyre model presented in Section 1.1.1. In this case, the function F is given by (1.11), $\mathcal{H} = \{ \underline{v} \in H^1(\Omega)^3 \mid \underline{v}|_{\Gamma_0} = 0\}$, and the space shift operator S is defined through rotation of the coordinate:

$$\forall u \in \mathcal{H} \qquad S : u(\underline{X}) \mapsto u(\underline{\underline{R}}_{\omega T}\underline{X})$$

with $\underline{\underline{R}}_{\omega T}$ rotation of angle ωT.

It is obvious in fact to see that all examples of Chapter 1 enter in the present framework (2.1)-(2.2), the simplest situation being the cardiac model where the space shift is the identity.

Back to the abstract formulation (2.1)-(2.2), let us denote by $\varphi(t; t_*, u_*)$ solution at time t (integral line or trajectory) of the differential equation (2.1), passing through the point (t_*, u_*). Then, we can define the monodromy operator:

$$\Phi_t : u \mapsto \varphi(t + T; t, u)$$

which represents the solution after one period of the initial value problem starting from the point (t, u). Under this notation, our problem written with the space-time periodicity condition (2.2) takes the form

$$\Phi_t(u(t)) = Su(t).$$

Thus, the space-time periodic solution of (2.1)-(2.2) is given by

$$u(t) = \varphi(t; 0, u_0),$$

where the initial data u_0 is defined as the solution to the space-time periodicity equation

$$\Phi_0(u_0) - Su_0 = 0. \tag{2.3}$$

Indeed, if we know the "true" initial data (i.e. corresponding to the periodic solution), then the solution of (2.1)-(2.2) is obtained for the first period by solving

$$\begin{aligned} &F(t, u, \dot{u}) = 0, \quad t \in [0, T] \\ &u(0) = u_0 \end{aligned} \tag{2.4}$$

and for any further period it is given by (2.2), provided that we have the space-time shift invariance property

$$\forall t \in \mathbb{R},\ \forall u, w \in \mathcal{H}: \quad F(t+T, Su, Sw) = 0, \quad \text{when} \quad F(t,u,w) = 0. \tag{2.5}$$

This space-time shift invariance has been proved to hold in Lemmas 1-3 for all systems studied in Chapter 1. We will take this assumption (2.5) as a general assumption to be satisfied by the abstract problem (2.1) under study.

So, to find the solution of the problem (2.1)-(2.2) we have to solve the equation (2.3) on the unknown u_0, which is simply the value of $u(t)$ at the point $t = 0$. As for the existence of a solution of (2.3), it has to be checked on a case by case basis. The theoretical framework of Chapter 3 introduces a general class of linear problems for which existence and stability of periodic solutions can be proved. For nonlinear problems, existence and uniqueness results can be proved when $S^{-1}\Phi_0$ is contracting by a simple application of the fixed point theorem.

2.2.2 Time discrete problem

Time discretization of evolution problem (2.1) consists in introducing a sequence of calculation times $t_0 < t_i < t_m = t_0 + T$ with time steps $\Delta t_i = t_{i+1} - t_i$, and in replacing the implicit time evolution (2.1) by the induction [Quarteroni et al. 2010]

$$u_{i+1} = u_i + \Delta t_i\, \phi_{\Delta t}(t_i, u_i, \Delta t_i; F),$$

where the increment $\phi_{\Delta t}$ is defined by the time scheme. For an implicit Euler scheme, the increment $\phi_{\Delta t}$ is solution of the non-linear equation

$$F(t_i + \Delta t_i, u_i + \Delta t_i\, \phi_{\Delta t}, \phi_{\Delta t}) = 0. \tag{2.6}$$

After such a discretization, the non-linear evolution problem (2.1) with space-time periodicity condition (2.2) becomes

$$\begin{aligned} u_{i+1} &= u_i + \Delta t_i\, \phi_{\Delta t}(t_i, u_i, \Delta t_i; F), \qquad i = 0 \dots m-1 \\ u_m &= S u_0. \end{aligned} \tag{2.7}$$

If we introduce the discrete monodromy operator operator

$$\Phi_0^{\Delta t} : u_0 \mapsto u_m \quad \textit{obtained by solving (2.7) from } i = 0 \textit{ to } i = m-1,$$

the time discrete equivalent of (2.3) becomes

$$\Phi_0^{\Delta t}(u_0) - S u_0 = 0. \tag{2.8}$$

In what follows, we will consider the present time discrete problem to be discretized in space too, with solution living in the finite space $\mathbb{R}^d$. In this case, the matrix, representing the space shift S, depends on the mesh and does not change

until the mesh is modified. For a general mesh, the space shift is defined through interpolation. It is strictly sparse and contains no more than N_{nodes} non-zeros by line, where N_{nodes} denotes the maximal number of nodes by element. If the mesh is periodic with respect to the sculpture size, the space shift is simply a permutation matrix.

2.3 Newton shooting technique

We are looking for the initial data u_0 solution of the non-linear equation (2.3). This is a nonlinear problem for the unknown u_0. We apply the Newton-Raphson method to solve it, which leads to the iterative correction process:

$$u_0^{n+1} = u_0^n + \delta u_0^{n+1}$$

with the correction δu_0^n being solution of the linear problem

$$(\mathrm{D}\Phi_0(u_0^n) - S) \underbrace{(u_0^{n+1} - u_0^n)}_{=\delta u_0^{n+1}} = - \underbrace{\Big(\Phi_0(u_0^n) - S u_0^n\Big)}_{=\varepsilon_{per}^n}$$

where $\mathrm{D}\Phi_0$ denotes the gradient of Φ_0 with respect to the initial data u_0. On the right part we have the periodicity error (denoted by ε_{per}^n) calculated during the n-th iteration. Thus the correction δu_0^{n+1} is defined by solving

$$(S - \mathrm{D}\Phi_0(u_0^n))\, \delta u_0^{n+1} = \varepsilon_{per}^n, \tag{2.9}$$

which leads to the iteration process:

$$u_0^{n+1} = u_0^n + (S - \mathrm{D}\Phi_0(u_0^n))^{-1} \Big(\Phi_0(u_0^n) - S u_0^n\Big). \tag{2.10}$$

The key question here is how to compute $\mathrm{D}\Phi_0$, the gradient of the monodromy operator (which we call the tangent monodromy matrix). An approach is proposed and discussed in the following section.

Note that, during each Newton iteration n, computing the periodicity error ε_{per}^n requires to perform all the evolution from $t = 0$ to $t = T$, i.e. to solve the initial value problem (2.4) with initial value u_0^n, in order to obtain $\Phi_0(u_0^n)$. So, the residual computation for the "global" Newton loop, solving (2.3) or its time approximation (2.8), includes solving the nonlinear evolution problem (2.1), or respectively (2.7), with "local" Newton loops at each time step during one period.

This technique can be also considered as a kind of shooting method. Indeed, starting with an arbitrary left boundary value, we go through one period evolution to obtain the right boundary value and use it for correction of the left boundary value and so on.

2.4 Approximation of the Jacobian

For $u(t)$, solution to (2.1), it holds

$$u(t+T) = \Phi_t(u(t)).$$

Hence, its variation satisfies

$$\delta u(t+T) = \mathrm{D}\Phi_t(u(t))\ \delta u(t). \tag{2.11}$$

Meanwhile, from the evolution equation

$$F(t, u, \dot{u}) = 0,$$

we can obtain its linearized form governing the evolution of any initial perturbation of the solution:

$$\mathrm{D}_{\dot{\mathrm{u}}}F\ \dot{\delta u} + \mathrm{D}_{\mathrm{u}}F\ \delta u = 0, \tag{2.12}$$

whose integration from t to $t+T$ with initial value $\delta u(t)$ defines the tangent monodromy operator in (2.11). Similarly, the time discrete equivalent of (2.12) is obtained from (2.7):

$$\delta u_{i+1} = \underbrace{\left(\mathrm{Id} + \Delta t_i \frac{\partial \phi_{\Delta t}}{\partial u_i}\right)}_{\mathcal{W}_i} \delta u_i, \tag{2.13}$$

where we introduce the forward operator $\mathcal{W}_i = \mathrm{Id} + \Delta t_i \frac{\partial \phi_{\Delta t}}{\partial u_i}$. In the case of the implicit Euler time scheme, the operator $\frac{\partial \phi_{\Delta t}}{\partial u_i}$ is defined by linearization of (2.6):

$$\frac{\partial \phi_{\Delta t}}{\partial u_i} = -\left(B_i + \Delta t_i \cdot A_i\right)^{-1} A_i,$$

where

$$A_i = \mathrm{D}_{\mathrm{u}}F(t_{i+1}, u_{i+1}, \frac{u_{i+1}-u_i}{\Delta t_i}), \qquad B_i = \mathrm{D}_{\dot{\mathrm{u}}}F(t_{i+1}, u_{i+1}, \frac{u_{i+1}-u_i}{\Delta t_i}). \tag{2.14}$$

Then, the forward operator is

$$\mathcal{W}_i = \mathrm{Id} + \Delta t_i \frac{\partial \phi_{\Delta t}}{\partial u_i} = \left(B_i + \Delta t_i \cdot A_i\right)^{-1} B_i. \tag{2.15}$$

Note that if A_i and B_i are positive definite, $\mathcal{W}_i$ is contracting. For a general time scheme, by induction from (2.13) it yields

$$\delta u_m = \mathcal{W}_{m-1}\mathcal{W}_{m-2}\ldots\mathcal{W}_0\ \delta u_0.$$

That is, after time discretization, the tangent monodromy operator is a superposition of the forward operators:

$$\begin{aligned} \mathrm{D}\Phi_0^{\Delta t} &= \mathcal{W}_{m-1} \circ \mathcal{W}_{m-2} \circ \ldots \circ \mathcal{W}_0 \\ &= \prod_{i=0}^{m-1} \mathcal{W}_i \\ &= \prod_{i=0}^{m-1} \left(\mathrm{Id} + \Delta t_i \, \frac{\partial \phi_{\Delta t}}{\partial u_i} \right), \end{aligned} \tag{2.16}$$

where the product is non-commutative with the factors ordered from right to left. For example, for the implicit Euler scheme, it writes

$$\mathrm{D}\Phi_0^{\Delta t} = \prod_{i=0}^{m-1} \left\{ \left(B_i + \Delta t_i \cdot A_i \right)^{-1} B_i \right\}. \tag{2.17}$$

On the n-th global Newton step, all tangent matrices A_i and B_i, necessary to approach $\mathrm{D}\Phi_0^{\Delta t}$, have been already obtained during the computation of the periodicity error ε_{per}^n, where $\Phi_0^{\Delta t}(u_0)$ is computed by numerical integration of the initial value problem (2.4). More precisely, for each i, A_i and B_i are parts of the Jacobian at the last local Newton iteration solving the i-th time step. In fact, for an implicit Euler scheme, we can store directly the local Jacobian $B_i + \Delta t \cdot A_i$ (or its matrix factorization) and its part B_i to compose the forward operator $\mathcal{W}_i = \left(B_i + \Delta t \cdot A_i \right)^{-1} B_i$.

Matrix associated to $\mathrm{D}\Phi_0$ is not assembled explicitly, which is quite expensive numerically, but is defined implicitly by its matrix-vector multiplication:

$$\forall u \quad \mathrm{D}\Phi_0^{\Delta t} \, u = \mathcal{W}_{m-1} \cdot \mathcal{W}_{m-2} \cdot \ldots \cdot \mathcal{W}_1 \cdot \mathcal{W}_0 \, u.$$

Then the matrix-free GMRES (see the following section) is used to solve the global Newton linear system with matrix $\mathrm{D}\Phi_0^{\Delta t}$.

If during the local Newton resolution of a time step any matrix factorization of the associated local Jacobian $B_i + \Delta t \, A_i$ (ex., LU or Cholesky decomposition) is used, it can be stored directly along with the Jacobian itself. Though this will require more memory space, this can strongly decrease the computational time, since each forward operator $\mathcal{W}_i$ requires to solve a linear system with an already once-factorized matrix. So, each stored factorization will be used multiple times during Krylov iterations.

2.5 Matrix-free Krylov technique: GMRES method

Let us now consider in details the solution of the system (2.9), appearing during the n-th Newton step to compute the unknown increment δu_0^n by solving

$$\left(S - \mathrm{D}\Phi_0^{\Delta t}(u_0^n)\right) \delta u_0^{n+1} = \varepsilon_{per}^n, \tag{2.18}$$

where the periodicity error ε_{per}^n is already computed and the tangent monodromy matrix $\mathrm{D}\Phi_0^{\Delta t}$ is not assembled but is defined through its multiplication operation, as discussed in the previous section. In particular, for the implicit Euler time scheme $\mathrm{D}\Phi_0^{\Delta t}$ is defined by (2.17).

We solve the system (2.18) using the Generalized Minimal Residual method (GMRES) [Saad and Schultz 1986]. As any Krylov subspaces method, it does not require to know the system's matrix explicitly, but only needs computing the matrix-vector product.

Let us rewrite (2.18) in the form

$$Ax = b$$

with the matrix $A = \left(S - \mathrm{D}\Phi_0^{\Delta t}(u_0^n)\right)$, the right hand side $b = \varepsilon_{per}^n$, and the unknown $x = \delta u_0^{n+1}$. We also denote by d the dimension of x. The idea of GMRES algorithm consists in approximation of solution x by vector x_k, the element of the Krylov subspace

$$\mathcal{K}_k = \mathrm{span}\{b, Ab, \ldots, A^{k-1}b\}, \qquad k \in \mathbb{N},\ k \le d,$$

which minimizes the norm of the residual

$$r_k = Ax_k - b.$$

Instead of the basis $b, Ab, \ldots, A^{k-1}b$, the algorithm computes an orthonormal basis $\{q_i\}_{i=1}^k$ in $\mathcal{K}_k$, using the Arnoldi iteration method. Let $q_1 = b/\|b\|$. Given $\{q\}_{i=1}^k$, the Arnoldi iteration uses the stabilized Gram-Schmidt orthogonalization to construct q_{k+1}:

$$\begin{aligned}
&q_{k+1}^{(0)} = Aq_k,\\
&\text{for } i = 1 \ldots k\\
&\qquad h_{i,k} = \langle q_{k+1}^{(i-1)},\ q_i\rangle,\\
&\qquad q_{k+1}^{(i)} = q_{k+1}^{(i-1)} - h_{i,k}\, q_i,\\
&h_{k+1,k} = \|q_{k+1}^{(k)}\|,\\
&q_{k+1} = q_{k+1}^{(k)}/h_{k+1,k}.
\end{aligned} \tag{2.19}$$

So, every such Arnoldi iteration requires to compute one matrix-vector product Aq_k. However, for $A = (S - \mathrm{D}\Phi_0)$ this operation, according to (2.16), is defined by

$$Aq_k = Sq_k - \mathcal{W}_{m-1} \cdot \mathcal{W}_{m-2} \cdot \ldots \cdot \mathcal{W}_1 \cdot \mathcal{W}_0 \, q_k, \tag{2.20}$$

where $m = T/\Delta t$ is the number of time steps per cycle T. It thus requires m consecutive applications of the forward operators $\mathcal{W}_i$ and one space shift Sq_k. Moreover, to apply a forward operators $\mathcal{W}_i$ one has to solve the associated linear system, which however has been already solved once with a different right hand side, while computing ε^n_{per}. That is, the corresponding factorization (LU or Cholesky) is already computed and stored. In particular, for the implicit Euler scheme the forward operator is given by (2.15) with the local tangent matrices A_i and B_i defined in (2.14). So, let L_i and U_i be the stored LU decomposition of the local Jacobian

$$B_i + \Delta t_i \cdot A_i = L_i \, U_i, \qquad i = 1..m.$$

Then for any vector v the product Av is computed by the following algorithm:

$$\begin{aligned} &v_0 = v, \\ &\text{for } i = 1 \ldots m \\ &\qquad v_i = U_i^{-1} L_i^{-1} B_i v_{i-1}, \\ &Av = Sv - v_m. \end{aligned} \tag{2.21}$$

Altogether, computing of Aq_k requires to execute successively m matrix-vector multiplication operation, m linear system resolutions with known factorizations and one space shift operation.

Let us denote by Q_k the $d \times k$ matrix with columns q_i, $i = 1..k$. Then, any vector x_k of size d from the Krylov subspace $\mathcal{K}_k$ can be represented in the basis Q_k as

$$x_k = Q_k y_k,$$

where the vector y_k of size k represents the coordinates of x_k in this basis. Finally, the linear least squares method is used to find y_k minimizing the residual norm $\|r_k\| = \|Ax_k - b\|$, which leads to the $k \times k$ linear system

$$\left(H_k^t H_k\right) y_k = \|b\| h_1, \tag{2.22}$$

where H_k is an upper Hessenberg matrix of the coefficients $h_{i,j}$ from the Arnoldi algorithm (2.19), and h_1 is its transposed first row.

To summarize, for each global Newton step we solve the linear system (2.9) using the GMRES method, whose iteration k is defined as follows:

1. Given Q_k, construct q_{k+1} using the Arnoldi iteration (2.19). This requires to compute one matrix-vector product Aq_k, which is defined by (2.20). In particular, in case of implicit Euler time scheme, Aq_k is computed by (2.21).

2. Solve the least squares problem (2.22) to find y_k, where the upper Hessenberg matrix H_k was constructed during the Arnoldi iteration.

3. Repeat, increasing k, if the residual norm $\|r_k\|$ is not small enough, otherwise compute $x_k = Q_k y_k$, the Krylov approximation of solution of (2.9).

Let us present now some convergence results for the discussed algorithm. In the following proposition, we denote by $\langle \cdot, \cdot \rangle$ the inner product (typically ℓ_2), same as in the Arnoldi process (2.19), and by $\|\cdot\|$ the associated norm.

Proposition 2. *Let the tangent monodromy operator* $\mathrm{D}\Phi_0$ *be strictly contracting, i.e. there exists* $\gamma \in (0, 1)$ *such that* $\|\mathrm{D}\Phi_0 v\| < \gamma \|v\|$ *for any non-zero vector* v. *Then the above GMRES algorithm, solving (2.18) and using the left or right preconditioner* S^{-1}, *converges linearly at worst in* $\mathcal{O}(\sqrt{\gamma})$.

Proof. According to [Saad and Schultz 1986], the GMRES method for the preconditioned system $Ax = b$ converges if the operator A is positive real, i.e. if there exists $c > 0$ such that $\langle Av,\ v\rangle > c\|v\|^2$ for any non-zero vector v. Moreover, it holds the estimation for the residual $r_k = Ax_k - b$

$$\|r_k\| \leq \left(1 - \frac{\alpha^2}{\sigma}\right)^{k/2} \|r_0\|,$$

where α is the minimal eigenvalue of $\frac{1}{2}(A + A^t)$ and σ is the maximal eigenvalue of $A^t A$. That is,

$$\alpha = \inf_{v \neq 0} \frac{\langle \frac{1}{2}(A + A^t)v,\ v\rangle}{\|v\|^2} = \inf_{v \neq 0} \frac{\langle Av,\ v\rangle}{\|v\|^2},$$
$$\sigma = \sup_{v \neq 0} \frac{\langle A^t Av,\ v\rangle}{\|v\|^2} = \sup_{v \neq 0} \frac{\|Av\|^2}{\|v\|^2}.$$

In our case, the preconditioned operator is $A_r = AS^{-1} = \mathrm{Id} - \mathrm{D}\Phi_0\, S^{-1}$ or $A_\ell = S^{-1}A = \mathrm{Id} - S^{-1}\,\mathrm{D}\Phi_0$. We use successively the Cauchy-Schwartz inequality and that $\mathrm{D}\Phi_0$ is strictly contracting and S is unitary, to obtain for any non-zero vector v

$$|\langle \mathrm{D}\Phi_0\, S^{-1}v,\ v\rangle| \leq \|\mathrm{D}\Phi_0 S^{-1}v\| \cdot \|v\| < \gamma \|S^{-1}v\| \cdot \|v\| = \gamma \|v\|^2,$$

or equivalently

$$|\langle S^{-1}\,\mathrm{D}\Phi_0 v,\ v\rangle| = \langle \mathrm{D}\Phi_0 v,\ Sv\rangle \leq \|\mathrm{D}\Phi_0\, v\| \cdot \|Sv\| < \gamma \|v\|^2.$$

Hence follows the positiveness of the preconditioned operators A_r:

$$\langle A_r v,\ v\rangle = \langle v,\ v\rangle - \langle \mathrm{D}\Phi_0\, S^{-1}v,\ v\rangle > (1 - \gamma)\|v\|^2.$$

From the other side, we can estimate

$$\begin{aligned}\|A_r v\|^2 &= \|v\|^2 - 2\langle \mathrm{D}\Phi_0\, S^{-1} v,\ v\rangle + \|\mathrm{D}\Phi_0\, S^{-1} v\|^2 \\ &\le \|v\|^2 + 2\,|\langle \mathrm{D}\Phi_0\, S^{-1} v,\ v\rangle| + \|\mathrm{D}\Phi_0\, S^{-1} v\|^2 \\ &< (1 + 2\gamma + \gamma^2)\|v\|^2 = (1+\gamma)^2\|v\|^2.\end{aligned}$$

Similarly, we can obtain the same results for A_ℓ:

$$\langle A_\ell v,\ v\rangle > (1-\gamma)\|v\|^2, \qquad \|A_\ell v\|^2 < (1+\gamma)^2\|v\|^2.$$

Thus,

$$\begin{aligned}\alpha &= \inf_{v\neq 0} \frac{\langle A_{r,\ell}\, v,\ v\rangle}{\|v\|^2} > 1-\gamma, \\ \sigma &= \sup_{v\neq 0} \frac{\|A_{r,\ell}\, v\|^2}{\|v\|^2} < (1+\gamma)^2,\end{aligned}$$

and the residual estimation becomes

$$\begin{aligned}\|r_k\| &\le \left(1 - \frac{\alpha^2}{\sigma}\right)^{k/2} \|r_0\| \\ &< \left(1 - \left(\frac{1-\gamma}{1+\gamma}\right)^2\right)^{k/2} \|r_0\| \\ &= \left(\frac{2\sqrt{\gamma}}{1+\gamma}\right)^k \|r_0\|,\end{aligned}$$

where $\frac{2\sqrt{\gamma}}{1+\gamma} \in (\gamma,\, 1)$, when $\gamma \in (0,\, 1)$. □

Remark 2. *Note that we need to use a preconditioner S^{-1} to ensure the convergence of the algorithm.*

2.6 Alternative realization

In the classical Newton algorithm discussed above, at each Newton step we modify the global initial state at time $t = 0$. However, sometimes it can be more convenient to work at each Newton step on the initial state of the current time period, i.e. at time $t = nT$, where n is the number of the current Newton step (which is also the number of the current time period). To do this, we change the variable in the Newton algorithm, introducing a new variable $\hat{u}^n$, defined by

$$\hat{u}^n = S^n u_0^n, \quad n \in \mathbb{N}, \tag{2.23}$$

which can be considered as an approximation at the n-th Newton step of $u(nT)$, solution at time nT obtained from the space-time periodicity condition. This

change of variable can be interpreted as a non-linear preconditioner. Then, the Newton algorithm can be rewritten as

$$\begin{aligned}\hat{u}^{n+1} &= S^{n+1}u_0^{n+1} = S^{n+1}(u_0^n + \delta u_0^{n+1}) \\ &= S\left(S^n u_0^n\right) + S^{n+1}\delta u_0^{n+1} \\ &= S\hat{u}^n + S^{n+1}\delta u_0^{n+1},\end{aligned} \tag{2.24}$$

where δu_0^{n+1} is defined by (2.9):

$$\delta u_0^{n+1} = \left(S - \mathrm{D}\Phi_0(u_0^n)\right)^{-1} \varepsilon_{per}^n \tag{2.25}$$

with the periodicity error

$$\varepsilon_{per}^n = \Phi_0(u_0^n) - Su_0^n.$$

We now assume that the function $F(t, u, \dot{u})$, defining the implicit form of the evolution law, is invariant under the action of the space-time shift in the sense that for any u and w the assumption (2.5) is true, that is

$$F(t+T, Su, Sw) = 0, \quad \text{when} \quad F(t, u, w) = 0.$$

Then, Φ_t "commutes" with S in the sense that for any u

$$S\Phi_t(u) = \Phi_{t+T}(Su). \tag{2.26}$$

This assumption is satisfied in the space-time periodic problems of Chapter 1 (see Lemmas 1-3).

Thus, we obtain from (2.26) by induction for any u

$$\begin{aligned}S^n\Phi_0(u) &= S^{n-1}\left(S\Phi_0(u)\right) \\ &= S^{n-1}\Phi_T(Su) \\ &= S^{n-2}\Phi_{2T}(S^2u) \\ &= \Phi_{nT}\left(S^n u\right).\end{aligned}$$

Hence, substituting u_0^n, we get

$$S^n\Phi_0(u_0^n) = \Phi_{nT}\left(\hat{u}^n\right), \tag{2.27}$$

where $\hat{u}^n$ is given by (2.23). Moreover, differentiation of (2.26) with respect to u gives for the tangent operator

$$S^n\,\mathrm{D}\Phi_0(u_0^n) = \mathrm{D}\Phi_{nT}\left(\hat{u}^n\right)S^n.$$

Applying this "commutation" identity in (2.25), we develop the last term in (2.24):

$$\begin{aligned}S^{n+1}\delta u_0^{n+1} &= S^{n+1}\left(S - \mathrm{D}\Phi_0(u_0^n)\right)^{-1}\varepsilon_{per}^n \\ &= \left(S^{-n} - \mathrm{D}\Phi_0(u_0^n)S^{-n-1}\right)^{-1}\varepsilon_{per}^n \\ &= \left(S^{-n} - S^{-n}\,\mathrm{D}\Phi_{nT}(\hat{u}^n)S^{-1}\right)^{-1}\varepsilon_{per}^n \\ &= \left(\mathrm{Id} - \mathrm{D}\Phi_{nT}(\hat{u}^n)S^{-1}\right)^{-1}S^n\varepsilon_{per}^n,\end{aligned} \tag{2.28}$$

where $S^n\varepsilon^n_{per}$ can be expressed in terms of $\hat{u}^n$ using (2.27):

$$\begin{aligned} S^n\varepsilon^n_{per} &= S^n\Big(\Phi_0(u^n_0) - Su^n_0\Big) \\ &= \underbrace{\Phi_{nT}\left(\hat{u}^n\right) - S\hat{u}^n}_{=\hat{\varepsilon}^n_{per}}. \end{aligned} \tag{2.29}$$

Here we introduce the current periodicity error $\hat{\varepsilon}^n_{per} = \Phi_{nT}\left(\hat{u}^n\right) - S\hat{u}^n$. Thus, from (2.24), (2.28) and (2.29), we can rewrite the previously discussed classical Newton algorithm as an iterative method for computing $\hat{u}^{n+1}$ as

$$\hat{u}^{n+1} = S\hat{u}^n + \Big(\mathrm{Id} - \mathrm{D}\Phi_{nT}(\hat{u}^n)\, S^{-1}\Big)^{-1} \hat{\varepsilon}^n_{per}$$

from the current periodicity error

$$\hat{\varepsilon}^n_{per} = \Phi_{nT}(\hat{u}^n) - S\hat{u}^n.$$

This equivalently writes:

$$\hat{u}^{n+1} = \Phi_{nT}(\hat{u}^n) + \delta\hat{u}^{n+1},$$

with the correction $\delta\hat{u}^{n+1}$ defined by

$$\delta\hat{u}^{n+1} = -\hat{\varepsilon}^n_{per} + \Big(\mathrm{Id} - \mathrm{D}\Phi_{nT}(\hat{u}^n)\, S^{-1}\Big)^{-1} \hat{\varepsilon}^n_{per}. \tag{2.30}$$

Recall that $\hat{u}^n$ is supposed to approximate $u(nT)$. So, while the classical shooting Newton-Krylov algorithm (2.10) computes the initial state of the first cycle $[0, T]$, the present alternative way to implement the same algorithm proposes to compute the initial state of the n-th cycle $[(n-1)T, nT]$. From the other point of view, it modifies the standard asymptotic method (where the cyclic steady state is computed as the asymptotic limit solution) by introducing the correction (2.30) of the transient solution after each cycle, equivalent to a global Newton iteration. Such a correction provides discontinuities of the transient solution, which "jumps" after each cycle to approach the desired space-time periodic state. Correction term can be also considered as a controller of the system, based on the observation during the last cycle, where the periodicity error plays role of the observer.

Matrix-free Krylov algorithm. To compute the increment (2.30), one has to solve the linear system

$$Ax = b \tag{2.31}$$

with $A = \mathrm{Id} - \mathrm{D}\Phi_{nT}(\hat{u}^n)\, S^{-1}$ and $b = \hat{\varepsilon}^n_{per}$, which is precisely the preconditioned version of (2.18), discussed in Proposition 2. Again, we solve it using the matrix-free GMRES method, discussed in Section 2.5. Here, the matrix-vector product Av is defined for any vector v by

$$Av = v - \mathcal{W}_{m-1} \cdot \mathcal{W}_{m-2} \cdot \ldots \cdot \mathcal{W}_1 \cdot \mathcal{W}_0\,(S^{-1}v),$$

where $m = T/\Delta t$ is the number of time steps per period T, $\mathcal{W}_i$ are the local forward operators during the cycle n, and S is the space shift. For example, in case of the implicit Euler scheme, where the forward operator is given by (2.15) with the local tangent matrices A_i and B_i defined in (2.14), the product Av for any vector v is computed by the following algorithm:

$$\begin{aligned} &v_0 = S^{-1}v, \\ &\text{for } i = 1 \dots m \\ &\qquad v_i = U_i^{-1} L_i^{-1} B_i v_{i-1}, \\ &Av = v - v_m. \end{aligned} \tag{2.32}$$

Above, the matrices L_i and U_i stand for the known LU decomposition of the local Jacobian $(B_i + \Delta t_i \cdot A_i) = L_i U_i,\ \ i = 1..m$.

Proposition 3. *Let the tangent monodromy operator $\mathrm{D}\Phi_{nT}$ be strictly contracting, i.e. there exists $\gamma \in (0,\, 1)$ such that $\|\mathrm{D}\Phi_{nT}\, v\| < \gamma \|v\|$ for any non-zero vector v. Then the GMRES algorithm, solving the linear system (2.31) at the Newton step n, converges linearly at worst in $\mathcal{O}(\sqrt{\gamma})$.*

Proof. See the proof of Proposition 2. □

Remark 3. *In contrast to Proposition 2, in this algorithm realization no preconditioner is needed to guarantee the convergence.*

2.7 Detailed Newton-Krylov algorithm

Shooting type realization. As it was seen above, the proposed Newton-Krylov technique approximates the "correct" initial state u_0, proceeding as for a shooting method. That is, at each Newton step we evaluate $u(T) = \Phi_0(u_0)$ from a given u_0, which is then corrected, using the periodicity error $\varepsilon_{per} = u(T) - Su_0$. We describe below the detailed algorithm in the case of implicit Euler scheme.

We fix an arbitrary initial state u_0^1 for the first iteration. Then, the n-th iteration of the global Newton loop is as follows:

1. Given an initial value u_0^n, compute $u_m^n = \Phi_0(u_0^n)$ by solving the initial value problem:

$$F\left(t_{i+1}, u_{i+1}^n, \frac{u_{i+1}^n - u_i^n}{\Delta t_i}\right) = 0, \quad i = 0 \dots m-1,$$

where $m \cdot \Delta t = T$. On each time step $i = 0..m-1$, a nonlinear problem is solved using Newton-Raphson method (local Newton loop).

2. We store m local Jacobians $(B_i + \Delta t \cdot A_i)$ and m matrices B_i, $i = 0..m-1$, where

$$A_i = \mathrm{D_u} F(t_{i+1}, u^n_{i+1}, \frac{u^n_{i+1} - u^n_i}{\Delta t_i}),$$
$$B_i = \mathrm{D_{\dot u}} F(t_{i+1}, u^n_{i+1}, \frac{u^n_{i+1} - u^n_i}{\Delta t_i}),$$

computed on the last Newton iteration for each time step i. Note that we store the factorization (LU or Cholesky) of the Jacobians.

3. Estimate the residual (periodicity error):

$$\varepsilon^n_{per} = u^n_m - S u^n_0.$$

If $|\varepsilon^n_{per}|$ is less than desired precision, then u^n_j, $j = 1..m$, provides the desired space-time periodic solution. Otherwise, continue the algorithm to proceed to the correction step.

4. Use the preconditioned matrix-free GMRES method (see Section 2.5) to compute the increment

$$\delta u^{n+1}_0 = (S - \mathrm{D}\Phi^n_0)^{-1} \varepsilon^n_{per},$$

where S is the space shift matrix. The tangent monodromy matrix $\mathrm{D}\Phi^n_0$, given by (2.17), is defined implicitly by its matrix-vector product for any vector v:

$$\mathrm{D}\Phi^n_0 \, v = \mathcal{W}_{m-1} \cdot \mathcal{W}_{m-2} \cdot \ldots \cdot \mathcal{W}_0$$

with forward operators $\mathcal{W}_i = (B_i + \Delta t \cdot A_i)^{-1} B_i$ (implicit Euler), where the matrices $(B_i + \Delta t \cdot A_i)$ and B_i are computed and stored during the step 1. The already computed and stored factorizations of the local Jacobian $(B_i + \Delta t \cdot A_i)$ are used for multiplication by their inverses.

5. Correction: $u^{n+1}_0 = u^n_0 + \delta u^{n+1}_0$. Pass to the next iteration.

Observer-controller type realization. This alternative realization of the Newton-Krylov algorithm consists in a modification of the standard time evolution by introducing a correction (controller) of the current solution after each time period, based on the current periodicity error (observer). The following algorithm, applied in conjunction with an implicit Euler time scheme, is schematically depicted in Figure 2.1.

First, we fix an arbitrary initial state u_0. Then the n-th time period is as follows:

1. Proceed with one-period time integration from $u_{(n-1)m}$ to u_{nm}, where $u_{nm} = \Phi_{nT}(u_{(n-1)m})$ is given by solution of the initial value problem:

$$F\left(t_{i+1}, u_{i+1}, \frac{u_{i+1}-u_i}{\Delta t}\right) = 0, \quad i = (n-1)m \dots nm-1,$$

where $m \cdot \Delta t = T$. On each time step i, a nonlinear problem is solved using Newton method (local Newton loop).

2. We store m local Jacobians $(B_i + \Delta t \cdot A_i)$ and m matrices B_i, where

$$\begin{aligned} i &= (n-1)m \dots nm-1, \\ A_i &= \mathrm{D_u} F(t_{i+1}, u^n_{i+1}, \frac{u^n_{i+1}-u^n_i}{\Delta t_i}), \\ B_i &= \mathrm{D_{\dot u}} F(t_{i+1}, u^n_{i+1}, \frac{u^n_{i+1}-u^n_i}{\Delta t_i}), \end{aligned}$$

computed on the last Newton iteration for each time step i during the last time period. Note that we store the factorization (LU or Cholesky) of the Jacobians.

3. Estimate the periodicity error:

$$\hat\varepsilon^n_{per} = u_{nm} - S u_{(n-1)m}.$$

If $|\hat\varepsilon^n_{per}|$ is less than desired precision, then $u_{(n-1)m+j}$, $j = 1..m$, provides the desired space-time periodic solution. Otherwise, continue the algorithm to proceed to the correction step.

4. Use the matrix-free GMRES method (see Section 2.5 and algorithm (2.32)) to compute the increment

$$\delta\hat u^{n+1} = -\hat\varepsilon^n_{per} + \left(\mathrm{Id} - \mathrm{D}\Phi^n\, S^{-1}\right)^{-1} \hat\varepsilon^n_{per},$$

where S is the space shift matrix. The tangent monodromy matrix $\mathrm{D}\Phi^n$ is defined implicitly by its matrix-vector product for any vector v:

$$\mathrm{D}\Phi^n\, v = \mathcal{W}_{m-1} \cdot \mathcal{W}_{m-2} \cdot \ldots \cdot \mathcal{W}_0$$

with the forward operators $\mathcal{W}_i = (B_i + \Delta t \cdot A_i)^{-1} B_i$ (implicit Euler), where the matrices $(B_i + \Delta t \cdot A_i)$ and B_i are computed and stored during the step 1. The already computed and stored factorizations of the local Jacobians $(B_i + \Delta t \cdot A_i)$ are used for multiplication by their inverses.

5. Correction $u_{nm} := u_{nm} + \delta\hat u^{n+1}$. Pass to the next cycle.

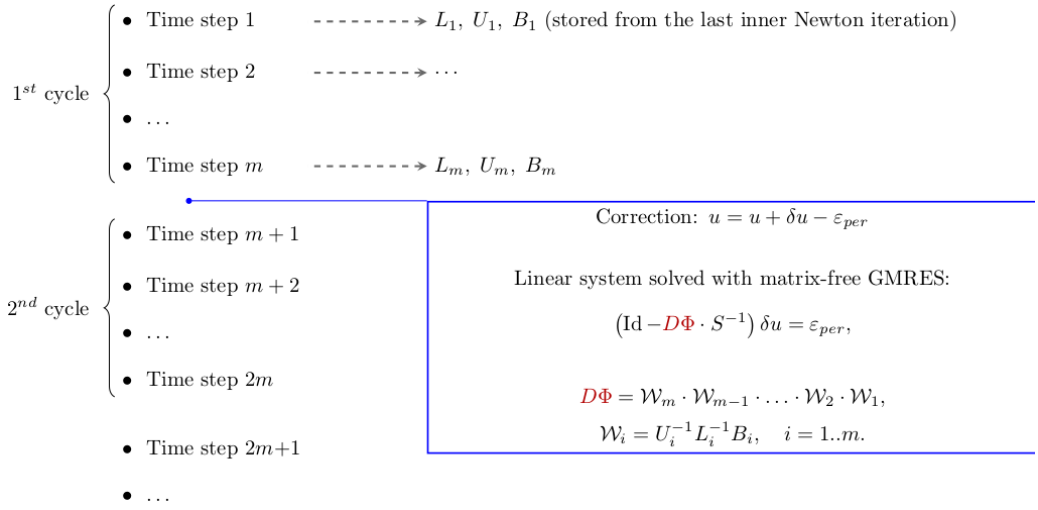

Figure 2.1: Scheme of the Newton-Krylov algorithm (observer-controller realization) in case of implicit Euler time scheme. The time-evolution solution u is corrected in the end of each cycle with the increment δu. Here, ε_{per} is the current periodicity error computed during the last cycle, S is the space shift operator, $\mathcal{W}_i$ denotes the forward operator, and the matrices L_i and U_i stand for the LU decomposition of the local Jacobian $(A_i + \Delta t_i B_i) = L_i U_i$.

2.8 Application. Linear 2D heat problem

We first start our application examples with a linear problem. Obviously, the Newton-based method will give the solution immediately after the first global iteration (i.e. after the first cycle). However, one Newton iteration requires to compute a correction term (2.30), solving a linear problem with GMRES, where each Krylov iteration is of the same complexity as computing one cycle evolution. That is, in linear case we can understand a Krylov iteration as one cycle computation. Thus, it is interesting to compare performance of the Newton-Krylov and the asymptotic methods on a linear example.

We apply both methods to a 2D heat model, described in Section 1.2, where a planar disk is heated with a periodically moving source (Figure 2.2). We have performed five simulations with different values of the disk radius, which leads to different relaxation times. The results are compared in Table 2.1. We can observe that in each case Newton-Krylov method requires less iterations with better accuracy than the asymptotic method. Besides, Newton-Krylov is less sensitive to the relaxation time growth.

For example, in case of radius $R = 10\,mm$, the asymptotic method reaches the cyclic solution with the accuracy 10^{-4} (periodicity error ℓ_∞-norm) in 25 time

periods (cycles). Meanwhile, the Newton-Krylov algorithm obtains the same result after the first cycle, including 8 Krylov iterations during GMRES (with accuracy 10^{-4}). Moreover, it reaches the accuracy 10^{-10} after 14 Krylov iterations.

R,		Asymptotic		Newton-Krylov	
$[mm]$	$\|\mathrm{D}\Phi\|$	# cycles	accuracy	# cycles	accuracy
5	0.3168	7	9.63e-5	4 (8)	3.94e-5 (7.44e-13)
10	0.7404	25	9.19e-5	9 (15)	3.37e-5 (1.61e-11)
20	0.9268	97	9.93e-5	22 (33)	4.56e-5 (5.93e-11)
30	0.9667	217	9.99e-5	37 (55)	5.97e-5 (8.99e-11)
40	0.9811	385	9.99e-5	54 (76)	7.67e-5 (4.31e-11)

Table 2.1: Comparison of the asymptotic and the Newton-Krylov methods for a linear 2D heat problem (see Section 1.2). The table presents the results of five simulations performed with different values of the disk radius, which leads to different relaxation times (illustrated here by the value of the norm of monodromy operator $\|\mathrm{D}\Phi\|$). In a linear case, complexities of one Krylov iteration and one cycle evolution are equivalent. For the Newton-Krylov, along with the number of cycles (1 cycle + Krylov iterations) needed to reach the periodicity error accuracy 10^{-4}, it is also indicated in parentheses the cycle number needed to reach accuracy 10^{-10}. We can observe that Newton-Krylov method requires less iterations with better accuracy than the asymptotic method. Besides, Newton-Krylov is less sensitive to the relaxation time growth.

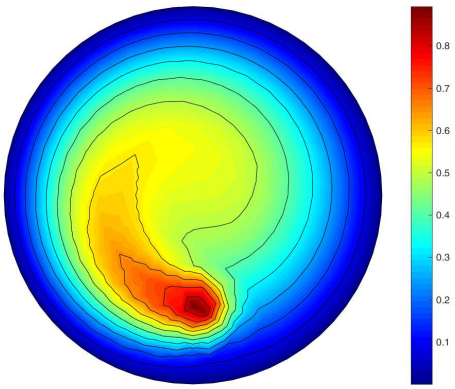

Figure 2.2: Planar disk heated with a periodically moving source (model described in Section 1.2). Finite elements solution (temperature).

2.9 Application. Rolling tyre

In order to justify the performance of the proposed Newton-based technique, we want to compare it with the classical asymptotic method, when the space-time periodic state is sought as an asymptotic limit of the standard time evolution solution with arbitrary initial data. For this purpose, we consider the alternative Newton algorithm implementation, discussed in Section 2.6, and as an initial guess we take the initial state of the asymptotic method. In this case, the only difference in implementation between two methods is the correction of the solution in the end of each time period in the Newton method (see Figure 2.1).

First, we implement the methods in MatLab R2016b for the simplified tyre rolling model, proposed in Section 1.1.4. It allows us to test the technique on a simple mathematical problem with memory effects provided by the stick friction and by the viscoelasticity of the material.

Then, we will present an industrial application, where the Newton algorithm has been implemented into the Michelin industrial code. The results demonstrate the practical value of the proposed techniques.

2.9.1 Simplified academic model

Let us consider the simplified tyre model, described in Section 1.1.4, which presents a 3D ring, where periodicity of the sculptures is represented by periodic material properties, instead of geometric periodicity. Mathematical definition of the problem is given in (1.17) and writes

$$F(t, \underline{u}, \dot{\underline{u}}) = 0,$$
$$\underline{u}(t) = S\underline{u}(t - T),$$

where F is defined by (1.18), T is the time period. The space shift operator S is defined in the rotating coordinate system (connected to the tyre rim with the origin on the axle) by

$$\forall \underline{v} \quad S : \underline{v}(\underline{X}) \mapsto \underline{\underline{R}}_\theta^{-1}\, \underline{v}(\underline{\underline{R}}_\theta \underline{X}),$$

where $\underline{\underline{R}}_\theta$ denotes the rotation of angle θ (sculpture size). Remind that for the sake of simplicity, we use the small strains assumption (linearized strains), so the only non-linearity is produced by the contact forces, which involves the normal contact pressure and the stick-slip friction.

The rates of convergence to the space-time periodic state is characterized by decreasing of the periodicity error $\varepsilon_{per} = \underline{u}(t) - S\underline{u}(t - T)$, which is the residual in the global Newton algorithm. Solution is said to have converged to the cyclic steady state, when the periodicity error ℓ_∞-norm is less that the specified accuracy 10^{-4}.

We set the tyre external and internal radii $r_1 = 1\,m$ and $r_2 = 0.7\,m$ respectively and the width to $0.2\,m$. The ground is at the distance $r_{load} = 0.9\,r_1$ from the

wheel axle. The tyre has $M = 36$ sculptures of angle $\theta = 2\pi/M = 10^\circ$ and depth $(r_1 - r_{sculpture}) = 0.1\, r_1$. Material properties, periodic with respect to the angle, vanish at order 10^{-5} in the domains associated to voids in the sculpture (these domains are not affected by the contact). That is, the Young's modulus is in the form (1.16) with the reference value $E_0 = 10^2\, MPa$, associated to rubber. In a first step, we consider a purely elastic material, i.e. viscosity coefficient is set to zero. Thus, only frictional contact provides memory effects.

The finite elements simulations have been implemented in MatLab R2016b, using P_1-elements on a conforming tetrahedral θ-periodic mesh (Figure 2.3), composed of 4500 nodes and 19008 tetrahedral elements. The implicit Euler time scheme is used with step $\Delta t = 0.1\, T$, where $T = \frac{2\pi}{\omega M}$ is the time period of one sculpture turn. That is, we use 10 time steps per period (cycle). Each time iteration is solved with the complete Newton method, with the contact treated by penalization (see (1.3) and (1.4)) with penalty coefficients $\epsilon_N = \epsilon_\tau = 10^7$. A second test will use a lower tangent penalty factor $\epsilon_\tau = 10^6$. A loaded frictionless state is taken as the initial state.

The tyre advances with linear velocity $v_{ax} = 22.22222\ m/s (= 80\ km/h)$. The angular velocity of the rim is $\omega = v_{ax}/r_{load}$, which provides a small rim couple, and therefore a small friction force, ensuring that a large part of the contact zone is in the adherent regime, which is the most challenging case.

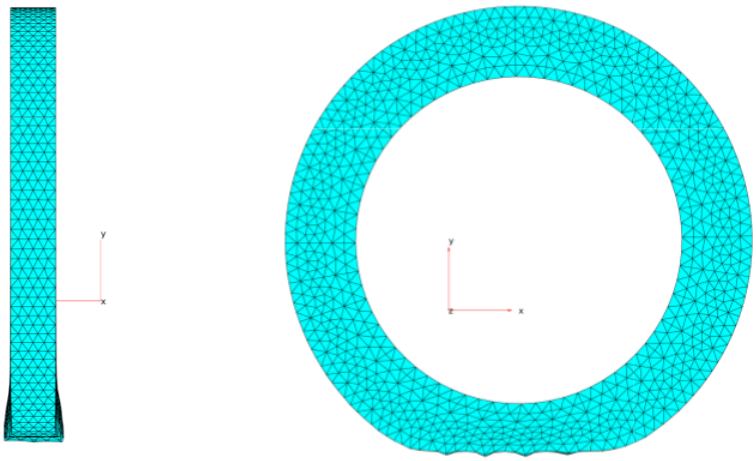

Figure 2.3: 10°-periodic mesh of rolling tyre (created in MatLab). Instead of geometric modification, periodicity of the sculpture is represented by periodicity of material properties (Young's modulus), which are negligibly small in the domains associated to voids. Moreover, these domains are not affected by the contact, which produces the surface irregularities observed on the contact surface.

Comparison of the asymptotic and the Newton-Krylov methods is presented in Table 2.2, demonstrating the evolution of the periodicity error ℓ_∞-norm after each cycle. The corresponding computation time is indicated in the bottom of the tables. Remark that Newton-Krylov method converges with quadratic rate. For penalty factors $\epsilon_\tau = 10^7$ and $\epsilon_\tau = 10^6$, it is respectively about 4 and 1.5 times more efficient than the asymptotic method.

The last column in Table 2.2 indicates the number of Krylov iterations needed to reach accuracy 10^{-6} while solving with GMRES [Saad and Schultz 1986] the linear system on each global Newton iteration (each cycle). We can see that the number of Krylov iterations has decreased with the penalty coefficient ϵ_τ, while the number of Newton iterations (cycles) has not changed much. Note that we do not solve the Newton linear system after the last cycle, which reconstructs the entire cyclic solution from the already converged initial data, i.e. there is no Krylov iterations at the last Newton step.

Once-performed LU factorizations are stored and reused multiple times during the GMRES algorithm, which allows to solve rapidly the linear systems, associated to the local Jacobians. In our simulation, one Krylov iteration requires about 0.08 s. To compare, if we do not store the factorization (i.e. factorizing Jacobian each time when we solve the associated linear system), one Krylov iteration will take about 2.3 s, which is about 30 times slower.

Let us now introduce viscosity inside the tyre material. Viscosity coefficient η is θ-periodic in the form (1.16) with the reference viscosity coefficient η_0, which takes values 0.1, 0.25, 0.5, 0.75, 1 and 10 $MPa \cdot s$. Young's modulus is still $10^2\, MPa$. A large viscosity coefficient provides large memory effects and increases the relaxation time of the problem. The friction is still present, tangent penalty coefficient is $\epsilon_\tau = 10^7$.

We apply the Newton-Krylov method using different values of the viscosity coefficient in order to study its sensitivity to the problem's relaxation time. As we can see in Table 2.3, increasing of the relaxation time does not affect much the number of Newton steps (number of cycles), but instead increases the number of Krylov iterations needed after each cycle. We can observe, however, that the overall computation time is not very sensitive to the number of Krylov iterations. This is because the time required to perform the GMRES is negligible with respect to the global Newton step computation time, which depends on the number of local Newton iterations during each time step.

$\epsilon_\tau = 10^7$

	Asymptotic	Newton-Krylov	
# cycles	Periodicity error	Periodicity error	# Krylov iter.
1	3.3464e-01	3.3464e-01	10
2	2.6088e-01	3.2516e-02	8
3	2.0938e-01	1.9033e-04	6
4	1.5360e-01	6.3073e-07	
5	9.9635e-02		
6	6.0135e-02		
7	3.6511e-02		
8	2.2581e-02		
9	1.4076e-02		
10	8.7888e-03		
11	5.4933e-03		
12	3.4350e-03		
13	2.1459e-03		
14	1.3404e-03		
15	8.3732e-04		
16	5.2302e-04		
17	3.2669e-04		
18	2.0406e-04		
19	1.2747e-04		
20	7.9633e-05		
Elapsed time	334.12 s	77.4 s	

$\epsilon_\tau = 10^6$

	Asymptotic	Newton-Krylov	
# cycles	Periodicity error	Periodicity error	# Krylov iter.
1	2.3370e-01	2.3370e-01	5
2	4.4157e-02	6.5393e-04	4
3	8.7853e-03	5.4066e-08	
4	1.7262e-03		
5	3.4142e-04		
6	6.7367e-05		
Elapsed time	79.807 s	55.752 s	

Table 2.2: Rolling elastic tyre (MatLab simulation). Comparison of the periodicity error evolution for the asymptotic and the Newton-Krylov methods. Two present tests use different values of the tangent penalty coefficient: $\epsilon_\tau = 10^7$ (top table) and $\epsilon_\tau = 10^6$ (bottom table). The last column indicates the number of Krylov iterations performed during GMRES at each cycle of the Newton-Krylov algorithm.

η_0,	Asymptotic		Newton-Krylov		
$[MPa \cdot s]$	# cycles	Elapsed time	# cycles	# Krylov iter.	Elapsed time
0.10	21	351 s	3	$11 + 8$	54 s
0.25	23	367 s	3	$20 + 10$	55 s
0.50	40	621 s	3	$36 + 15$	51 s
0.75	54	811 s	3	$48 + 22$	52 s
1.00	70	1060 s	3	$58 + 32$	60 s
10.00	406	4504 s	4	$148 + 95 + 10$	70 s

Table 2.3: Rolling viscoelastic tyre (MatLab simulation). Sensitivity of the Newton-Krylov algorithm to the relaxation time. The table shows the number of non-linear cycles and Krylov iterations, needed to reach periodicity error accuracy 10^{-4}, as well as the overall computation time for the asymptotic and the Newton-Krylov methods as functions of viscosity coefficient η_0. The relaxation time of the problem grows with the viscosity. For the Newton-Krylov, this does not affect much the number of global Newton steps (number of cycles), but increases instead the number of Krylov iterations.

2.9.2 Industrial model

In order to justify the performance of the proposed Newton-Krylov method, we have implemented the algorithm into the Michelin industrial code. In its evolutionary form (alternative realization from Section 2.6), it is easy to compare with the classical industrial way to obtain the periodic solution as an asymptotic limit of the standard time evolution from an arbitrary initial state.

The non-linear mechanics of the steady rolling tyre is described in Section 1.1.1 with the mathematical definition of the problem given by (1.10):

$$F(t, \underline{\tilde{u}}, \dot{\underline{\tilde{u}}}) = 0,$$
$$\underline{\tilde{u}}(t) = S\underline{\tilde{u}}(t - T),$$

where F is defined by (1.11), T is the time period. The space shift operator S is defined through the rotation of the argument:

$$\forall \underline{v} \quad S : \underline{v}(\underline{X}) \mapsto \underline{v}(\underline{\underline{R}}_\theta \underline{X}),$$

where $\underline{\underline{R}}_\theta$ denotes rotation of angle θ (sculpture size). We are looking for the space-time periodic solution $\underline{\tilde{u}}$. So the criterion of convergence to the limit cycle is the periodicity error $\varepsilon_{per} = \underline{\tilde{u}}(t) - S\underline{\tilde{u}}(t - T)$, which is the residual in the global Newton algorithm. Solution is said to have converged to the cyclic steady state, when the periodicity error ℓ_∞-norm is less that the chosen tolerance 10^{-4}.

We consider a simple geometric model of our test tyre (Figure 2.4) with $M = 36$ periodic sculptures. It is a conforming (almost uniform) hexahedral mesh, periodic with respect to the angle $\theta = 2\pi/M = 10°$. The periodicity is presented by the

periodic void spaces in the sculpture. The mesh has 9830 nodes and 6624 "brick" Q_1-elements. Radius of the tyre is $270\,mm$, and the loaded radius (given constant distance from the tyre axle to the ground) is $r_{load} = 250\,mm$.

The time period of one sculpture turn is $T = \theta/\omega = \frac{2\pi}{\omega M}$. We consider a time discretization with $m = 10$ time steps per period. That is, the time step is $\Delta t = T/m = 0.1 \cdot T$.

All materials are incompressible (treated by penalty) and elastic, i.e. with no viscosity in the constitutive law. We do not take in account the inertia terms. So, all the memory effects come from the frictional contact (in the adherent regime), defined with the regularized Coulomb law (1.4).

The rolling configuration is defined by two parameters: the linear velocity of the wheel axle v_{ax} and the angular velocity of the rim ω. We consider a high speed regime with $v_{ax} = 22222.22\,mm/s$ $(= 80\,km/h)$ and two rotation regimes: $\omega = v_{ax}/r_{load} = 88.88888\ s^{-1}$, which provides a small rim couple, and a greater $\omega = 1.25 \cdot v_{ax}/r_{load} = 111.1111\ s^{-1}$, providing a greater couple, since the couple depends on the difference $\omega - v_{ax}/r_{load}$.

We take the same initial state for both Newton-Krylov and asymptotic methods. Starting from an undeformed state, we perform one standard time step iteration to obtain a loaded state, which takes the friction into account. This state, obtained after one time iteration, is taken as the initial state for our simulations.

Newton-Krylov and asymptotic methods are compared in Table 2.4 for two rotation configurations. There is shown the evolution of the ℓ_∞-norm of the periodicity error as function of the number of computed cycles (time-periods). The corresponding computation time is indicated in the bottom of the tables. Comparing two methods, we observe that in case $\omega = v_{ax}/r_{load}$, Newton-Krylov method is more than twice more efficient than the asymptotic method. But for a greater angular velocity, efficiency of both methods is almost the same. Asymptotic method converges even a little faster. That is because increasing of the rim couple leads to the friction force growth. So a larger part of the contact surface enters into a sliding regime. Since the memory effects are provided only by the adherent regime, the relaxation time of the problem decreases, and therefore it converges faster. However, the Newton method shows still the same rate and converges in 6 periods independently of the relaxation time.

Note that, in contrast to the previous MatLab implementation, Newton method here does not demonstrate quadratic convergence rate. That is due to the fact that the local Newton resolutions on each time step use non-exact Jacobians.

The last column in Table 2.4 indicates the number of Krylov iterations needed to reach the accuracy 10^{-6} while solving with GMRES [Saad and Schultz 1986] the linear system on each global Newton iteration (each cycle). We use the matrix-free Krylov subspaces iterative solver, provided by PETSc (Portable Extensible Toolkit for Scientific Computation [Balay et al. 2016]). Direct solver (also by PETSc), using LU factorization, is used to solve multiple linear systems, arising from inversion of the local Jacobians in the forward operator (2.15). Once performed factoriza-

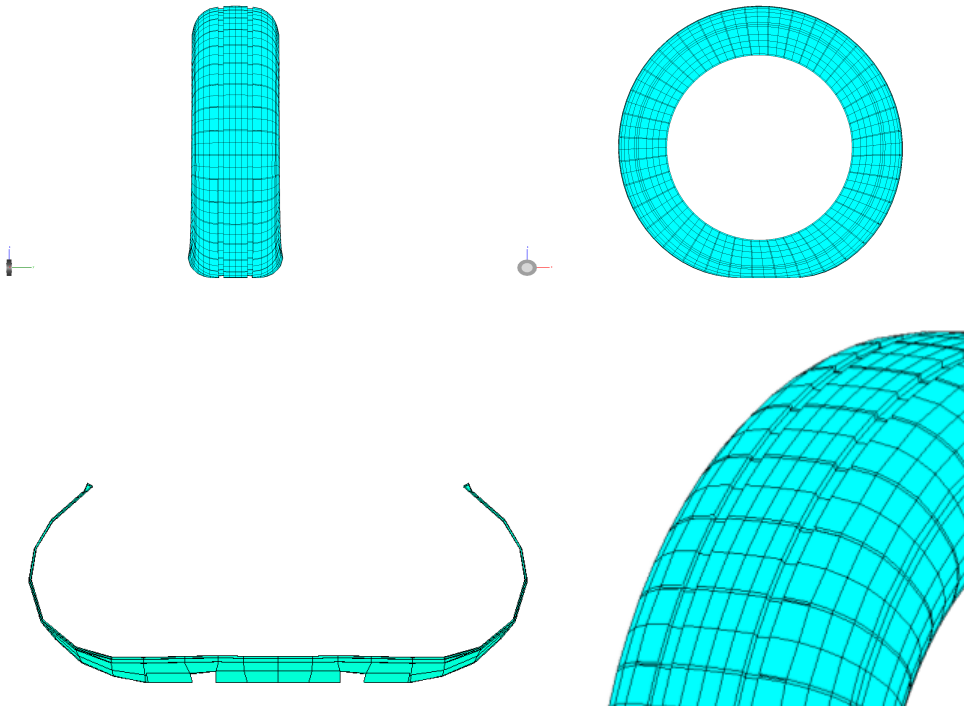

Figure 2.4: Hexahedral mesh of the tyre with $10°$-periodic sculptures.

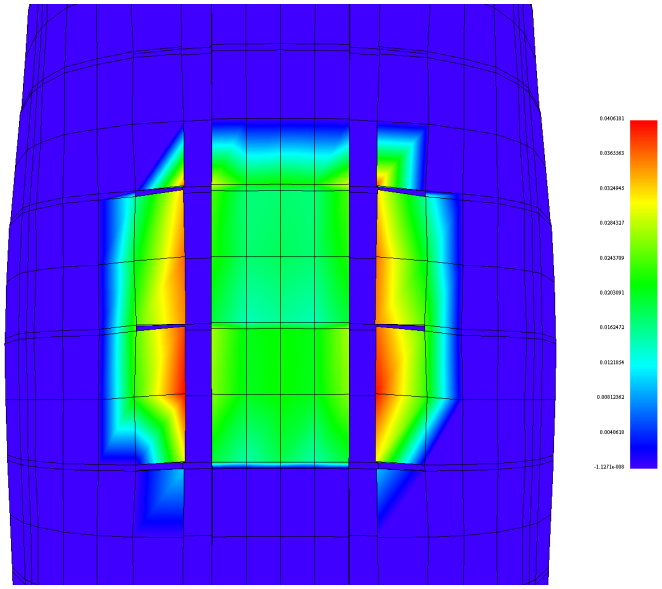

Figure 2.5: Finite elements solution: nodal pressure in contact zone.

tion is stored and reused multiple times, which allows to solve rapidly the global linear systems. In our simulation, one Krylov iteration requires about one second, which is negligible in comparison to one cycle overall computation time about $500 - 1000\ s$.

Regular tyre. If we take a regular tyre, that is with no sculptures (see Figure 2.6), the cyclic solution is simply the steady state. The number of sculptures here is set to $M = 120$, which corresponds to the number of angular mesh steps. In absence of voids, the contact zone is increased, thus the relaxation time becomes larger too. Comparison of Newton-Krylov and asymptotic methods in the case $\omega = v_{ax}/r_{load}$ is presented in Table 2.5. We observe that the asymptotic solution has not yet converged after 32 cycles, while Newton-Krylov always converges in 6 iterations (cycles), though the number of Krylov iterations is increased.

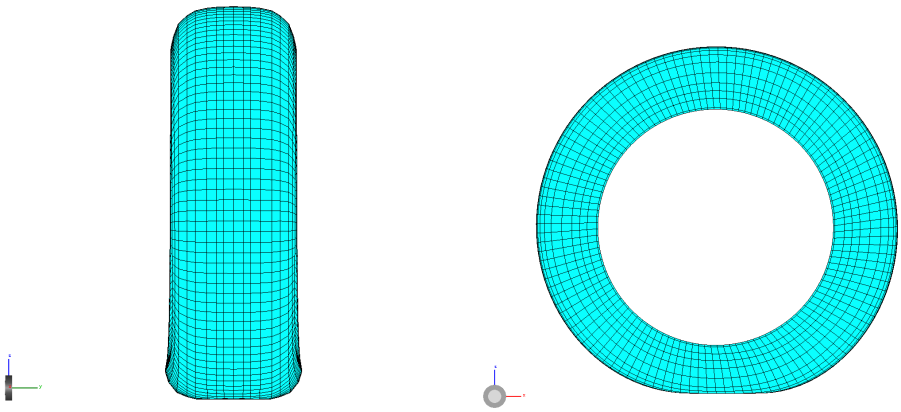

Figure 2.6: Hexahedral tyre mesh with no sculpture. Number of motifs is taken $M = 120$, which corresponds to the number of angular mesh steps.

$\boxed{\omega = v_{ax}/r_{load}}$

	Asymptotic	Newton-Krylov	
# cycles	Periodicity error	Periodicity error	# Krylov iter.
1	2.58695	2.58695	16
2	2.57251	33.3906	4
3	2.27233	0.164569	7
4	2.05147	0.0038217	6
5	1.84092	0.000153063	4
6	1.63789	5.65882e-05	
7	0.865028		
8	0.377441		
9	0.0670852		
10	0.0112266		
11	0.00192364		
12	0.000366376		
13	0.000501187		
14	0.000453552		
15	9.30607e-05		
Elapsed time	15596.7 s	7098.97 s	

$\boxed{\omega = 1.25 \cdot v_{ax}/r_{load}}$

	Asymptotic	Newton-Krylov	
# cycles	Periodicity error	Periodicity error	# Krylov iter.
1	11.0188	11.0188	12
2	2.08072	60.162	3
3	0.00542872	0.00504267	4
4	0.000166966	0.000880275	3
5	5.46415e-05	0.000258374	3
6		7.78401e-05	
Elapsed time	3217.31 s	4579.4 s	

Table 2.4: Rolling tyre (Michelin industrial simulation). Comparison of the periodicity error evolution for the asymptotic and the Newton-Krylov methods, searching for the steady cyclic state. Two present tests use different values of the angular velocity: $\omega = \underline{v}_{ax}/r_{load}$ (top table) and $\omega = 1.25 \cdot v_{ax}/r_{load}$ (bottom table). Greater ω induces a greater couple, which leads to a larger slip zone, decreasing memory effects. However, Newton-Krylov convergence rate always remains 6 cycles. So, in the second case, asymptotic method has converged a little bit faster. The last column indicates the number of Krylov iterations performed during GMRES at each cycle of the Newton-Krylov algorithm.

$\boxed{\omega = v_{ax}/r_{load}}$

	Asymptotic	Newton-Krylov	
# cycles	Periodicity error	Periodicity error	# Krylov iter.
1	0.86779	0.86779	53
2	0.829639	51.5665	3
3	0.827099	0.0702491	12
4	0.824896	0.0114307	11
5	0.822508	1.45e-04	9
6	0.820009	3.85e-05	
...	...		
30	1.66e-03		
31	6.24e-04		
32	2.04e-04		
Elapsed time	34747.3 s	6455.95 s	

Table 2.5: Rolling tyre with no sculpture (Michelin industrial simulation). Comparison of the periodicity error evolution for the asymptotic and the Newton-Krylov methods, searching for the steady state of a rolling regular tyre. In absence of empty spaces in the sculpture, the contact zone is larger, so that memory effects are large too. However, Newton-Krylov convergence rate does not change and is still 6 cycles. Meanwhile, the number of Krylov iterations (last column) is increased. Here, the angular velocity of the rim is $\omega = v_{ax}/r_{load}$.

2.10 Conclusion

In this chapter, we have considered an alternative method for calculating the space-time periodic solution to non-linear evolution problems. For large problems, direct methods are not very convenient, since they require the inversion of very large matrices. Usually, such a cyclic solution is computed as an asymptotic limit of the associated initial value problem with arbitrary initial data. However, when the relaxation time is large, convergence to the limit cycle can be very slow. Another possibility is to use Newton-Krylov method to compute the "correct" initial state that provides the cyclic solution. That means to consider the periodicity condition as an equation for the unknown "true" initial state. Once the "correct" initial data is found, the desired space-time periodic solution is provided by solving the initial value problem during one time period.

The equation on the unknown initial state includes a non-linear evolution function, requiring to solve an initial value problem during one time period. Applying Newton-Raphson technique, we obtain a linear system, where the residual is defined by the periodicity error, and the Jacobian includes the gradient of the evolution function (called tangent monodromy operator or global Jacobian). Construction of this operator, which can not be expressed explicitly, is quite challenging.

One Newton iteration corresponds to one time period and, after time discretization, includes several time steps. Each time step solves a local non-linear problem, using an internal Newton loop. Successive solutions of the linear systems, arising at the end of each such loop, are the constitutive parts of the global Jacobian. Thus, local Jacobians, stored during one cycle, can be used to construct the corresponding tangent monodromy matrix. However, in practice, for efficiency, this matrix is never assembled, but defined implicitly by the multiplication operation, using the stored operators. Then, one of the matrix-free Krylov iterative methods (GMRES, for example) can be used to solve the linear system that appears at each global Newton iteration.

During GMRES, each Krylov iteration is equivalent to the integration of one linearized cycle. That is, one Krylov iteration requires to solve a sequence of linear systems, associated to the local Jacobians. However, each of these systems has been already solved during a corresponding time step. So, if its factorization (LU or Cholesky) is already performed, it has to be stored instead of the matrix itself. Using once-performed factorizations reduces considerably the numerical cost of local Jacobians inversion during Krylov iterations. In our simulations, it allowed to accelerate one Krylov iteration in about 30 times. In this way, computing time needed to apply the global Jacobian (tangent monodromy operator) becomes negligible with respect to the time to compute the residual (periodicity error), which is the time to compute one time period (cycle).

To summarize, on each global Newton step, given an initial state (starting with an arbitrary guess), the method solves the non-linear initial value problem during the first period, in order to estimate the periodicity error and to store the tangent matrices. If the periodicity error is sufficiently small, the current initial state is accepted. Otherwise, a correction step is performed, where the increment (correction) is found from the periodicity error and the monodromy matrix, and the initial state is then updated for the next step.

The method can be considered as a kind of shooting method. Indeed, starting with an arbitrary left boundary value, we go through one period evolution to obtain the right boundary value and use it for correction of the left boundary value and so on.

In the proposed algorithm, each Newton step approximates the global initial state at time $t = 0$. However, it is more convenient to approximate the initial state of the current time period, i.e. at time $t = nT$, where n is the number of the current cycle, which corresponds to a Newton step. This can be achieved by change of variable in the Newton algorithm, and leads to modification of a standard time evolution by introducing a correction of the current transient solution after each cycle. The correcting step involves the current periodicity error and the tangent monodromy matrix, defined implicitly, using operators stored during the cycle (along with the corresponding factorizations). Such a correction induces discontinuities of the transient solution, which "jumps" at each time cycle.

Both implementation are equivalent and present just two points of view to

the same algorithm. The advantage of the last formulation is that it can be easily derived from the classic time evolution by adding the correction step in the end of each cycle (Figure 2.1). Besides, it can be compared with the methods searching the periodic state as an asymptotic limit of solution, in particular those accelerating convergence to the limit state (ex., Delayed Feedback Control method, which will be discussed in the next chapter). Indeed, it may be considered as an observer-controller process, where correction, performed in the end of each period, is based on the observation during this period.

On the other hand, the present Newton-Krylov algorithm is memory greedy, because one needs to store a number of matrices, proportional to the number of time steps per cycle. That is, a fine time discretization of a large problem (with a lot of degrees of freedom) implies a large number of large matrices to be stored (even along with their factorizations). Thus, the method favors problems either with few time steps per cycle, or with few degrees of freedom in space domain, which ensures a reasonable memory usage.

Implementing applications, we started with a linear problem. As expected, Newton algorithm gives the solution after the first iteration (i.e. after the first cycle). However, one Newton iteration solves a linear problem using GMRES, where each Krylov iteration is of the same complexity as the calculation of one cycle evolution. We have compared performance of the Newton-Krylov algorithm with the classic asymptotic method (where the space-time periodic state is sought as an asymptotic limit of the standard time evolution solution with arbitrary initial data) on a linear 2D heat model, described in Section 1.2, where a planar disk is heated with a periodically moving source. We have observed that Newton-Krylov method requires less iterations with better accuracy than the asymptotic method. Besides, Newton-Krylov was less sensitive to the relaxation time growth.

Further, the Newton-Krylov technique has been applied to our main model problem: a rolling 3D tyre in presence of stick-slip frictional contact with the soil (Section 1.1.1). This problem is three dimensional and non-linear. First, we have studied the method on a simplified academic model (Section 1.1.4) using MatLab R2016b. Newton-Krylov method has converged with quadratic rate and has reached better accuracy four times faster than the asymptotic method. Storing LU factorizations of local Jacobians during the cycle and reusing them during the GMRES allowed to reduce computing time of one Krylov iteration in about 30 times.

Finally, Newton-Krylov algorithm has been integrated into the Michelin industrial code. There, the method has not demonstrated quadratic convergence rate, because of using non-exact local Jacobians for the local Newton resolutions on each time step. In case of small rim couple, Newton-Krylov has been twice more efficient than the asymptotic method. But for a greater couple, efficiency of both methods was almost the same (asymptotic method converges even a little faster). In the case of a regular tyre (with no sculpture), when the cyclic solution is simply the steady state, Newton-Krylov has been more than five times faster.

While convergence time of the asymptotic method depends on the size of memory effects of the problem, Newton-Krylov method always converged within the same number of iterations/cycles. Instead, the variation of the relaxation time affected only the number of Krylov iterations on each cycle. Given that one Krylov iteration (equivalent to a linearized cycle, but with known factorization) is more than 100 times faster than one non-linear cycle, such a trade is quite advantageous. Thus, Newton-Krylov convergence time should be of the same order independently of the problem's relaxation time. We conclude that Newton-Krylov shooting method is very efficient and is a robust technique for computing space-time periodic solution of evolution problems.

CHAPTER 3

Delayed feedback control method for computing the space-time periodic solution of evolution problems

Summary

3.1 Introduction

Mechanics of nonlinear continua have been the topic of many developments. Nowadays, these problems are faced with new challenges, such as handling large memory and diffusion effects or solving time dependent coupled problems on multiscale geometries with space or time periodicity conditions. In industrial applications, in order to avoid the inversion of very large matrices, time periodic states are often computed as the asymptotic limit solution of an initial value boundary value problem with arbitrarily chosen initial data. This kind of problems can be faced, for instance, in the cardiac contractions modeling. Another example concerns the steady rolling of a viscoelastic tyre [Le Tallec and Rahier 1994, Govindjee et al. 2014] with a periodic sculpture. In this case, the stable state satisfies a "rolling" periodicity condition (cyclic steady state [Govindjee et al. 2014]), including shifts both in time and space: the state $\underline{u}(x,t)$ at any point $\underline{x}$ is the same that at the corresponding point observed at the next sculpture one time period T ago

$$\underline{u}(t,\underline{x}) = R_{\omega T}^{-1}\,\underline{u}(t-T, R_{\omega T}\underline{x}).$$

Above, R_θ denotes the rotation of angle θ and ω the rotation speed. Calculating such initial value problems until the asymptotic limit may take a lot of time for "viscous" problems, when memory effects are very large. In such cases nonetheless, one is not interested in the evolution history, but only in a fast access to the asymptotic limit cycle. Thus developing methods accelerating convergence to this limit is of high interest.

Here, even if the asymptotic limit is periodic, the solution of the initial value evolution problem is not. The lack of periodicity of the calculated solution is then an extra information (observation) on which one can apply control techniques. In other words, we can modify the initial value problem by introducing a feedback control term [Pyragas 1992, Hövel and Schöll 2005], based on this observation (periodicity error). So, the state shifted in space as well as in time (time-delay) is present in equation. This way we introduce an artificial force, proportional to the periodicity error and attracting our solution to the cyclic steady state. When the solution of the modified initial value problem converges to the limit cycle, the control term vanishes, and the modified and original problems have thus the same asymptotic limit. The control in this case is the factor operator (or gain operator), applied to the periodicity error in the control term. Thus, the technique consists to find the optimal gain operator providing the fastest convergence of the modified problem solution to the limit cyclic steady state.

The present technique is similar to the time-delayed feedback control (or time-delay autosynchronization), first suggested by [Pyragas 1992] and further extended by [Socolar et al. 1994]. It is a powerful tool widely used for stabilization of unstable periodic orbits in deterministic chaotic systems [Kittel et al. 1995, Pyragas 1995, 2002, Bleich and Socolar 1996] or unstable steady states [Hövel and Schöll 2005, Yanchuk et al. 2006]. Detailed overview on the time-delayed feedback control can be found in [Pyragas 2012] and in [Hövel 2010].

In this work, the time-delayed feedback technique is applied to an a priori stable system in order to accelerate its convergence to the stable limit cycle (space-time periodic solution). Moreover, given the space-time periodicity, along with the time-delay the feedback term includes also a shift in space. Our main result is the optimal form of the gain operator in the feedback term for a linear problem, providing the fastest convergence to the steady cyclic solution. This form of the feedback control has been also adapted and tested for nonlinear problems.

In the following section, we present an analytical analysis of an abstract linear evolution problem, modified by introducing a feedback control term. The introduced feedback term includes both temporal (time-delay) and spacial shifts. So the modified (controlled) problem leads to a delayed differential system [Bellman and Cooke 1963, Yi et al. 2010, Asl and Ulsoy 2003], whose explicit solution uses the Lambert W function [Corless et al. 1996, 1997, Valluri et al. 2000, Shinozaki and Mori 2006]. Having studied the influence of the control on the convergence rate, we propose then the optimal control, by optimizing the spectrum of the problem and minimizing thus the convergence time. We also study the influence of the magnitude of the memory effects on the efficiency of the method. Then, we propose a simplified modification of the optimal control, which is numerically cheaper and preserves the efficiency. Moreover, a predictor-corrector form of the proposed feedback control is introduced, which is quite easy in implementation. In this form, the present control technique has been extended and adapted to the non-linear case.

To confirm the theoretical results, Sections 3.4 and 3.5 are devoted to applications of the discussed method to a couple of model problems. In the first one, we consider a planar disk heated with a source periodically moving along a circular path, which may be a simple model problem for additive manufacturing. This problem corresponds exactly to the theoretical framework. The second problem considers the steady rolling of a viscoelastic tyre with periodic sculptures. This problem is three dimensional and non-linear, and is further complexified in a second step by adding stick-slip boundary conditions. So the proposed control technique has been extended and adapted to the non-linear case. Both problems have been solved numerically with the finite element method, using MatLab R2016b, while comparing the controlled and non-controlled solutions. Finally, the present feedback control method in the predictor-corrector form has been integrated into Michelin industrial code.

3.2 Linear problem

3.2.1 Abstract problem formulation

We consider an abstract evolution problem with a space-time periodic condition. Let $\mathcal{H}$ be a separable Hilbert space with duality product $\langle \cdot, \cdot \rangle$. We are

looking for a state $u(t) \in \mathcal{H}$ such that

$$\langle B\,\partial_t u(t) + Au(t) - f(t),\ v\rangle = 0 \qquad \forall v \in \mathcal{H}, \forall t, \tag{3.1}$$

$$u(t) = Su(t-T), \tag{3.2}$$

where we make the following fundamental assumptions which are satisfied in many problems:

1. A is a linear bounded symmetric elliptic operators from $\mathcal{H}$ to its dual $\mathcal{H}'$, which means that $\langle Au,\ v\rangle$ can be used as scalar product on $\mathcal{H}$ and B is a bounded symmetric positive operator, i.e $\forall u, v \in \mathcal{H}\ \ \langle Bu,\ v\rangle = \langle Bv,\ u\rangle$ and $\langle Bu,\ u\rangle \geq 0$.

2. The space shift S is a linear unitary operator from $\mathcal{H}$ onto $\mathcal{H}$ for the A-norm, i.e. $S^* = S^{-1}$, where S^* is the conjugate of S, defined by $\langle AS^*u,\ v\rangle = \langle Au,\ Sv\rangle$, $\forall u, v \in \mathcal{H}$. Moreover, S commutes with B, i.e.

$$\forall\, u, v \in \mathcal{H} \quad \langle BSu,\ v\rangle = \langle Bu,\ S^*v\rangle.$$

   Note that A and B may not commute.

3. $f(t) \in \mathcal{H}'$ satisfies the space-time periodicity condition with a time period T:

$$f(t) = Sf(t-T).$$

In practice, the solution of such problems is often computed as an asymptotic limit of the solution to the initial value evolution problem (3.1) with an arbitrary initial condition. As it will be observed in Section 3.2.2, due to the ellipticity assumption 1, this asymptotic limit exists. And due to the assumptions 2 and 3, its is space-time periodic. In the frame of this work, we are going to propose an optimal control method, accelerating the convergence of the initial value problem solution to the solution of (3.1)-(3.2).

3.2.2 Controlled problem. Explicit solution

Periodicity condition (3.2) can be considered as an observation. Then the periodicity error $\Delta u(t) = u(t) - Su(t-T)$ can be used to construct a controller for the initial value problem. So we modify it by introducing a feedback control term [Pyragas 1992, Hövel and Schöll 2005], based on the periodicity error:

$$\begin{aligned} \langle B\,\partial_t u(t) + Au(t) + \overbrace{G\left(u(t) - Su(t-T)\right)}^{\text{control term}} - f(t),\ v\rangle = 0, \qquad & t > 0, \\ u(t) = \phi(t), \qquad & t \in [-T,\, 0], \end{aligned} \tag{3.3}$$

for any $v \in \mathcal{H}$, where $\phi(t)$ represents an arbitrary initial data. Remark that the introduced feedback control term includes both temporal and spacial shifts (time-delay and unitary spacial operator S respectively). The gain operator $G : \mathcal{H} \to \mathcal{H}'$

acting on this observation error is actually our control and has to be properly identified. The case $G \equiv 0$ corresponds to the non-controlled initial value problem. We will check below that the solution $u(t)$ to the modified problem (3.3) converges to the periodic solution of the original problem (3.1). The question is whether there exists a gain operator G, providing the fastest convergence. This amounts to analyze the influence of G on the asymptotic behavior of the controlled solution and to choose the one leading to the optimal convergence rate. We will restrict ourselves to gains $G = G(A, B, S)$ which can be defined as analytical function of the operators A, B and of the space shift S. Therefore, by construction, G will commute with S.

In this general frame work, we begin by studying the general solution of the controlled problem (Theorem 1). For its demonstration, we first recall a fundamental lemma expliciting the solution of (3.3) in the scalar case.

Lemma 4. *[Bellman and Cooke 1963, Yi et al. 2010, Asl and Ulsoy 2003]. Let α, γ and σ be given complex numbers, let $\beta \geq 0 \in \mathbb{R}$ be given and g be a function of time satisfying $g(t) = \sigma g(t - T)$. Then the solution $u(t)$ to the problem*

$$\begin{aligned} \beta\, \partial_t u(t) + \alpha\, u(t) + \gamma\, (u(t) - \sigma\, u(t - T)) - g(t) = 0, \qquad & t > 0, \\ u(t) = \phi(t), \qquad & t \leq 0, \end{aligned} \tag{3.4}$$

is in the form

$$u(t) = \sum_{k \in \mathbb{Z}} u_k\, e^{\lambda_k\, t} + u_\infty(t),$$

with coefficients $\lambda_k \in \mathbb{C}$ and time periodic fundamental solution u_∞ given by

$$\lambda_k = -\frac{1}{\beta}\,(\alpha + \gamma) + \frac{1}{T}\, W_k \left[\frac{T}{\beta}\, \gamma\sigma\, e^{T(\alpha+\gamma)/\beta} \right], \qquad k \in \mathbb{Z}$$

$$u_\infty(t) = \int_0^\infty e^{-\alpha s} g(t - \beta s) ds.$$

Above, the function W_k denotes the k-th branch of the multivalued Lambert function W [Corless et al. 1996] and u_k are coefficients depending on the initial data $\phi(t)$ to be defined later.

Proof. Problem (3.4) is a simple delay-differential equation [Bellman and Cooke 1963, Yi et al. 2010, 2006, Yi and Ulsoy 2006, Asl and Ulsoy 2003]. We first observe that by construction, for all values of $\beta \geq 0$, the fundamental solution u_∞ satisfies

$$\begin{gathered} \beta\, \partial_t u_\infty(t) + \alpha\, u_\infty(t) - g(t) = 0, \\ u_\infty(t) = \sigma u_\infty(t - T). \end{gathered}$$

We apply the Laplace transform to the function $\mathring{u} = u - u_\infty$

$$\mathfrak{L}\{\mathring{u}\}(s) = \int_0^\infty e^{-st} (u - u_\infty)(t) dt.$$

Our original problem then classically reduces to

$$\beta s\,\mathfrak{L}\{\mathring{u}\}(s) - \beta\phi(0) + (\alpha+\gamma)\,\mathfrak{L}\{\mathring{u}\}(s) - \gamma\sigma\,e^{-Ts}\mathfrak{L}\{\mathring{u}\}(s) - \gamma\sigma\Phi(s) = 0,$$

where $\Phi(s)$ is defined from the initial data:

$$\Phi(s) = e^{-Ts}\int_{-T}^{0}\phi(t)\,e^{-st}\,dt.$$

The Laplace transform of $\mathring{u} = u - u_\infty$ is thus given by

$$\mathfrak{L}\{\mathring{u}\}(s) = \frac{\beta\phi(0) + \gamma\sigma\Phi(s)}{\beta s + (\alpha+\gamma) - \gamma\sigma\,e^{-Ts}}. \tag{3.5}$$

Its poles λ_k are roots of the denominator, i.e. satisfy the transcendental equation

$$\lambda + (\alpha+\gamma)/\beta - (\gamma\sigma/\beta)\,e^{-T\lambda} = 0.$$

Multiplying by $Te^{T(\lambda+\alpha/\beta+\gamma/\beta)}$, we obtain

$$T\,(\lambda + \alpha/\beta + \gamma/\beta)\,e^{T(\lambda+\alpha/\beta+\gamma/\beta)} = (T\gamma\sigma/\beta)\,e^{T(\alpha+\gamma)/\beta}. \tag{3.6}$$

To represent a solution of this equation, let us introduce the Lambert W function [Corless et al. 1996, Shinozaki 2007, Yi et al. 2010]. It is a complex-valued function denoted by $W\,[z]$ and satisfying $W\,[z]\,e^{W[z]} = z$, $\forall z \in \mathbb{C}$. See Appendix A for a brief overview. Note that the Lambert W function is multivalued and has an infinite number of branches W_k, $k \in \mathbb{Z}$. Thus, the characteristic equation (3.6) has an infinite number of roots corresponding to different branches W_k of the Lambert function:

$$\lambda_k = -\frac{1}{\beta}\,(\alpha+\gamma) + \frac{1}{T}\,W_k\left[\frac{T}{\beta}\,\gamma\sigma\,e^{T(\alpha+\gamma)/\beta}\right], \qquad k \in \mathbb{Z}. \tag{3.7}$$

All these poles are simple. Using then the Cauchy residue theorem, the inverse transform of (3.5) takes the form

$$u(t) - u_\infty(t) = \sum_{k\in\mathbb{Z}} u_k\,e^{\lambda_k\,t}.$$

Its rate of convergence to zero is controlled by the real parts of the poles λ_k. Coefficients u_k are obtained using the L'Hôpital's rule:

$$\begin{aligned} u_k = \operatorname*{Res}_{s\to\lambda_k}\mathfrak{L}\{\mathring{u}\}(s) &= \lim_{s\to\lambda_k}\frac{(s-\lambda_k)(\beta\phi(0)+\gamma\sigma\Phi(s))}{\beta s + (\alpha+\gamma) - \gamma\sigma\,e^{-Ts}} \\ &= \frac{\beta\phi(0)+\gamma\sigma\Phi(\lambda_k)}{\beta + T\gamma\sigma e^{-\lambda_k T}}. \end{aligned} \tag{3.8}$$

□

Remark 4. *At the limit β goes to zero, when $\mathfrak{Re}\alpha > 0$ and if we choose the gain γ as a function $\gamma(\beta)$ such that*

$$\lim_{\beta\to 0}\gamma(\beta) = 0 \quad \textit{and} \quad \lim_{\beta\to 0}\frac{T}{\beta}\,\gamma(\beta)\,e^{T(\alpha+\gamma(\beta))/\beta} \leq C,$$

then the transient solution $u_k e^{\lambda_k t}$ behaves asymptotically at worst like $e^{-\alpha t/\beta}$ which converges exponentially fast towards zero for small values of β. At the limit $\beta = 0$, the asymptotic solution $g(t)/\alpha$ is reached instantaneously.

To prove our fundamental result, we also introduce a spectral representation of operators $\hat{B} = A^{-1}B$ and S using the spectral theorem (multiplication representation version) for normal operators commuting together (see [de Dormale and Gautrin 1975, Kowalski 2009, Jazar 2004, Weidmann 2012]).

Proposition 4 (Spectral representation)**.** *Under our assumptions, endowing $\mathcal{H}$ with the scalar product $\langle A\,\cdot\,,\,\cdot\rangle$, the operator $\hat{B}$ is self-adjoint. Indeed, B being symmetric, we have for $\hat{B}:\mathcal{H}\to\mathcal{H}$ that*

$$\langle A\hat{B}u,\,v\rangle = \langle Bu,\,v\rangle = \langle u,\,Bv\rangle = \langle u,\,A\hat{B}v\rangle = \langle Au,\,\hat{B}v\rangle.$$

Moreover, since B and S commute, $\hat{B}$ and S commute with respect to the inner product $\langle A\,\cdot\,,\,\cdot\rangle$, that is

$$\langle A\hat{B}Su,\,v\rangle = \langle BSu,\,v\rangle = \langle Bu,\,S^*v\rangle = \langle A\hat{B}u,\,S^*v\rangle = \langle AS\hat{B}u,\,v\rangle.$$

Since S commutes with its adjoint $S^* = S^{-1}$, like for any normal operator, we can write $S = S_1 + \mathrm{i}\,S_2$, where $S_1 = \frac{1}{2}(S+S^*)$ and $S_2 = \frac{1}{2\mathrm{i}}(S-S^*)$ are self-adjoint and commuting. Then S_1, S_2 and $\hat{A}$ are two-by-two commuting self-adjoint operators, so there exists a spectral representation (see [de Dormale and Gautrin 1975, Theorem 4]), i.e. there exists a finite measure space (Y,μ), together with measurable complex-valued functions on Y β and σ , and a unitary map $U:\mathcal{H}\mapsto L^2(Y,\mu)$, such that $\forall\, v\in\mathcal{H}$

$$U\hat{B}v = \beta\,Uv,$$
$$USv = \sigma\,Uv.$$

Since $\hat{G} = A^{-1}G$ is supposed to be analytical function of $\hat{B}$ and S, there will exist a complex valued function γ defined on Y such that we have

$$U\hat{G}v = \gamma\,Uv,$$
$$U\hat{G}Sv = \gamma\,USv = \gamma\sigma\,Uv.$$

Besides, since $\hat{B}$ is positive and bounded, and S is unitary on $\mathcal{H}$, then β is non-negative (possibly zero) and bounded, and $|\sigma| = 1$ on Y.

Theorem 1 (General solution of a controlled problem)**.** *Under our assumptions, the solution to our controlled problem (3.3) is given by :*

$$u(t) = U^{-1}\left(\sum_{k\in\mathbb{Z}} u_k\, e^{\lambda_k\, t}\right) + u_\infty(t),$$

where λ_k are measurable complex-valued functions on Y, $u_k \in L^2(Y,\mu)$ are defined from the initial data $\phi(0)$ and $u_\infty(t) : \mathbb{R} \mapsto \mathcal{H}$ is the space-time periodic solution of the problem.

Proof. After multiplication by A^{-1}, the controlled problem (3.3) writes

$$\begin{aligned} \hat{B}\,\partial_t u + u(t) + \hat{G}\,(u(t) - Su(t-T)) - A^{-1}f(t) = 0 \in \mathcal{H}, \qquad & t > 0 \\ u(t) = \phi(t), \qquad & t \in [-T,\, 0]. \end{aligned}$$

According to Proposition 4, we define $\tilde{u}(t,y) = Uu \in L^2(Y,\mu)$, where $y \in Y$ defines a spectral index. After multiplication by U, the problem becomes

$$\beta\partial_t\tilde{u}(t,y) + (1+\gamma)\,\tilde{u}(t,y) - \gamma\sigma\,\tilde{u}(t-T,y) - (UA^{-1}f)(t,y) = 0 \in Y,$$

and for a given y, its solution is provided by Lemma 4. Hence, the solution to problem (3.3) is

$$u(t) = U^{-1}\left(\sum_{k\in\mathbb{Z}} u_k(y)\, e^{\lambda_k(y)\, t} + \tilde{u}_\infty(t)\right)$$

with u_k defined by (3.8), λ_k by (3.7) and $\tilde{u}_\infty(t)$ by

$$\tilde{u}_\infty(t,y) = \int_0^\infty e^{-s}\,(UA^{-1}f)(t-\beta s, y)ds.$$

Observe that by construction $\tilde{u}_\infty(t,y) \in L^\infty(\mathbb{R}; L^2(Y,\mu))$ if $f \in L^\infty(\mathbb{R};\mathcal{H}')$, meaning that the space time periodic solution $u_\infty = U^{-1}\tilde{u}_\infty$ that we have exhibited is well defined in $L^\infty(\mathbb{R};\mathcal{H})$. Since in the absence of control ($\gamma = 0$), we have $\mathfrak{Re}\lambda_k(y) = -\frac{1}{\beta} < -\frac{1}{\beta_{max}}$, we also see that the solution of the initial value problem does converge asymptotically in time to the space time periodic solution of the problem. So does the controlled solution if we can construct a control G such that $\mathfrak{Re}\lambda_k(y)$ is uniformly negative. This will be the purpose of Section 3.2.3. □

3.2.3 Optimal gain operator

The next theorem presents the main result of the current chapter, namely the characterization of the optimal control for the problem (3.3).

Theorem 2. *Under the assumptions of Section 3.2.1, the optimal gain operator for the problem (3.3), providing the fastest convergence to the asymptotic solution, is given by*

$$G_{opt} = -\frac{1}{T}\, B \sum_{n=1}^{\infty} c_n \cdot \left(e^{-T\, B^{-1} A}\, S^{-1}\right)^n \quad \textit{with} \;\; c_n = \frac{n^{n-1}}{n!\, e^n}. \tag{3.9}$$

When B is not invertible, the quantity $e^{-T\, B^{-1} A}$ corresponds to the well defined limit $\lim_{\epsilon \to 0} e^{-T\,(B+\epsilon A)^{-1} A}$.

Proof. According to Theorem 1 (keeping its notations), the difference between the solution of the controlled problem and the asymptotic solution is in the form:

$$u(t) - u_\infty(t) = U^{-1} \left(\sum_{k \in \mathbb{Z}} u_k\, e^{\lambda_k\, t} \right).$$

When $\mathfrak{Re}\lambda_k < 0$ for all k , the solution converges in time to the asymptotic limit, corresponding to the space time periodic solution of the problem. We accelerate convergence by decreasing their real part which, according to (3.7), can be achieved by acting on the spectrum γ of $\hat{G}$ to be optimized in function of the spectra β and σ of $\hat{B}$ and S. According to (A.2), the principal branch λ_0 is always the rightmost. So the optimal control, providing the fastest convergence, moves λ_0 on the left as much as possible. Let us consider it as a function of γ:

$$\lambda_0 = -1/\beta - \underbrace{\left(\gamma/\beta - \frac{1}{T}\, W_0 \left[\frac{T}{\beta} \sigma\gamma\, e^{T(\gamma+1)/\beta} \right] \right)}_{\text{controlled part of the spectrum}}.$$

Let us also introduce the accelerating term

$$J(\gamma) = \mathfrak{Re} \left(\gamma/\beta - \frac{1}{T}\, W_0 \left[\frac{T}{\beta} \sigma\gamma\, e^{T(\gamma+1)/\beta} \right] \right), \qquad \gamma \in \mathbb{C},$$

which defines the acceleration of convergence of the controlled problem as function of the gain spectrum γ. For the non-controlled solution, when $\gamma \equiv 0$, this term is zero. Convergence slows down relative to the non-controlled case, if J is negative, and accelerates, if it is positive. Thus we are looking for the optimal γ_{opt} providing the maximum of $J(\gamma)$:

$$\gamma_{opt} = \arg \max_{\gamma \in \mathbb{C}} J(\gamma).$$

We can prove (see Appendix B) that this maximum is attained at

$$z := \frac{T}{\beta} \sigma\gamma\, e^{T(\gamma+1)/\beta} = -1/e$$

and that we have thus

$$\begin{aligned}\gamma_{opt} &= \frac{\beta}{T} W_0\left[-\tfrac{1}{e}\,\sigma^{-1}e^{-T/\beta}\right] \\ &= -\frac{\beta}{T}\sum_{n=1}^{\infty}\frac{n^{n-1}}{n!\,e^n}\cdot\left(\sigma^{-1}e^{-T/\beta}\right)^n, \\ J_{opt} &= \frac{1}{T}\left(\mathfrak{Re}W_0\left[-e^{-T/\beta-1}\sigma^{-1}\right] - W_0(e^{-1})\right),\end{aligned}$$

where we have used the representation (A.3) of W_0 which is legal since we have $|\sigma^{-1}e^{-T/\beta}| = |e^{-T/\beta}| < 1$. Observe that this choice does satisfy the convergence criteria of Remark 4:

$$\lim_{\beta\to 0}\gamma_{opt} = 0 \quad \text{and} \quad \lim_{\beta\to 0}\frac{T}{\beta}\,\gamma_{opt}\,e^{T(\alpha+\gamma_{opt})/\beta}\sigma = -1/e.$$

Returning back to the operator terms, under the notation $c_n = \dfrac{n^{n-1}}{n!\,e^n}$ and using the series expansion of the exponential, the optimal gain operator becomes

$$\begin{aligned}G_{opt} &= AU^{-1}\gamma_{opt}U \\ &= -\frac{1}{T}AU^{-1}\beta\left(\sum_{n=1}^{\infty}c_n\cdot\left(e^{-T/\beta}\sigma^{-1}\right)^n\right)U \\ &= -\frac{1}{T}AU^{-1}\beta U\left(\sum_{n=1}^{\infty}c_n\cdot\left(U^{-1}e^{-T/\beta}UU^{-1}\sigma^{-1}U\right)^n\right) \\ &= -\frac{1}{T}A\hat{B}\left(\sum_{n=1}^{\infty}c_n\cdot\left(\left\{\sum_{k=0}^{\infty}(-TU^{-1}\frac{1}{\beta}U)^k/k!\right\}U^{-1}\sigma^{-1}U\right)^n\right) \\ &= -\frac{1}{T}A\hat{B}\left(\sum_{n=1}^{\infty}c_n\cdot\left(\left\{\sum_{k=0}^{\infty}(-T\hat{B}^{-1})^k/k!\right\}S^{-1}\right)^n\right) \\ &= -\frac{1}{T}\,B\sum_{n=1}^{\infty}c_n\cdot\left(e^{-T\,\hat{B}^{-1}}\,S^{-1}\right)^n \\ &= -\frac{1}{T}\,B\sum_{n=1}^{\infty}c_n\cdot\left(e^{-T\,B^{-1}A}\,S^{-1}\right)^n.\end{aligned}$$

□

Remark 5. *Note that $e^{-t\,B^{-1}A}$ is a fundamental solution of the non-controlled problem, i.e. $u(t,x) = e^{-t\,B^{-1}A}u(0,x)$, when $G \equiv 0$ and $f \equiv 0$. That is $e^{-T\,B^{-1}A}$ plays role of the T-shift in time for the non-controlled solution. Thus the proposed control can be interpreted as a correction of the present solution by combining all*

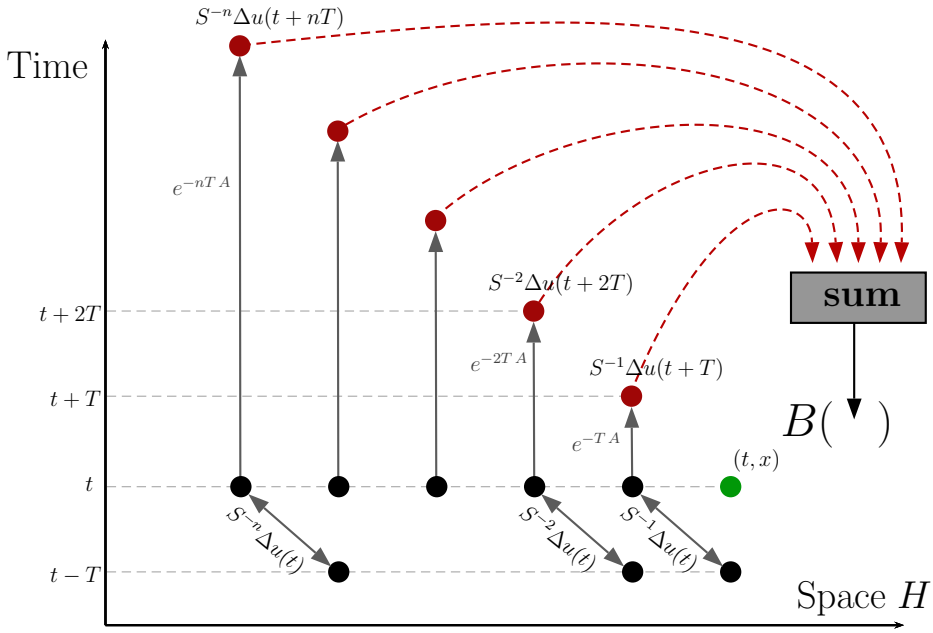

Figure 3.1: Geometrical interpretation of the control term at (t, x), which combines all the "future" space-time shifted periodicity errors Δu inside the evolution term B.

the "future" space-time shifted periodicity errors inside the evolution term B (see Figure 3.1):

$$G_{opt}\Delta u(t) \simeq -\frac{1}{T}\, B \sum_{n=1}^{\infty} c_n\, S^{-n}\Delta u(t+nT),$$

where the periodicity error is defined by $\Delta u(t) = u(t) - Su(t-T)$. Remark that the control is non-local by construction, since it uses the periodicity errors computed at shifted locations.

3.2.4 Efficiency analysis

We have developed an optimal control for an abstract evolution problem, accelerating convergence to the periodic solution. Now we want to estimate the efficiency of the proposed control. It is characterized by the ratio η between the

real parts of the controlled and non-controlled poles:

$$\begin{aligned}\eta := \frac{\lambda_0}{1/\beta} &= \frac{1/\beta + J_{opt}}{1/\beta} \\ &= 1 + \frac{\beta}{T}\left(1 + \mathfrak{Re} W_0\left[-e^{-T/\beta - 1}\sigma^{-1}\right]\right), \\ &\geq 1 + \frac{\beta}{T}\left(1 + W_0\left[-e^{-T/\beta - 1}\right]\right),\end{aligned}$$

where the inequality comes from (A.4), given $|\sigma^{-1}| = 1$. Thus the acceleration ratio can be estimated from below:

$$\eta \geq g\left(\beta/T\right)$$

with the minorant function g given by

$$g(x) = 1 + x\left(1 + W_0\left[-e^{-1/x - 1}\right]\right), \qquad x \in \mathbb{R}.$$

So the efficiency estimator g is a function of the original problem relaxation time $\tau = \beta$ normalized by the time period T (see Figure 3.2).

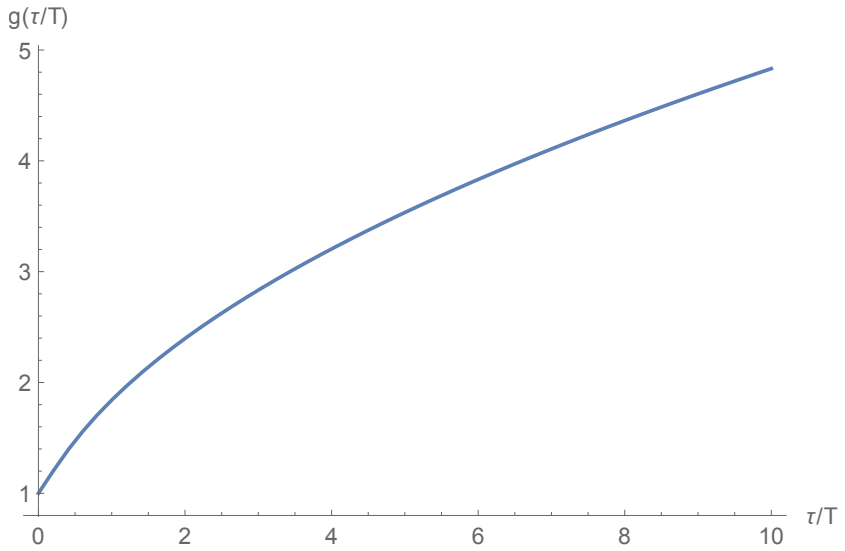

Figure 3.2: Efficiency estimator $g(\tau/T)$, a minorant of the acceleration ratio η, as a function of the original problem relaxation time τ normalized by the time period T.

We can conclude that the acceleration, provided by the optimal control, grows with the relaxation time of the problem. While there is no gain when the non-controlled solution converges very fast (which is the case where no acceleration

is required), the efficiency increases when memory effects grows, that is when the underlying problem becomes more and more "viscous". Thus the proposed control method is much more efficient for the slowly convergent problems.

Note that the efficiency depends also on the time period T, that means the method is more efficient for small periods. In the limit case, when $T \to 0$, the controlled problem converges immediately towards the steady solution.

3.2.5 Quasi-optimal practical approach

The application of the proposed control requires to compute $e^{-T\,B^{-1}A}$. However, computation of an operator exponential is quite expensive. In a finite element framework, this amounts to compute the exponential of a very large matrix. Moreover the matrix vector multiplication is very expensive because a matrix exponential is not sparse in general. So if we want to use the proposed control technique in practice, we have to develop a more convenient (cheaper and simpler) approach, avoiding the matrix exponential calculation.

The idea is to optimize only the active pole. Indeed, asymptotically only the active pole is responsible for the rate of convergence, so any control minimizing the greatest pole provides asymptotically the same gain as the optimal one.

Let us be more precise. Recall that the optimal gain operator

$$G_{opt} = -\frac{1}{T}\,B\sum_{n=1}^{\infty} c_n \cdot \left(e^{-T\,B^{-1}A}\,S^{-1}\right)^n \quad \text{with} \;\; c_n = \frac{n^{n-1}}{n!\,e^n} \tag{3.10}$$

has the spectrum

$$\gamma^{opt}(y) = \frac{\beta(y)}{T}\,W_0\left[-\tfrac{1}{e}\,e^{-T/\beta(y)}\sigma(y)^{-1}\right]$$

with $\beta(y)$ and $\sigma(y)$, $|\sigma| = 1$, representing respectively the spectra of $A^{-1}B$ and S, where y is a spectral index (omitted further for the sake of simplicity). That yields convergence rates of the different branches $k \in \mathbb{Z}$, given in (3.7), by

$$\lambda_k^{opt} = -\frac{1}{\beta} - \frac{1}{T}\left(W_0\left[-\tfrac{1}{e}\,e^{-T/\beta}\sigma^{-1}\right] - W_k\left[-e^{-1}\right]\right),$$

with the principle branch (which is the rightmost among all k)

$$\lambda_0^{opt} = -\frac{1}{\beta} - \frac{1}{T}\left(W_0\left[-\tfrac{1}{e}\,e^{-T/\beta}\sigma^{-1}\right] + 1\right).$$

Let us consider now a simplified gain operator

$$G_{\hat\alpha} = -\frac{1}{T}\,B\sum_{n=1}^{\infty} c_n \cdot \left(e^{-T\,\hat\alpha}\,S^{-1}\right)^n, \qquad \hat\alpha \in \mathbb{R}_+, \tag{3.11}$$

which is a modification of the optimal one (3.10), where the operator $A^{-1}B$ in the exponential is replaced by $\hat{\alpha}\cdot\mathrm{Id}$, $\hat{\alpha} \in \mathbb{R}_+$. Construction of such an operator requires computing only a scalar exponential. Spectrum of this operator is

$$\gamma^{\hat{\alpha}}(y) = \frac{\beta(y)}{T} W_0\left[-\tfrac{1}{e}\, e^{-T\hat{\alpha}} \sigma(y)^{-1}\right],$$

which by definition of W_0 satisfies

$$\frac{T\gamma^{\hat{\alpha}}}{\beta} e^{\frac{T\gamma^{\hat{\alpha}}}{\beta}} = -\frac{1}{e}\, e^{-T\hat{\alpha}} \sigma^{-1}.$$

Remark that $\hat{\alpha}$ does not depend on y, that is, it does not change over the spectral space. The associated convergence rate is now from a direct application of (3.7)

$$\lambda_0^{\hat{\alpha}}(y) = -\frac{1}{\beta(y)} - \frac{1}{T}\left(W_0\left[-\tfrac{1}{e}\,\sigma(y)^{-1} e^{-T\hat{\alpha}}\right] - W_0\left[-e^{T(1/\beta(y)-\hat{\alpha})-1}\right]\right). \tag{3.12}$$

We claim that the best choice of the scalar $\hat{\alpha}$ in the simplified gain operator (3.11), allowing approximate the optimal gain (3.10), is the minimal generalized eigenvalue α_0 of A and B:

$$\begin{aligned}\alpha_0 &= \min\{\alpha > 0 \mid \exists v \in \mathcal{H} \ :\ Av = \alpha Bv\} \\ &= \frac{1}{\max\{\beta > 0 \mid \exists v \in \mathcal{H} \ :\ Bv = \beta Av\}}.\end{aligned}$$

So the simplified gain operator becomes

$$G_{m.e.} = -\frac{1}{T}\, B \sum_{n=1}^{\infty} c_n \cdot \left(e^{-T\alpha_0}\, S^{-1}\right)^n, \tag{3.13}$$

where the subscript "m.e." is after "minimal eigenvalue". The associated convergence rate is

$$\lambda_0^{m.e.}(y) = -\frac{1}{\beta(y)} - \frac{1}{T}\left(W_0\left[-\tfrac{1}{e}\,\sigma(y)^{-1} e^{-T\alpha_0}\right] - W_0\left[-e^{T(1/\beta(y)-\alpha_0)-1}\right]\right).$$

It is easily seen, that for y_0, such that $1/\beta(y_0) = \alpha_0$, we have $\lambda_0^{m.e.}(y_0) = \lambda_0^{opt}(y_0)$. However, it is not clear that y_0 provides the leading exponent over the whole spectrum. The following theorem states the relation between the leading exponents for the optimal and minimal eigenvalue gain operators.

Theorem 3. *The poles, provided by the optimal and the minimal eigenvalue controls, have the same upper bound:*

$$\max_{\substack{1/\beta \geq \alpha_0 \\ |\sigma| = 1}} \mathfrak{Re}(\lambda_0^{m.e.}) = \max_{\substack{1/\beta \geq \alpha_0 \\ |\sigma| = 1}} \mathfrak{Re}(\lambda_0^{opt}) \tag{3.14}$$

Proof. Let us consider λ_0^{opt} and $\lambda_0^{m.e.}$ as functions of $\alpha \stackrel{\text{def}}{=} 1/\beta$ and σ:

$$\lambda_0^{opt}(\alpha,\sigma) = -\alpha - \frac{1}{T}\left(W_0\left[-\tfrac{1}{e}\,\sigma^{-1}e^{-T\alpha}\right]+1\right),$$
$$\lambda_0^{m.e.}(\alpha,\sigma) = -\alpha - \frac{1}{T}\left(W_0\left[-\tfrac{1}{e}\,\sigma^{-1}e^{-T\alpha_0}\right] - W_0\left[-\tfrac{1}{e}\,e^{T(\alpha-\alpha_0)}\right]\right).$$

It is easy to see that both poles are equal at $\alpha=\alpha_0$ and $\sigma=1$:

$$\lambda_0^{m.e.}(\alpha_0,1) = -\alpha_0 - \frac{1}{T}\left(W_0\left[-\tfrac{1}{e}\,e^{-T\alpha_0}\right]+1\right) = \lambda_0^{opt}(\alpha_0,1). \tag{3.15}$$

First, let us see that

$$\mathfrak{Re}\lambda_0^{opt}(\alpha_0,1) = \max_{\substack{\alpha\,\geq\,\alpha_0\\ |\sigma|\,=\,1}} \mathfrak{Re}\lambda_0^{opt}(\alpha,\sigma). \tag{3.16}$$

This follows from the fact that for σ, such that $|\sigma|=1$, and $\alpha\geq\alpha_0>0$, it holds

$$\mathfrak{Re}W_0\left[-\tfrac{1}{e}\sigma^{-1}e^{-T\alpha}\right] \geq \mathfrak{Re}W_0\left[-\tfrac{1}{e}e^{-T\alpha}\right] \geq \mathfrak{Re}W_0\left[-\tfrac{1}{e}e^{-T\alpha_0}\right],$$

where (A.4) is used for the first inequality.

Now, in order to prove that

$$\mathfrak{Re}\lambda_0^{m.e.}(\alpha_0,1) = \max_{\substack{\alpha\,\geq\,\alpha_0\\ |\sigma|\,=\,1}} \mathfrak{Re}\lambda_0^{m.e.}(\alpha,\sigma), \tag{3.17}$$

we consider the difference

$$T\left(\lambda_0^{m.e.}(\alpha_0,1) - \lambda_0^{m.e.}(\alpha,\sigma)\right) = T(\alpha-\alpha_0) - 1 - W_0\left[-e^{T(\alpha-\alpha_0)-1}\right] - W_0\left[-e^{-T\alpha_0-1}\right] + W_0\left[-\sigma^{-1}e^{-T\alpha_0-1}\right].$$

Using again (A.4), we have for all $\sigma\in\mathbb{C}$, $|\sigma|=1$, and all $\alpha_0>0$ that

$$\mathfrak{Re}W_0\left[-\tfrac{1}{e}e^{-T\alpha_0}\right] \leq \mathfrak{Re}W_0\left[-\tfrac{1}{e}\sigma^{-1}e^{-T\alpha_0}\right].$$

Thus, we have

$$T\cdot\mathfrak{Re}\left(\lambda_0^{m.e.}(\alpha_0,1) - \lambda_0^{m.e.}(\alpha,\sigma)\right) \geq \mathfrak{Re}\left(T(\alpha-\alpha_0) - 1 - W_0\left[-e^{T(\alpha-\alpha_0)-1}\right]\right).$$

To estimate the right hand side, we examine the function

$$f(x) = \mathfrak{Re}\left(x - W_0\left[-e^x\right]\right), \qquad x\geq -1.$$

Its derivative is

$$\partial_x f(x) = \mathfrak{Re}\left(1 - \frac{W_0\left[-e^x\right]}{1+W_0\left[-e^x\right]}\right) = \mathfrak{Re}\left(\frac{1}{1+W_0\left[-e^x\right]}\right).$$

Recall that $1 + \mathfrak{Re} W_0[z] \geq 0$ for all $z \in \mathbb{C}$. So $\partial_x f(x) \geq 0$ for all x. That is, the function $f(x)$ is increasing with $x \in \mathbb{R}$. Furthermore, it is easy to see that $f(-1) = 0$. Hence, substituting x by $T(\alpha - \alpha_0) - 1$, we obtain for $\alpha \geq \alpha_0$

$$\mathfrak{Re}\left(T(\alpha - \alpha_0) - 1 - W_0\left[-e^{T(\alpha-\alpha_0)-1}\right]\right) \geq 0,$$

which proves (3.17).

The statement of the theorem follows from (3.15), (3.16) and (3.17). □

Corollary 2. *If the minimal mode of $B^{-1}A$ (i.e. associated to α_0) is S-periodic (thus associated to $\sigma = 1$), the minimal eigenvalue control $G^{m.e}$ provides **exactly the same** rate of convergence of the initial value problem solution to the periodic state than the optimal control G^{opt}.*

If the minimal mode is not S-periodic, we expect anyway, due to the upper bound (3.14), the rate of convergence of the modified control to be close to the optimal one.

Proposition 5. *In the general case, when the spectrum of $B^{-1}A$ is complex, we can use the polar decomposition of the monodromy operator $\Phi = e^{-T\,B^{-1}A} = \sqrt{\Phi^t\Phi}\,Q$, where $\sqrt{\Phi^t\Phi}$ denotes the unique positive square root of $\Phi^t\Phi$ and Q is a unitary operator. So (3.10) can be rewritten as*

$$\begin{aligned} G_{opt} &= -\frac{1}{T}\,B\sum_{n=1}^{\infty} c_n \cdot \left(\sqrt{\Phi^t\Phi}\,Q\,S^{-1}\right)^n \\ &= -\frac{1}{T}\,B\sum_{n=1}^{\infty} c_n \cdot \left(\sqrt{\Phi^t\Phi}\;\hat{S}^{-1}\right)^n \end{aligned} \tag{3.18}$$

with a redefined shift $\hat{S} = SQ^t$. All the above results can be applied in this case, and the practical version of the gain operator (3.18) can thus be written as

$$G_{opt} = -\frac{1}{T}\,B\sum_{n=1}^{\infty} c_n \cdot \left(e^{-T\alpha_0}\;\hat{S}^{-1}\right)^n,$$

where the scalar α_0 is such that $e^{-T\alpha_0} = \|\Phi\|$ is the spectral norm of the monodromy operator.

If the operator $B^{-1}A$ is normal, i.e. $(B^{-1}A)^t(B^{-1}A) = (B^{-1}A)(B^{-1}A)^t$, then α_0 is the minimal eigenvalue of the symmetric part of $B^{-1}A$ and $Q = e^{-T(B^{-1}A)_{asym}}$, where $(\,)_{asym}$ denotes the asymmetric part.

Remark 6. *If in the simplified gain operator (3.11) we take $\hat{\alpha}$ such that $0 < \hat{\alpha} < \alpha_0$, then $-e^{T(1/\beta(y)-\hat{\alpha})-1} < -\frac{1}{e}$ for all y and thus the last term in (3.12) will always provide a non-zero imaginary part*

$$\mathfrak{Im}\{W_0\left[-e^{T(1/\beta(y)-\hat{\alpha})-1}\right]\} \neq 0 \quad \forall y.$$

So, in this case, all the exponents $\lambda_k^{\hat{\alpha}}$, $k \in \mathbb{Z}$, will have, generally speaking, an imaginary part, which will generate an oscillating solution. Moreover, when $\hat{\alpha}$ approaches zero, the above imaginary part grows, and thus the oscillation periods become smaller. Meanwhile, the real part of $\lambda_k^{\hat{\alpha}}$ increases, and thus, although locally the oscillations could accelerate the convergence, asymptotically it slows down with $\hat{\alpha}$ going to zero ($\hat{\alpha} < \alpha_0$).

Remark 7. *Our feedback control with the quasi-optimal gain (3.13) has been constructed on the space-continuous problem with infinite dimensional space $\mathcal{H}$. As it will be confirmed further by the numerical experiments, finite element approximation does not alter the optimality of the control. The analysis can be identically applied to the finite element version with a formula (3.13), which converges to the continuous limit when the space discretization step goes to zero.*

3.2.6 Time-discrete feedback

The optimal time controlled problem that we have defined above assumes that we use exact time integration of the space time periodic solution and of the uncontrolled or controlled initial value problems. Numerical time integration affects the space time periodic solution and impacts the efficiency of our optimally controlled problem, thus limiting the practical efficiency of our proposed technique in practical applications. To restore or even improve the performances of our controlled problem in presence of numerical time integration, we need to construct the optimal control for the time discretized problem. There are two ways to do this. The first consists in time discretization of the controlled problem with the optimal gain, discussed before. In the second way to be followed hereafter, we discretize in time the non-controlled problem before applying the control. Then we modify the discretized equation through the delayed feedback control term. In this case, the optimal gain operator has to be constructed, which is the purpose of the present section.

Let us thus divide the period T by $m \in \mathbb{Z}$ time steps $\Delta t = T/m$, and define the time discrete approximations $u_i = u(t_i)$, $t_i = i\Delta t$, $i \in \mathbb{Z}$. Then the implicit Euler scheme for the abstract homogeneous problem (3.1) writes

$$B\frac{u_i - u_{i-1}}{\Delta t} + Au_i = 0.$$

The time-discretization of the associated controlled problem 3.1 then becomes

$$B\frac{u_i - u_{i-1}}{\Delta t} + Au_i + G\left(u_i - Su_{i-m}\right) = 0. \tag{3.19}$$

The optimal form (3.9) of the gain operator G has been developed for the time-continuous problem (3.1), that is it is optimal for the case $m \to \infty$. Now we want to construct the optimal gain for a time-discrete problem (3.19). To do this

in all generality, let us consider an abstract time scheme for the homogeneous problem (3.1):

$$u_i = \mathcal{W}_{\Delta t}\, u_{i-1},$$

where the forward operator $\mathcal{W}_{\Delta t} = \mathcal{W}_{\Delta t}(\Delta t; A, B)$ is a function of A and B, defined by the choice of the time scheme. For example, in the implicit Euler case, we have $\mathcal{W}_{\Delta t} = (B + \Delta t\, A)^{-1} B$. Then we modify this discrete problem by introducing a feedback control term, based on the periodicity error:

$$u_i = \mathcal{W}_{\Delta t}\, u_{i-1} - \mathcal{G}(u_i - S u_{i-m}), \tag{3.20}$$

where the discrete gain operator $\mathcal{G}$ has to be constructed such that the convergence to the limit cycle be the fastest. Note that in order to recover the abstract form (3.20) from (3.19) in the implicit Euler case, we should set $G = (B\,\Delta t^{-1} + A)\,\mathcal{G}$. Putting all u_i terms on the left to obtain

$$(\mathrm{Id} + \mathcal{G}) u_i = \mathcal{W}_{\Delta t}\, u_{i-1} + \mathcal{G} S u_{i-m},$$

and using spectral representation of $\mathcal{W}_{\Delta t}$, $\mathcal{G}$ and S, we write the problem in spectral form

$$(1+\gamma) u_i = w u_{i-1} + \gamma\sigma u_{i-m},$$

where w, γ and σ are the spectra of $\mathcal{W}_{\Delta t}$, $\mathcal{G}$ and S respectively. The general solution of this induction formula is of the form $u_i = \sum_{p=1}^{m} \hat{u}_p z_p^i$, where $\hat{u}_p$ are the weights of the poles z_p, which are solutions of the polynomial equation

$$(1+\gamma) z^i = w z^{i-1} + \gamma\sigma z^{i-m}.$$

Excluding zero solution, we divide it by z^{i-m}:

$$(1+\gamma) z^m - w z^{m-1} - \gamma\sigma = 0. \tag{3.21}$$

Considering the solution $z = z(\gamma)$ as a function of the control γ, we want to find the optimal γ_{opt}, which provides the minimum of $|z|$. That is, we are looking for

$$\gamma_{opt} = \arg\min_{\gamma\in\mathbb{C}} z(\gamma).$$

According to the theoretical analysis of the optimal control in the continuous case (Section 3.2.3), the fastest convergence is reached in the point, where the derivative of solution with respect to the control γ explodes. Thus, taking derivative with respect to γ in the polynomial equation (3.21) gives

$$z^m + (1+\gamma)\, m z^{m-1} \frac{\partial z}{\partial \gamma} - w\,(m-1) z^{m-2} \frac{\partial z}{\partial \gamma} - \sigma = 0.$$

Hence, the derivative is

$$\frac{\partial z}{\partial \gamma} = \frac{z^m - \sigma}{(1+\gamma)\, m z^{m-1} - w\,(m-1) z^{m-2}}.$$

Then the non-zero solution, exploding the derivative, is provided by

$$(1+\gamma)mz^{m-1} = w(m-1)z^{m-2}.$$

Hence, we have

$$z = \frac{w}{1+\gamma}\,(1-1/m).$$

Substituting this back to the polynomial equation (3.21), we obtain the equation, defining the optimal γ:

$$\frac{w^m}{(1+\gamma)^{m-1}}\,(1-1/m)^m - \frac{w^m}{(1+\gamma)^{m-1}}\,(1-1/m)^{m-1} - \gamma\sigma = 0.$$

Rearranging, we have

$$(1+\gamma)^{m-1}\gamma = \underbrace{-\frac{1}{m-1}\,(1-1/m)^m w^m \sigma^{-1}}_{=y}. \tag{3.22}$$

Let us denote the right hand side by $y = -\frac{1}{m-1}\,(1-1/m)^m w^m \sigma^{-1}$ and introduce the function $f(\gamma) = (1+\gamma)^{m-1}\gamma$. Then the optimal γ solves

$$f(\gamma) = y.$$

To obtain a solution we use Lagrange inversion theorem at some point γ_0:

$$\gamma = \gamma_0 + \sum_{n=1}^{\infty} \hat{c}_n \frac{(y - f(\gamma_0))^n}{n!},$$

where

$$\hat{c}_n = \lim_{\gamma\to\gamma_0} \frac{d^{n-1}}{d\gamma^{n-1}} \left(\frac{\gamma-\gamma_0}{f(\gamma)-f(\gamma_0)}\right)^n.$$

At $\gamma_0 = 0$ it gives

$$\gamma = \sum_{n=1}^{\infty} \hat{c}_n \frac{y^n}{n!},$$

with

$$\begin{aligned}
\hat{c}_n &= \lim_{\gamma\to 0} \frac{d^{n-1}}{d\gamma^{n-1}} \left(\frac{1}{(1+\gamma)^{m-1}}\right)^n \\
&= (-1)^{n-1}((m-1)n)((m-1)n+1)((m-1)n+2)\dots((m-1)n+n-2) \\
&= (-1)^{n-1}(mn-n)(mn-(n-1))\dots(mn-3)(mn-2).
\end{aligned}$$

So the optimal γ is defined by the series

$$\gamma = -\frac{1}{m}\sum_{n=1}^{\infty} c_{m,n}\, w^{mn}\sigma^{-n},$$

with coefficients

$$c_{m,n} = \frac{1}{n!} \cdot \frac{\big((m-1)n\big)_{n-1}}{(m-1)^{n-1}} \cdot \left(1 - \frac{1}{m}\right)^{mn-1}, \tag{3.23}$$

where $(k)_n$ denotes the Pochhammer symbol:

$$(k)_n = k(k+1)(k+2)\dots(k+n-1).$$

Restoring back the operator $\mathcal{G}$ with its spectrum γ, we get the optimal gain operator:

$$\mathcal{G} = -\frac{1}{m} \sum_{n=1}^{\infty} c_{m,n}\, \mathcal{W}_{\Delta t}^{mn} S^{-n}. \tag{3.24}$$

Thus, the formula (3.24) gives the form of optimal gain operator for the discrete controlled problem

$$u_i = \mathcal{W}_{\Delta t}\, u_{i-1} - \mathcal{G}(u_i - S u_{i-m}). \tag{3.25}$$

Remark 8. *If we denote the monodromy operator by* $\Phi = \lim_{m\to\infty} \mathcal{W}_{\Delta t}^m = \mathrm{Exp}\left(-T\, B^{-1} A\right)$, *then the limit*

$$\lim_{\Delta t \to 0} (\Delta t^{-1} \mathcal{G}) = -\frac{1}{T} \sum_{n=1}^{\infty} \frac{n^{n-1}}{n!\, e^n}\, \Phi^n S^{-n}$$

gives the optimal gain operator G_{opt} *(3.9) for the continuous case (Theorem 2), taken without the factor* B.

3.2.7 Predictor-corrector form

The controlled problem (3.25) can be written in the predictor-corrector form

$$\begin{aligned} u_i^{\#} &= \mathcal{W}_{\Delta t}\, u_{i-1}, \\ u_i &= u_i^{\#} - (\mathrm{Id} + \mathcal{G})^{-1} \mathcal{G} (u_i^{\#} - S u_{i-m}), \end{aligned}$$

where $u_i^{\#}$, solution of a non-controlled iteration, plays role of a predictor. The operator $\hat{\mathcal{G}} = -(\mathrm{Id} + \mathcal{G})^{-1}\mathcal{G}$ can be expressed through a series, similar to (3.24), but with different coefficients. Such an explicit form of the control term would allow to avoid any inversion of the operator $\mathrm{Id} + \mathcal{G}$ at the correction step. To construct this series, let us denote by $\hat{\gamma} = -(1+\gamma)^{-1}\gamma$ the spectrum of $\hat{\mathcal{G}}$. So, $1 + \gamma = (1 + \hat{\gamma})^{-1}$. And then, equation (3.22) rewrites in terms of $\hat{\gamma}$ as

$$\frac{\hat{\gamma}}{(1+\hat{\gamma})^m} = \frac{1}{m-1}\, (1 - 1/m)^m w^m \sigma^{-1}.$$

We use again Lagrange inversion theorem to obtain

$$\hat{\gamma} = \sum_{n=1}^{\infty} \frac{\hat{c}_n}{n!} \left(\frac{1}{m-1}\, (1-1/m)^m w^m \sigma^{-1}\right)^n,$$

where

$$\begin{aligned}\hat{c}_n &= \lim_{\hat{\gamma}\to 0} \frac{d^{n-1}}{d\hat{\gamma}^{n-1}}(1+\hat{\gamma})^{mn} \\ &= mn(mn-1)\dots(mn-(n-2)) \\ &= \frac{(mn)!}{(mn-(n-1))!}.\end{aligned}$$

Then, we obtain

$$\hat{\mathcal{G}} = -(\mathrm{Id}+\mathcal{G})^{-1}\mathcal{G} = \frac{1}{m}\sum_{n=1}^{\infty} c_{m,n}\,\mathcal{W}_{\Delta t}^{mn} S^{-n},$$

with coefficients

$$c_{m,n} = \frac{1}{n!}\cdot\frac{(mn)!}{(mn-n+1)!\cdot(m-1)^{n-1}}\cdot\left(1-\frac{1}{m}\right)^{mn-1}. \tag{3.26}$$

Thus, for the discrete controlled system (3.20) written in the predictor-corrector form

$$\begin{aligned} u_i^{\#} &= \mathcal{W}_{\Delta t}\, u_{i-1}, \\ u_i &= u_i^{\#} + \hat{\mathcal{G}}(u_i^{\#} - S u_{i-m}), \end{aligned} \tag{3.27}$$

or equivalently

$$u_i = \mathcal{W}_{\Delta t}\, u_{i-1} + \hat{\mathcal{G}}\left(\mathcal{W}_{\Delta t}\, u_{i-1} - S u_{i-m}\right),$$

the optimal gain operator is given by

$$\hat{\mathcal{G}} = \frac{1}{m}\sum_{n=1}^{\infty} c_{m,n}\,\mathcal{W}_{\Delta t}^{mn} S^{-n},$$

where coefficients $c_{m,n}$ are defined by (3.26), and S is the space shift operator.

Remark 9. *Note that operators $\hat{\mathcal{G}}$ and $-\mathcal{G}$ have the same limit when m goes to infinity:*

$$\lim_{\Delta t\to 0}(\Delta t^{-1}\hat{\mathcal{G}}) = \frac{1}{T}\sum_{n=1}^{\infty}\frac{n^{n-1}}{n!\,e^n}\,\Phi^n S^{-n},$$

where $\Phi = \lim_{m\to\infty}\mathcal{W}_{\Delta t}^{m} = \mathrm{Exp}\left(-T\,B^{-1}A\right)$ is the monodromy operator defining one cycle evolution. The above limit corresponds to the optimal gain operator G_{opt} (3.9) for the continuous controlled problem (Theorem 2).

Limiting case $\Delta t \to 0$. To illustrate the previous remark, let us once again consider the example of the implicit Euler scheme, applied to a linear problem defined through an implicit function $F(u, \dot{u}) = B\dot{u} + Au$. The associated controlled problem in the predictor-correction form writes

$$F\left(u_i^{\#}, \frac{u_i^{\#} - u_{i-1}}{\Delta t}\right) = 0,$$
$$u_i = u_i^{\#} + \hat{\mathcal{G}}(u_i^{\#} - Su_{i-m}).$$

Recall that $\hat{\mathcal{G}} = -(Id + \mathcal{G})^{-1}\mathcal{G}$ and that the correction step can be thus written implicitly as $u_i = u_i^{\#} - \mathcal{G}(u_i - Su_{i-m})$. Then, given the limits

$$\lim_{\Delta t \to 0} \mathcal{G} = 0 \qquad \text{and} \qquad \lim_{\Delta t \to 0} (\Delta t^{-1}\mathcal{G}) = B^{-1}G_{opt},$$

we have

$$\lim_{\Delta t \to 0} u_i^{\#} = u_i,$$
$$\lim_{\Delta t \to 0}\left(\frac{u_i^{\#} - u_{i-1}}{\Delta t}\right) = \lim_{\Delta t \to 0}\left(\frac{u_i - u_{i-1}}{\Delta t} + \Delta t^{-1}\mathcal{G}(u_i - Su_{i-m})\right)$$
$$= \dot{u}_i + B^{-1}G_{opt}\big(u_i - Su_{i-m}\big).$$

This leads to the continuous controlled problem

$$F\left(u_i, \dot{u}_i + B^{-1}G_{opt}\big(u_i - Su_{i-m}\big)\right) = 0,$$

or equivalently

$$B\dot{u}(t) + A(t) + G_{opt}\big(u(t) - Su(t-T)\big) = 0,$$

where the optimal gain operator G_{opt} is given by (3.9). Thus, the proposed discrete feedback control in the predictor-correction form (3.27) leads in continuous case to a correction of the time derivative by the delayed feedback control term, based on the periodicity error, with the continuous optimal gain operator proposed in Theorem 2.

Practical version. Similarly to Section 3.2.5, we propose a practical modification of the above gain operator $\hat{\mathcal{G}}$. We simplify it by replacing the forward operator $\mathcal{W}_{\Delta t}$ in the series by $w_{max}\mathrm{Id}$, where w_{max} denotes its maximal eigenvalue, or equivalently the spectral norm, i.e. $w_{max} = \|\mathcal{W}_{\Delta t}\|$. The maximal eigenmode of $\mathcal{W}_{\Delta t}(A, B)$ corresponds to α_0, the minimal generalized eigenmode of A and B. For example, for the implicit Euler scheme $w_{max} = (1 + \Delta t\, \alpha_0)^{-1}$, and the simplified gain writes

$$\hat{\mathcal{G}} = \frac{1}{m}\sum_{n=1}^{\infty} c_{m,n}\,(1 + \Delta t\, \alpha_0)^{-mn} S^{-n}$$

with coefficients $c_{m,n}$ defined by (3.26). And in case of a general forward operator $\mathcal{W}_{\Delta t}$, it has form

$$\hat{\mathcal{G}} = \frac{1}{m} \sum_{n=1}^{\infty} c_{m,n} \, \|\mathcal{W}_{\Delta t}^m\|^n S^{-n}. \tag{3.28}$$

Note that $\|\mathcal{W}_{\Delta t}^m\|$ is the norm of the time-discrete monodromy operator, defining one cycle of evolution.

Altogether, in predictor corrector form, the practical discrete control system writes

$$\begin{aligned} u_i^{\#} &= \mathcal{W}_{\Delta t} \, u_{i-1}, \\ u_i &= u_i^{\#} + \frac{1}{m} \sum_n c_{m,n} \|\mathcal{W}_{\Delta t}^m\|^n \, S^{-n} (u_i^{\#} - S u_{i-m}). \end{aligned}$$

3.2.8 Gain coefficients

We have represented the gain operator in form of a series (3.28). In practice, to apply the gain operator, a finite number N_{terms} of terms in series is computed. Its coefficients are strictly positive and compose an infinite decreasing sequence $\{c_{m,n}\}_{n\in\mathbb{N}}$ for a given number m of time steps per cycle. For a fixed m, the n-th coefficient is given by formula:

$$c_{m,n} = \frac{1}{n!} \cdot \frac{(mn)!}{(mn-n+1)! \cdot (m-1)^{n-1}} \cdot \left(1 - \frac{1}{m}\right)^{mn-1}, \quad n \in \mathbb{N}. \tag{3.29}$$

That is, the gain coefficients are independent of model and defined only by the time discretization parameter m. They can be thus predefined.

When m goes to infinity, the coefficients $c_{m,n}$ take the limit values

$$c_n = \lim_{m\to\infty} c_{m,n} = \frac{n^{n-1}}{n! \, e^n},$$

which are nothing else that the coefficients in the series decomposition of the function $-W_0[-\frac{1}{e}x]$, $x \in (0, 1)$, where W_0 is the principle branch of the Lambert W function.

For reference, values of the first 15 terms are given in Table 3.1 for $m = 10, 20, 30$ with the last column representing the limit case c_n when m goes to infinity.

To study how much the series (3.28) is affected by the number of coefficients, we introduce the series

$$\Sigma_N(x) = \sum_{n=1}^{N} c_{m,n} \, x^n, \tag{3.30}$$

n \ m	$m = 10$	$m = 20$	$m = 30$	$m = \infty$
1	0.3874	0.3774	0.3741	0.3679
2	0.1501	0.1424	0.14	0.1353
3	0.0843	0.0793	0.0777	0.0747
4	0.0556	0.0521	0.0509	0.0488
5	0.0402	0.0375	0.0367	0.0351
6	0.0308	0.0287	0.028	0.0268
7	0.0245	0.0228	0.0223	0.0213
8	0.0202	0.0187	0.0183	0.0174
9	0.0169	0.0157	0.0153	0.0146
10	0.0145	0.0134	0.0131	0.0125
11	0.0126	0.0117	0.0114	0.0109
12	0.0111	0.0102	0.01	0.0095
13	0.0098	0.0091	0.0089	0.0085
14	0.0088	0.0081	0.0079	0.0076
15	0.0079	0.0073	0.0072	0.0068

Table 3.1: First 15 gain coefficients $c_{m,n}$ defined by formula 3.29, for the discretization cases with $m = 10,\ 20,\ 30$ time steps per cycle. For a given m, they compose a strictly positive decreasing sequence $\{c_{m,n}\}_{n=1..N}$, which is model-independent. The last column represents the limit case $m \to \infty$, that is the coefficients $c_n = \frac{n^{n-1}}{n!\, e^n}$ in the series decomposition of the function $-W_0[-\frac{1}{e}x]$, $x \in (0,\ 1)$, where W_0 is the principle branch of the Lambert W function.

defined on the interval $[0,\ 1]$ for $N \in \mathbb{N}$. Let us fix $m = 10$ and observe the behavior of $\Sigma_N(x)$ as function of the coefficients number N. Functions $\Sigma_N(x)$ with $N = 2,\ 5,\ 10,\ 15,\ 20,\ 50$ and 100 are traced on Figure 3.3. We can conclude that the series $\Sigma_N(x)$ is more sensitive to N when x goes to one and indifferent to the number of coefficient in the vicinity of zero. It means that the number of coefficients in the gain operator (3.28) becomes more important when the norm of the monodromy operator is close to one, i.e. when the size of memory effects is large.

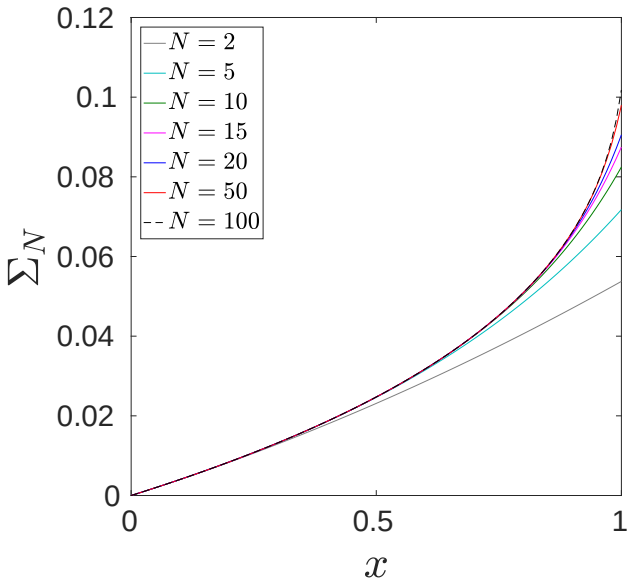

Figure 3.3: Behavior of the series (3.30) as function of the number of coefficients $c_{m,n}$ with $m = 10$ and $N = 2,\ 5,\ 10,\ 15,\ 20,\ 50$ and 100. We observe that it is more sensitive to N when x goes to one, from what it follows that the number N of coefficients retained in the gain operator (3.28) becomes more important when the norm of the monodromy operator is close to one, i.e. when the size of memory effects is large.

3.3 Non-linear problem

3.3.1 Predictor-corrector form

Let us consider an abstract non-linear evolution problem to be solved with the space-time periodicity condition:

$$F(t, u, \dot{u}) = 0,$$
$$u(t) = Su(t - T),$$

where S denotes a given shift in space. Let us thus divide the period T by $m \in \mathbb{Z}$ time steps $\Delta t = T/m$, and define the time discrete approximations $u_i = u(t_i)$, $t_i = i\Delta t$, $i \in \mathbb{Z}$. Then, the implicit Euler time scheme for the above non-linear system writes in the induction form

$$F\left(t_i, u_i, \frac{u_i - u_{i-1}}{\Delta t}\right) = 0,$$
$$u_i = Su_{i-m}.$$

Using the same strategy as in the previous sections, we propose the associated controlled non-linear problem in the predictor-corrector form

$$\begin{aligned} F\left(t_i, u_i^{\#}, \frac{u_i^{\#} - u_{i-1}}{\Delta t}\right) &= 0, \\ u_i = u_i^{\#} + \underbrace{\hat{\mathcal{G}}(u_i^{\#} - S u_{i-m})}_{\text{control term}}&, \end{aligned} \tag{3.31}$$

where $u_i^{\#}$ is a predicted state at time step i, computed by standard evolution iteration. It is then corrected with an increment $\hat{\mathcal{G}}(u_i^{\#} - S u_{i-m})$ computed from the periodicity error by applying a linear gain operator $\hat{G}$. Generalizing (3.31) to an arbitrary time scheme, we introduce the general time-discrete controlled problem

$$\begin{aligned} u_i^{\#} &= \mathcal{W}_{\Delta t}(t_i, u_{i-1}), \\ u_i &= u_i^{\#} + \hat{\mathcal{G}}(u_i^{\#} - S u_{i-m}), \end{aligned} \tag{3.32}$$

where the non-linear forward operator $\mathcal{W}_{\Delta t}$ is defined by function F and by the choice of time scheme. To further specify the optimal gain $\hat{\mathcal{G}}$, let us also introduce the non-linear monodromy operator $\Phi_{\Delta t}$ defining one cycle evolution

$$u_i = \Phi_{\Delta t}(t_i, u_{i-m}) = \mathcal{W}_{\Delta t}\left(t_i, \mathcal{W}_{\Delta t}\big(t_{i-1}, \dots \mathcal{W}_{\Delta t}(t_{i-m+1}, u_{i-m})\big)\right).$$

Its Jacobian $\mathrm{D}\Phi_{\Delta t}$ is a superposition of the tangent forward operators $\mathrm{D}\mathcal{W}_{\Delta t}$ computed during the last period T:

$$\mathrm{D}\Phi_{\Delta t}(t_i, u_{i-m}) = \mathrm{D}\mathcal{W}_{\Delta t}(t_i, u_{i-1}) \cdot \ldots \cdot \mathrm{D}\mathcal{W}_{\Delta t}(t_{i-(m-1)}, u_{i-m}). \tag{3.33}$$

Based on Section 3.2.7, we propose as gain operator for (3.32) the linear expansion

$$\hat{\mathcal{G}} = \frac{1}{m} \sum_{n=1}^{\infty} c_{m,n}\, a^n\, S^{-n},$$

with coefficients $c_{m,n}$ defined by (3.29) and the scalar parameter a approximating the norm of the tangent monodromy operator $\mathrm{D}\Phi_{\Delta t}$. Such an operator corresponds to the quasi-optimal gain (3.28) for the linearized problem. Hence, it will provide the fastest convergence in the vicinity of the limit cycle.

The practical choice of the parameter a is the key issue in the proposed technique. In what follows, we compare two ways for calculating a:

- The first way computes a directly as the maximal eigenvalue of $\mathrm{D}\Phi_{\Delta t}$ (i.e. the norm of the tangent monodromy operator of the problem) during the first cycle. To do this, we use the matrix-free power iteration method, where only the action of $\mathrm{D}\Phi_{\Delta t}$ to a vector is defined (and not the matrix $\mathrm{D}\Phi_{\Delta t}$

itself). This multiplication operation is defined as a sequence of matrix-vector products, given by (3.33). This procedure of computing the gain parameter a is rather expensive and its cost in memory use and CPU time amounts to a few Krylov iterations of Chapter 2. This cost will be reduced if any a priori information (estimation) on the tangent monodromy operator's norm is available to be used to construct the gain parameter a, within an acceptable loss in the provided acceleration.

- The second proposed technique for computing the gain parameter a consists in its continuous adaptive tuning [Guzenko et al. 2008, Pyragas and Pyragas 2011, 2013]. The gain parameter is considered as a time-dependent variable, and the gradient-descent method is used to make it converge to the optimal value, minimizing an objective function. This method is proposed in [Pyragas and Pyragas 2013] and is reviewed in the following section.

3.3.2 Adaptive tuning of the control parameter

Let us denote in this section the periodicity error by

$$p(t) = u(t) - Su(t - T).$$

We will also use a notation f_a to denote the derivative of any function f with respect to the gain parameter a. We write the controlled system in a generic continuous form

$$\dot{u} = F(t, u) + \mathcal{G}(a)\, p, \qquad \mathcal{G}(a) = \sum_{n=1}^{\infty} c_n\, a^n\, S^{-n} \tag{3.34}$$

with a space shift S and abstract coefficients c_n. Gain parameter a is to be tuned to the optimal value, minimizing an objective function ("cost" function).

Techniques of the continuous adaptive tuning of a feedback gain parameter include the speed-gradient method [Guzenko et al. 2008] and the gradient-descent method [Pyragas and Pyragas 2013, 2011]. The speed-gradient method continuously modifies the gain, minimizing locally the periodicity error. It is used in the framework of controlling initially unstable systems to bring the gain to the convergence region. However, it is not supposed to provide the optimal gain value. Given an initially stable system, the non-controlled case $a = 0$ is already in the convergence region, and we are looking for the optimal value. Meanwhile, the gradient-descent algorithm seeks to minimize the average periodicity error on a certain interval, which leads to a gain operator optimizing the convergence. Thus, in our framework, the gradient-descent method is of interest. In what follows, let us briefly review the algorithm, presented in [Pyragas and Pyragas 2013].

Instead of the norm of the current periodicity error p, we want to minimize the objective function

$$J(t) = \frac{1}{T} \int_{-\infty}^{t} e^{-(t-t')/T}\, \|p(t')\|^2\, \mathrm{d}t', \tag{3.35}$$

representing a "running" average on interval T of the periodicity error squared norm. The optimal a minimizing J is such that the gradient J_a is zero at this point. We use the gradient-descent (steepest gradient) method to define the evolution law of a by

$$\dot{a} = -\gamma J_a, \tag{3.36}$$

where γ is the scale of the relaxation time. In parallel, the objective function (3.35) satisfies by construction the evolution law

$$\dot{J} = \frac{1}{T}\,\|p\|^2 - \frac{1}{T}\,J.$$

Hence, a derivation with respect to a leads to the gradient evolution

$$\dot{J}_a = \frac{2}{T}\,\langle p,\ p_a\rangle - \frac{1}{T}\,J_a$$

to be used for the construction of the right hand side of the evolution equation in a. Above, $p_a(t) = u_a(t) - Su_a(t-T)$ and $u_a(t)$ denote respectively the derivatives of the periodicity error p and of the state variable u as functions of a. From (3.34) the state variable derivative u_a satisfies

$$\dot{u}_a = \mathrm{D}F(t,u)\,u_a + \mathcal{G}_a p + \mathcal{G} p_a$$

with the gradient of the gain operator given by $\mathcal{G}_a = \sum_{n=1}^{\infty} c_n\, n a^{n-1}\, S^{-n}$. Then the overall controlled system with adaptive tuning of a writes

$$\begin{aligned}
\dot{u} &= F(t,u) + \mathcal{G}p,\\
\dot{u}_a &= \mathrm{D}F(t,u)\,u_a + \mathcal{G}_a p + \mathcal{G} p_a,\\
T\dot{J}_a &= 2\,\langle p,\ p_a\rangle - J_a,\\
\dot{a} &= -\gamma J_a,
\end{aligned}$$

where $p(t) = u(t) - Su(t-T)$ is the periodicity error with derivative $p_a(t) = u_a(t) - Su_a(t-T)$, and the gain operator and its gradient are respectively given by

$$\mathcal{G} = \sum_{n=1}^{\infty} c_n\, a^n\, S^{-n}, \qquad \mathcal{G}_a = \sum_{n=1}^{\infty} c_n\, n a^{n-1}\, S^{-n}.$$

3.4 Application. Linear 2D heat problem

In this section we apply the developed control method to a linear problem, which exactly corresponds to the theoretical framework in Section 3.2.1. This allows us to verify in practice the analytical results of the current chapter. First, we

will demonstrate that the proposed control techniques indeed accelerate convergence to the space-time periodic solution. To do this, we will compare the convergence time for the controlled and non-controlled initial value problems. Then, by testing different relaxation times, we will verify if the efficiency of the method increases with the memory effects. Also, we want to check if the theoretical optimal control and its minimal eigenvalue approximation provide the same convergence rate. Finally, we are going to compare the efficiency of time-continuous and time-discrete versions of the optimal control.

The test problem considered herein is the linear 2D model, proposed in Section 1.2. It considers a planar disk, heated with a periodically moving source (see Figure 1.6). The source can take one of M positions on a circle path inside the disk. After having heated one spot during a time interval T, it moves to the next position, i.e. rotates to the angle $\theta = 2\pi/M$. All material parameters are supposed to be θ-periodic.

We are interested in the space-time periodic state, which is the asymptotic limit of the initial value problem with an arbitrary initial state. Applying the control technique described in this chapter, we expect to accelerate the convergence to the desired periodic solution. In what follows we will test and compare four previously discussed variants of the feedback control:

1. Feedback term operating on the time-continuous problem, using the optimal gain operator G^{opt} (3.9). Then, the modified problem is discretized in time.
2. The same but using the simplified gain operator $G^{m.e.}$ (3.13).
3. Feedback term operating on the time-discretized problem, using the associated optimal gain operator (3.24).
4. The same but using the simplified gain operator (3.28).

Note that in this simple 2D problem we can compute the exact optimal gain operator, including matrix exponential, and can compare it with its practical modification in terms of the provided acceleration rate.

Let us recall the problem formulation (see Section 1.2 for the details):

$$\begin{gathered}\text{Find } u : \mathbb{R}_+ \mapsto H^1(\Omega), \text{ such that } \forall v \in H^1(\Omega) \text{ and } \forall t \in \mathbb{R}_+ \\ \langle c\,\partial_t u,\ v\rangle + \langle \kappa\,\nabla u,\ \nabla v\rangle = \langle q,\ v\rangle - \int_\Gamma a\cdot(u-u_0)\,v, \\ u(t) = Su(t-T).\end{gathered} \tag{3.37}$$

We define the operators A and B, acting from $H^1(\Omega)$ to its dual H', and the function $f \in H'$ as follows:

$$\begin{array}{rrcl}\forall v \in H^1(\Omega): & \langle Au,\ v\rangle & = & \int_\Omega \kappa\,\nabla u\cdot\nabla v + \int_\Gamma a\,u\,v, \\ & \langle Bu,\ v\rangle & = & \int_\Omega c\,u\,v, \\ & \langle f,\ v\rangle & = & \int_\Omega q\,v + \int_\Gamma a\,u_0\,v.\end{array}$$

From our periodicity assumption, the above operators satisfy all hypotheses in Section 3.2.1. Under the above notation, the system (3.37) writes:

$$\begin{aligned} \langle B\,\partial_t u + Au - f,\ v\rangle_{H^{-1},H^1} = 0 \qquad & \forall v \in H^1(\Omega), \\ u(t) = Su(t-T), & \end{aligned}$$

which exactly corresponds to the theoretical framework of the delayed feedback control discussed in Section 3.2.1. Then, we write the associated controlled problem:

$$\begin{aligned} \langle B\,\partial_t u + Au + G\,(u(t) - Su(t-T)) - f,\ v\rangle = 0, \qquad & \forall v \in H^1(\Omega),\ \forall t > 0, \\ u(t) = \text{"arbitrary initial data"}, \qquad & t \le 0. \end{aligned}$$

We discretize this system in space with finite elements method, using P_1-elements on a conforming triangular mesh. The mesh is θ-periodic with respect to rotation. All simulations in this section have been implemented in MatLab R2016b. Thus, the space-discretized system writes

$$\begin{aligned} B_h\,\partial_t u_h + A_h u + G_h\,(u_h(t) - S_h u_h(t-T)) - f_h = 0, \qquad & t > 0, \\ u_h(t) = \text{"arbitrary initial data"}, \qquad & t \le 0, \end{aligned} \tag{3.38}$$

where u_h, A_h, B_h, G_h, S_h and f_h are the finite elements counterparts of u, A, B, G, S and f respectively. Since we use a θ-periodic mesh, S_h is a simple permutation matrix. In what follows we will only deal with the discretized entities and thus omit the subscribe h for the sake of simplicity.

According to Theorem 2, the optimal gain operator, providing the fastest convergence to the stable periodic solution, is in the form (3.9)

$$G^{opt} = -\frac{1}{T}\,B \sum_{n=1}^{N_{terms}} c_n\, e^{-nT\left(B^{-1}A\right)} S^{-n}, \qquad c_n = \frac{n^{n-1}}{n!\,e^n}. \tag{3.39}$$

The matrix exponential is computed here using the common spectral decomposition of A and B. For now the number of terms in the series N_{terms} is supposed to be large and is set to 100. Further, we will study the sensitivity of the control to the number of terms N_{terms}.

Along with the optimal control we want to test its minimal eigenvalue approximation $G^{m.e.}$ (proposed in Section 3.2.5), which is in the form (3.13)

$$G^{m.e.} = -\frac{1}{T}\,B \sum_{n=1}^{N_{terms}} c_n\, e^{-nT\alpha_0} S^{-n}, \qquad c_n = \frac{n^{n-1}}{n!\,e^n}, \tag{3.40}$$

where $\alpha_0 > 0$ is the minimal generalized eigenvalue of A and B, that is $\alpha_0 = \min\{\,\alpha \mid \exists\, \underline{v} \in V_0 :\ A\underline{v} = \alpha\, B\underline{v}\,\}$. This value is associated with the relaxation time of the problem and defines the size of memory effects.

Time-discretization of the controlled problem (3.38) using the implicit Euler scheme with time step $\Delta t = T/m$, $m \in \mathbb{Z}$, leads to the induction

$$\begin{aligned} B\,\frac{u_i - u_{i-1}}{\Delta t} + A\,u_i + G\,(u_i - S u_{i-m}) - f_i = 0, \qquad & i > 0, \\ u_i = \text{"arbitrary initial data"}, \qquad & i \le 0. \end{aligned} \tag{3.41}$$

In our simulations we set $m = 10$, that is $\Delta t = 0.1\,T$. Solution is said to have converged, when the periodicity error ℓ_2-norm reaches a specified accuracy 10^{-4}.

The optimal gain operator will slightly change, if we discretize the problem in time before applying the control. According to Section 3.2.6, the optimal gain operator G_m^{opt} for a discrete problem in form (3.41) is defined through operator $\mathcal{G}$ (3.24) as follows

$$\begin{aligned} G_m^{opt} &= (B + \Delta t A)\Delta t^{-1}\mathcal{G} \\ &= -\frac{1}{T}\,(B + \Delta t A) \sum_{n=1}^{N_{terms}} c_{m,n} \left((B + \Delta t A)^{-1} B \right)^{mn} S^{-n} \end{aligned} \tag{3.42}$$

with coefficients (3.23), and its practical version respectively writes

$$G_m^{m.e.} = -\frac{1}{T}\,(B + \Delta t A) \sum_{n=1}^{N_{terms}} c_{m,n}\,(1 + \Delta t\,\alpha_0)^{-mn} S^{-n}. \tag{3.43}$$

In what follows, we will solve the system (3.41), testing and comparing all the four controls G^{opt} and $G^{m.e.}$, G_m^{opt} and $G_m^{m.e.}$, given respectively by (3.39), (3.40), (3.42), (3.43). The initial condition u_{ini} in (3.41) is taken to be zero.

Let us introduce the normalized relaxation time of the problem by $(T\alpha_0)^{-1}$, where α_0 is the minimal generalized eigenvalue of A and B. As mentioned above, this value characterizes the magnitude of the memory effects of the problem. We perform several tests with different values of the disk radius R, which affects the problem's characteristic times $\rho\bar{c}_p R^2/\bar{\kappa}$ and $\rho\bar{c}_p R/\bar{a}$ and changes thus the relaxation time. So, varying R, we study the numbers of cycles needed to converge to the cyclic limit with the specified accuracy for the four discussed types of the gain operator. Then, these numbers are compared to those of the non-controlled evolution and of the Newton-Krylov method (see Section 2.8), where the cycle number includes one cycle plus the number of Krylov iterations.

We discretize the system in space with finite elements method (implemented in MatLab R2016b), using P_1-elements on a conforming triangular mesh, $\frac{2\pi}{M}$-periodic with respect to rotation. Simulation results on a 421 nodes mesh with $\Delta t = T/10$ are shown in the Table 3.2. We can see there that Newton-Krylov method requires the least number of cycles. We also observe that the discrete gain provides better convergence that the continuous one. Besides, in both cases, although much simpler to compute, the practical versions are as fast as the associated optimal gains. As noted in Section 3.2.5, this is due to the fact (numerically justified)

Radius	Relax.time	Number of cycles					
R, mm	$(T\alpha_0)^{-1}$	No control	G^{opt}	$G^{m.e.}$	G_m^{opt}	$G_m^{m.e.}$	Newton-Krylov
5	0.821	7	6	6	6	6	4
10	3.278	25	14	14	12	12	9
20	13.099	97	31	31	27	27	22
30	29.463	217	48	48	43	43	37
40	52.370	385	68	68	60	60	54

Table 3.2: Linear 2D heat equation.. Feedback control application results. We study the number of cycles needed to reach the accuracy 10^{-4} for different values of the relaxation time $(T\alpha_0)^{-1}$. We apply the delayed feedback control method using the continuous and discrete optimal gain operators G^{opt} (3.39) and G_m^{opt} (3.42), along with their practical versions $G^{m.e.}$ (3.40) and $G_m^{m.e.}$ (3.43). It is compared to the non-controlled evolution and to the Newton-Krylov method (see Section 2.8), where the cycle number includes one cycle plus the number of Krylov iterations. We observe that the discrete gain provides better convergence that the continuous one. Besides, in both cases, although much simpler to compute, the practical versions are as fast as the associated optimal gains. All methods have the same level of performance, Newton-Krylov being nevertheless the most efficient here.

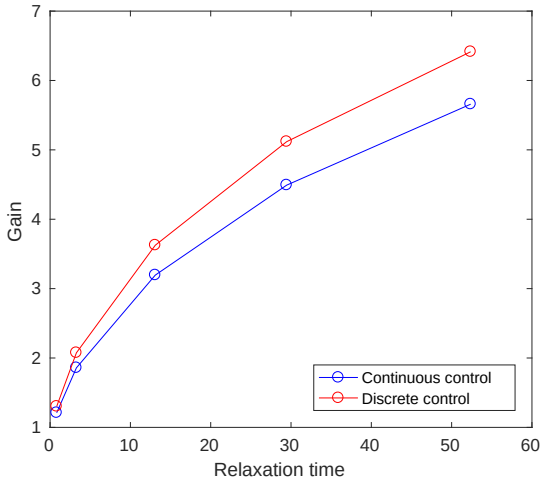

Figure 3.4: Linear 2D heat problem. Acceleration (gain) provided by the control as a function of relaxation time $(T\alpha_0)^{-1}$ of the problem. The simulation justifies the theoretical results of Section 3.2.4: the efficiency of the method indeed increases with the magnitude of the memory effects of the problem.

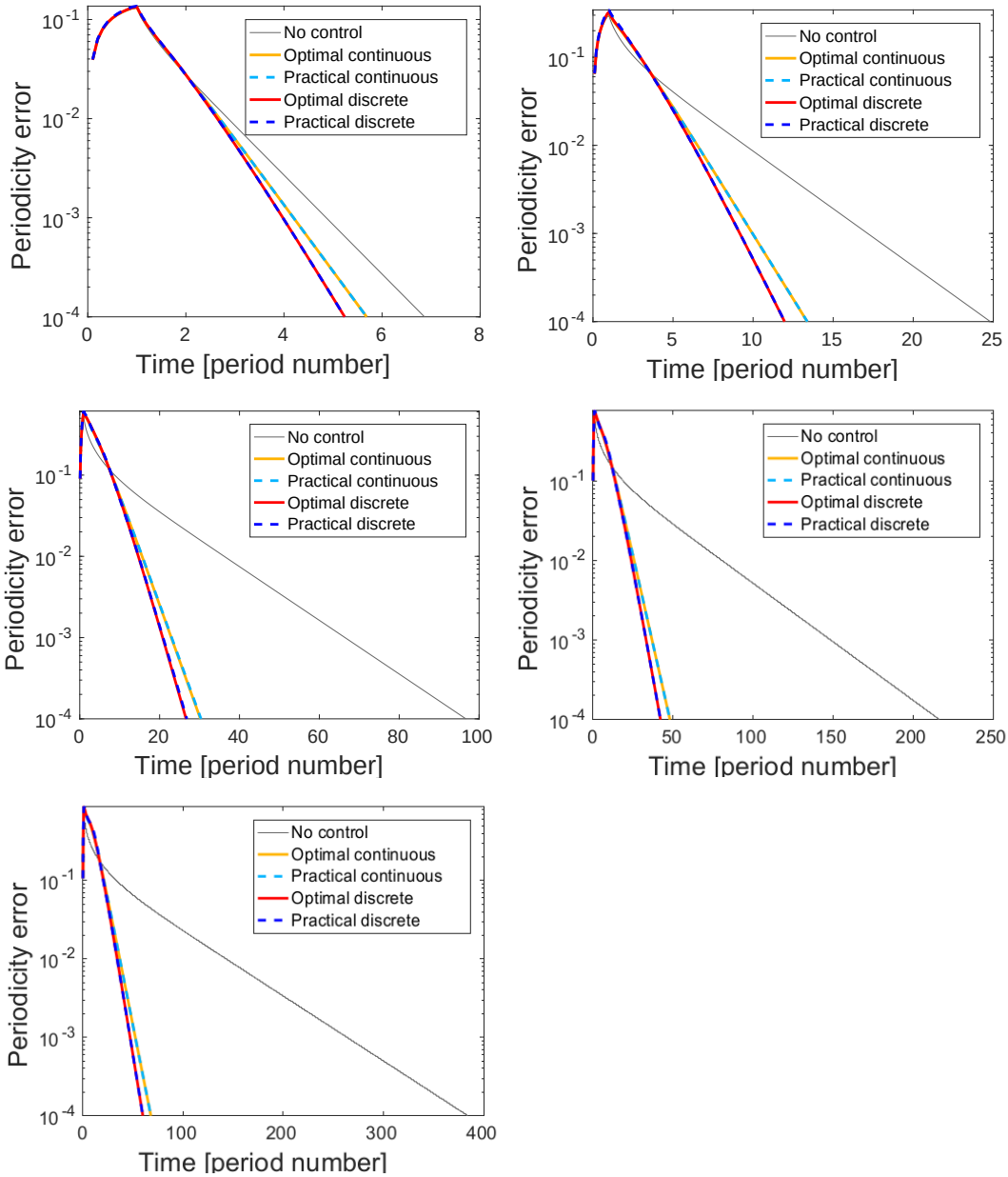

Figure 3.5: Linear 2D heat problem. Time-evolution of the periodicity error ℓ_2-norm (logarithmic scale) for the cases of $R = 5,\ 10,\ 20,\ 30,\ 40\ mm$ (left to right, top to bottom respectively). Varying the radius, we change the relaxation time of the problem. This affects the efficiency of the control. We compare four types of the gain operator – see (3.39), (3.40), (3.42) and (3.43). The discrete gain provides a better convergence that the continuous one. Besides, in both cases, the practical (minimal eigenvalue) versions are as fast as the associated optimal gains (coinciding solid and dashed lines).

that the minimal generalized eigenmode v_0 of A and B (i.e. associated to α_0) is S-periodic, that is $Sv_0 = v_0$.

Let us denote by N_c and N_{nc} the numbers of time iterations until convergence for the controlled and non-controlled problems respectively. The ratio N_{nc}/N_c is a measure of the acceleration of convergence which is provided by the feedback control. According to Section 3.2.4, the acceleration is expected to increase with the relaxation time. This result is shown on Figure 3.4, where the acceleration is presented as a function of relaxation time. We can observe that the efficiency of the method indeed increases with the magnitude of the memory effects of the problem.

Time evolutions of the periodicity error ℓ_2-norm for the discussed types of the gain operator are compared in logarithmic scale on Figure 3.5, where each plot corresponds to different values of the disk radius R (i.e. to different relaxation times).

To summarize, the discrete gain operator is more efficient than the continuous one, and the practical version, being much simpler in implementation, provides the same acceleration that the optimal gain. Thus, in what follows we will only use the discrete practical gain (3.43).

Sensitivity to the time step size. Let us study the sensitivity of the method's efficiency to the size of the time step $\Delta t = T/m$, where $m \in \mathbb{Z}$ is the number of time steps per period T. To do this, we perform several tests with various values of m in the case $R = 10\,mm$ using the discrete practical gain operator (3.43). The corresponding results are shown in Table 3.3, where we observe that the acceleration rate slightly decreases with the time step size Δt, until it reaches an asymptotic limit.

Number of time steps per period, $m = T/\Delta t$	5	10	20	30
Acceleration, N_{nc}/N_c	2.136	2.075	2.033	2.025

Table 3.3: Sensitivity of the control efficiency to the time step size $\Delta t = T/m$, where $m \in \mathbb{Z}$ is the number of time steps per period T. Case of $R = 10\,mm$. Acceleration rate slightly decreases when the discretization number m grows.

Sensitivity to the mesh size Now, we fix $R = 10\,mm$ and $m = 10$ (that is $\Delta t = 0.1\,T$), and we change the size of the mesh in order to study the sensitivity of the feedback control efficiency to the discretization in space (the state of Remark 7). In Table 3.4 there are compared the numbers of time steps N_{nc} and N_c, needed to reach the periodicity error accuracy 10^{-4}, respectively for the non-controlled and controlled problems, corresponding to the different mesh sizes. We see that the acceleration ratio N_{nc}/N_c, which depends on the relaxation time $(T\alpha_0)^{-1}$, moderately increases when the mesh size decreases, converging to the limit value corresponding to the space-continuous case.

Mesh size, nodes nb.	Relax.time $(T\alpha_0)^{-1}$	Number of time steps		Acceleration N_{nc}/N_c
		No control, N_{nc}	Controlled, N_c	
421	3.278	249	120	2.075
1051	3.632	274	128	2.140
2191	3.770	301	136	2.213
3571	3.815	315	141	2.234
5761	3.856	328	145	2.262
8641	3.871	338	148	2.284
13051	3.884	346	151	2.291

Table 3.4: Sensitivity of the control efficiency to the mesh size. Case of $R = 10\,mm$, $m = 10$.

Sensitivity to the number of terms in the series. Let us now study the sensitivity of the feedback control using the discrete practical gain operator to the number of terms N_{terms} taken into account in the series (3.43). The results (periodicity error norm evolution) of simulations with different values N_{terms} are depicted on Figure 3.6. We can observe that stating from $N_{terms} = 10$ the difference is negligible, and for $N_{terms} \geq 15$ the lines almost coincide. In what follows, if not specified, the number of coefficients in the gain operator is set to 12.

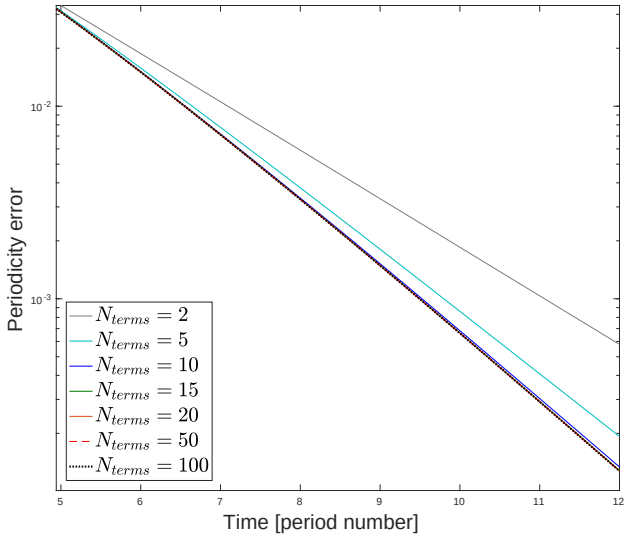

Figure 3.6: Linear 2D heat problem. Sensitivity of the periodicity error to the number N_{terms} of terms in the feedback gain series (3.43). For $N_{terms} \geq 10$ the difference is negligibly small.

Variation of the gain parameter. Let us consider a generic form of gain operator

$$G_m(\alpha) = (B + \Delta t A) \sum_{n=1}^{N_{terms}} c_{m,n} \, (1 + \Delta t \, \alpha)^{-mn} S^{-n},$$

where the scalar α plays role of the gain parameter. From Sections 3.2.3 and 3.2.5, we have already found that the optimal value of the parameter α is α_0 – the minimal generalized eigenvalue of the "stiffness" and "viscosity" matrices A and B. Nevertheless, we want to study how a change of the gain parameter α affects the evolution.

The simulation results with different values of α are depicted on Figure 3.7, where we compare the ℓ_2-norm evolutions of the periodicity error (top) and of the transient solution (bottom) for the disk of radius $R = 10\,mm$. Obviously, non-controlled case corresponds to $\alpha = \infty$. When it decreases, the convergence accelerates, attaining the steepest asymptotic rate at $\alpha = \alpha_0$. Beyond α_0, further decreasing of α illustrates the statement of Remark 6 from Section 3.2.5. That is, solution oscillates, since all the Floquet exponents have imaginary part (which grows with α decreasing). However, their real parts start to go to zero, so the asymptotic convergence rate slows down. Nevertheless, it is possible to make use of such oscillations when their periods are small (i.e. when $\alpha = \alpha_0 + \epsilon$ for small $\epsilon > 0$). In this case, by the moment when cosine starts to grow, the oscillation magnitude is already beyond the specified accuracy.

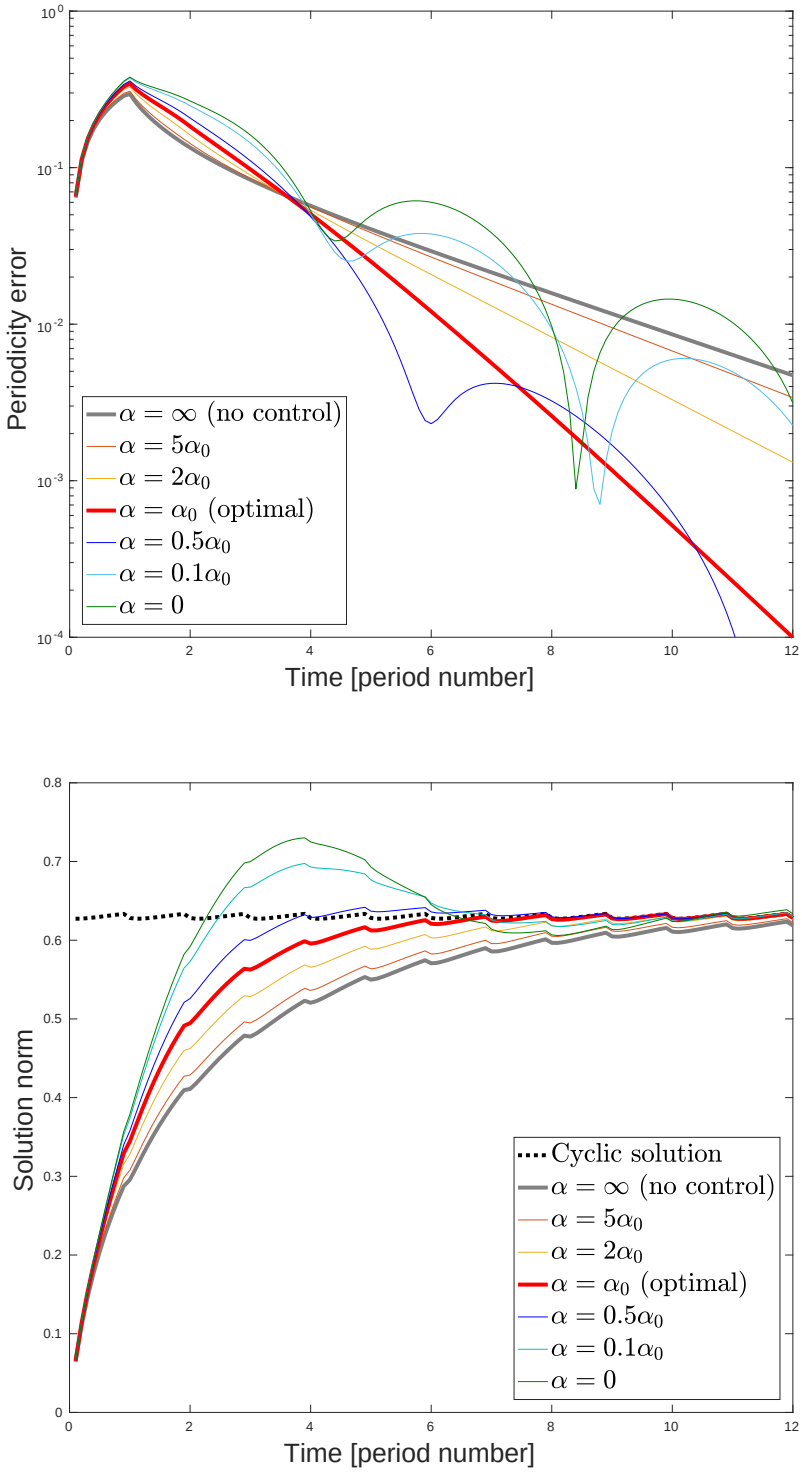

Figure 3.7: Linear 2D heat problem. Variation of the gain parameter. Time evolution of the ℓ_2-norm of the periodicity error (top) and of the transient solution (bottom). Case of $R = 10\,mm$.

3.5 Application. Rolling tyre

This section is devoted to application of the Delayed Feedback Control to a non-linear problem. We consider the steady rolling of a 3D viscoelastic tyre with periodic sculptures, in presence of stick-slip frictional contact with the soil. We are looking for the space-time periodic solution of this problem (cyclic steady state). This model is described in Section 1.1.1 and has been used in Section 2.9 to justify the Newton-Krylov method, discussed in Chapter 2. Now we will apply the feedback control technique, accelerating the convergence to the limit cyclic state, and will compare it with the classical asymptotic method as well as with the Newton-Krylov algorithm. We will start with the application to a simplified academic model, performed in MatLab R2016b, followed by the application to the complete model implemented in the Michelin industrial code.

3.5.1 Simplified academic model

Lets us consider first the simplified academic model described in Section 1.1.4. The mathematical definition of the problem is given in (1.17) and writes

$$F(t, \underline{u}, \dot{\underline{u}}) = 0,$$
$$\underline{u}(t) = S\underline{u}(t - T),$$

where F is defined by (1.18), T is the time period. The space shift operator S is defined in the rotating coordinate system (connected to the tyre rim with the origin on the axle) by

$$\forall \underline{v} \quad S : \underline{v}(\underline{X}) \mapsto \underline{\underline{R}}_\theta^{-1}\, \underline{v}(\underline{\underline{R}}_\theta \underline{X}),$$

where $\underline{\underline{R}}_\theta$ denotes the rotation of angle θ (sculpture size).

According to Section 3.3.1, the associated controlled problem, discretized in time with implicit Euler scheme, writes in the predictor-corrector form (3.32):

$$F\left(t_i,\ \underline{u}_i^{\#},\ \frac{\underline{u}_i^{\#} - \underline{u}_{i-1}}{\Delta t}\right) = 0,$$

$$\underline{u}_i = \underline{u}_i^{\#} + \hat{\mathcal{G}}\left(\underline{u}_i^{\#} - S\underline{u}_{i-m}\right),$$

where $\Delta t = T/m$, $m \in \mathbb{Z}$, is the time step, and the gain operator is in the form

$$\hat{\mathcal{G}} = \frac{1}{m} \sum_{n=1}^{N_{terms}} c_{m,n}\, a^n\, S^{-n} \tag{3.44}$$

with coefficients

$$c_{m,n} = \frac{1}{n!} \cdot \frac{(mn)!}{(mn - n + 1)! \cdot (m-1)^{n-1}} \cdot \left(1 - \frac{1}{m}\right)^{mn-1}.$$

Here, N_{terms} is set to 12. Gain parameter a has to approximate the norm of the tangent monodromy operator. In what follows, we are going to test two ways of computing of a as proposed in Section 3.3.1:

1. The first one consists in computing the **norm of the tangent monodromy operator** during the first cycle, using the matrix-free power iteration method.

2. The second way is the **adaptive tuning** technique using the gradient descent method, proposed in [Pyragas and Pyragas 2013]. See Section 3.3.2 for a brief review.

In addition, to test the feedback control method behavior with different memory sources, we will consider two different cases:

1. In the first case, stick-slip friction provides all memory effects. The material is purely elastic with no memory. In this test case we will compare the two above techniques for computing the gain parameter a.

2. In the second case, the material is viscoelastic. The friction is present, but viscosity-provided memory effects dominate. Varying the viscosity coefficient, we will study the sensitivity of the feedback control method to variations of the relaxation time.

We use the same model that in Section 2.9. In particular, we set the tyre external and internal radii $r_1 = 1\,m$ and $r_2 = 0.7\,m$ respectively and the width to $0.2\,m$. The ground is at the distance $r_{load} = 0.9\,r_1$ from the wheel axle. The tyre has $M = 36$ sculptures of angle $\theta = 2\pi/M = 10^\circ$ and depth $(r_1 - r_{sculpture}) = 0.1\,r_1$. Material properties, periodic with respect to the angle, vanishes in the domains associated to voids in the sculpture (these domains are not affected by the contact). That is, the Young's modulus E and the viscosity coefficient η are in the form (1.16) with the reference values $E_0 = 10^5\,KPa$, associated to rubber, and η_0 depending on the test case.

The tyre advances with linear velocity $v_{ax} = 22.22222\ m/s$ $(= 80\ km/h)$. The angular velocity of the rim is $\omega = v_{ax}/r_{load}$, which provides a small rim couple, and therefore a small friction force, ensuring that a large part of the contact zone is in the adherent regime. A loaded frictionless state is taken as the initial data.

The finite elements simulation have been implemented in MatLab R2016b, using P_1-elements on a conforming tetrahedral θ-periodic mesh (see Figure 2.3 in Section 2.9), composed of 4500 nodes and 19008 tetrahedral elements. The implicit Euler time scheme is used with step $\Delta t = 0.1\,T$, where $T = \frac{2\pi}{\omega M}$ is the time period of one sculpture turn. That is, we use 10 time steps per cycle. Each time iteration is solved with the complete Newton method, with the contact treated by penalization (see (1.3) and (1.4)) with penalty coefficients $\epsilon_N = \epsilon_\tau = 10^7$. Coulomb friction coefficient is $\mu = 0.8$. Solution is said to have converged, when the norm of the periodicity error $\varepsilon_{per} = \underline{u}(t) - S\underline{u}(t - T)$ reaches the specified accuracy 10^{-4}.

1. Stick-slip friction, elastic material. Let us consider first the stick-slip frictional contact case. For now, the material is purely elastic, i.e. we set $\eta \equiv 0$ in (1.18). Excluding material viscosity will allow us to observe the memory effects provided by friction. As mentioned before, we are testing two techniques of computing of a, proposed in Section 3.3.1.

Let a_0 be the norm of the tangent monodromy operator computed during the first cycle, using the matrix-free power iteration method. More precisely, we do not apply the control during the first period, but store the tangent matrices composing the local forward operators. Superposition (3.33) of this operators defines the action of the tangent monodromy operator as a sequence of matrix-vector products. Defined in this way the matrix-vector product is used in the power iteration algorithm to compute the norm a_0 (maximal eigenvalue) of the tangent monodromy operator.

Using the computed thus $a_0 = 0.8926$ as a reference, let us try different values of the gain parameter a in (3.44). In this way we study the sensitivity of the feedback control method to the gain parameter variation. Simulation results are depicted on Figure 3.8, illustrating in logarithmic scale the time-evolution of periodicity error ℓ_2-norm, using $a = 0,\ a_0^5,\ a_0^2,\ a_0,\ \sqrt{a_0},\ \sqrt[10]{a_0}$ and 1. Note that in two last cases the number of coefficients in the gain operator has been increased from 12 to 100, since the series becomes more sensitive to the coefficients number in the vicinity of identity (see Section 3.2.8 and Figure 3.3). Observe that, in contrast to linear case, the monodromy operator's norm does not provide the fastest convergence (even asymptotically). Here, the test value $a = \sqrt{a_0} = 0.9448$ is supposed to be closer to the asymptotically optimal gain. However, generally speaking, the variation of evolution as function of gain parameter is similar to that in linear case (compare Figure 3.8 and Figure 3.7). In particular, we can observe oscillations of the solution for large (close to one) values of a, illustrating the statement of Remark 6 from Section 3.2.5.

Applying adaptive tuning by the gradient descent method [Pyragas and Pyragas 2013], we start from the default value $a = 0$, i.e. from a non-controlled case. We set $\gamma = 10/\Delta t$ in (3.36). Gain parameter a has been successfully tuned to the value $a = a_{tuned} = 0.9421$, which is close to $\sqrt{a_0} = 0.9448$. Adaptive tuning is compared on Figure 3.9(top) to the previous results using the fixed gain parameter values $a = a_0$ and $a = \sqrt{a_0}$. We can see that the tuning takes a longer time than the other two tests. This is due to the fact that, given arbitrary initial data, the process needs several cycles to build a correct history. For this time, the gradient J_a of the objective function is positive, that would minimize a current periodicity error but not the future one. Since $a \in [0,\ 1]$, we restrict $a(t) := \min(\max(a(t), 0), 1)$. That prevents a from taking a negative value, which would lead to a slow down with respect to the non-controlled evolution. Time-evolutions of the gain parameter a and of the objective function gradient J_a are illustrated on Figure 3.9(bottom).

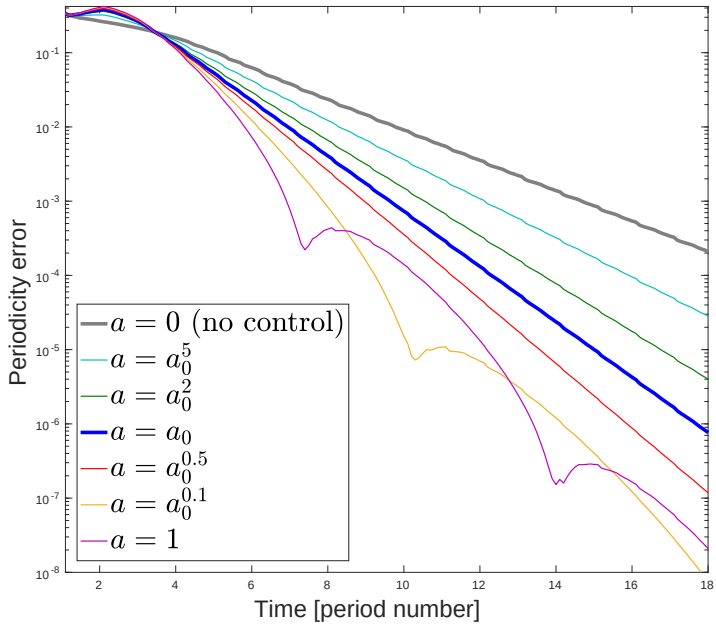

Figure 3.8: Rolling elastic tyre. Periodicity error evolutions (logarithmic scale) using different values of the gain parameter a. The reference value a_0 stands for the norm of the tangent monodromy operator of the problem, computed during the first cycle using the matrix-free power iteration method. We can see that in non-linear case the monodromy operator's norm does not give an optimal gain (here it is $\sqrt{a_0}$). However, in general the variation of evolution as function of gain is similar to that in linear case (compare with Figure 3.7).

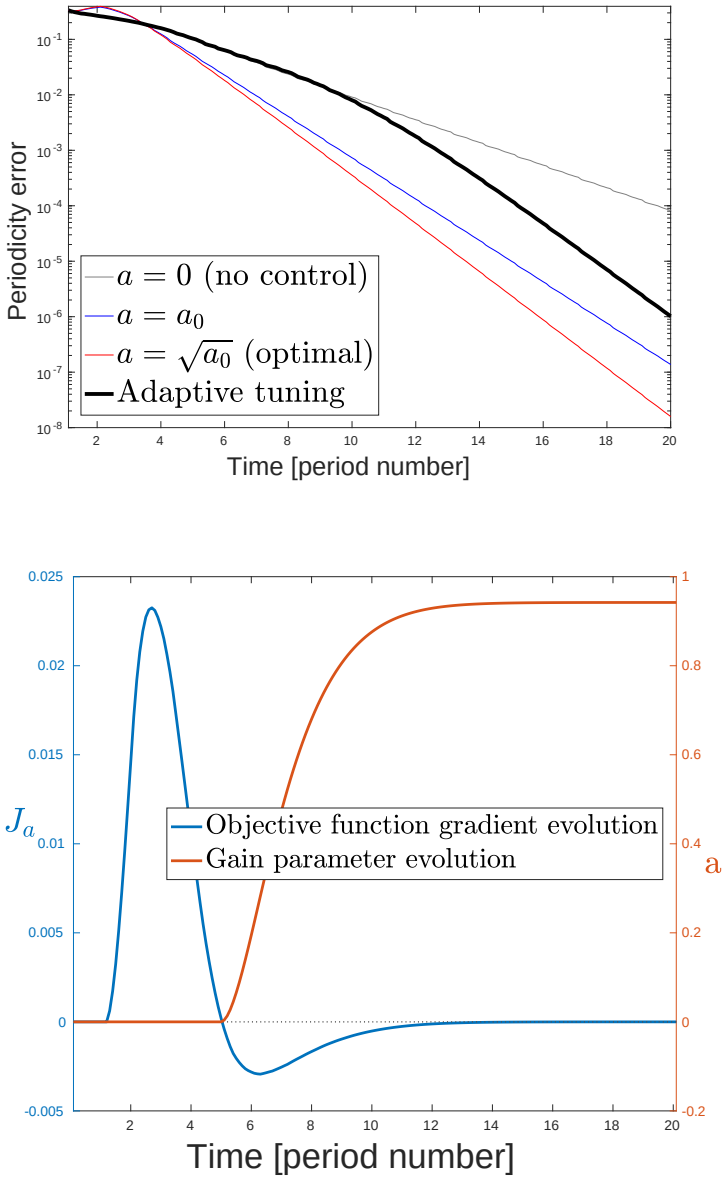

Figure 3.9: Rolling elastic tyre. Adaptive tuning of the gain parameter a to the optimal value, using the gradient descent method [Pyragas and Pyragas 2013]. Top: comparison of the periodicity error time-evolutions (logarithmic scale) using adaptive tuning and using fixed parameter values $a = a_0$ and $a = \sqrt{a_0}$ (nearly optimal), where a_0 denotes the norm of the tangent monodromy operator of the problem, computed during the first cycle. Gain parameter is successfully tuned to the optimal value, but for a longer time than the other two tests. Bottom: time evolution of the gain parameter a and of the objective function gradient. It is seen that, given arbitrary initial data, the process needs about five cycles to build a correct history, after what the adaptive tuning starts to converge to the optimal value. Here, a is forced to stay positive.

2. Viscoelastic material. Let us now introduce viscosity inside the tyre material. Viscosity coefficient η is θ-periodic in the form (1.16) with the reference viscosity coefficient η_0, which takes values 0.1, 0.25, 0.5, 0.75, 1 and 10 $MPa \cdot s$. Young's modulus is still $10^2\, MPa$. A large viscosity coefficient provides large memory effects and increases the relaxation time of the problem. The friction is still present, but viscosity-provided memory effects dominate.

Gain parameter a is set to a_0, that is the norm of the tangent monodromy operator computed during the first cycle.

Varying viscosity, we change the relaxation time of the problem, which affects the efficiency of the control. So we study the sensitivity of the feedback control to variation of the relaxation time. Simulation results are shown in Table 3.5, where we compare the number of cycles needed to reach periodicity error accuracy 10^{-4} for the non-controlled and controlled evolutions using different values of viscosity coefficient η_0. For reference, the last column represents the total iteration number for the Newton-Krylov method, that is together non-linear cycles and Krylov iterations (see also Table 2.3). Though the total cycles number is greater in case of the Newton-Krylov comparing to the feedback control, most of them are linear Krylov iterations, whose computation time is negligible with respect to that of the non-linear cycles (see Section 2.9) which are only 3-4 for the Newton-Krylov, provided that we can store the tangent matrices after factorization.

η_0,	Non-controlled		Controlled		Newton-Krylov	
$[MPa \cdot s]$	# cycles	Elapsed time	# cycles	Elapsed time	# cycles	Elapsed time
0.1	21	351 s	12	201 s	22	54 s
0.25	23	367 s	14	230 s	33	55 s
0.50	40	621 s	16	267 s	54	51 s
0.75	54	811 s	19	283 s	73	52 s
1.00	70	1060 s	21	317 s	93	60 s
10.00	406	4504 s	109	1189 s	257	70 s

Table 3.5: Rolling viscoelastic tyre (MatLab simulation). Sensitivity of the feedback control to relaxation time. The table compares the number of cycles and the computation time needed to reach periodicity error accuracy 10^{-4} for the non-controlled and controlled evolutions using different values of viscosity coefficient η_0. Varying viscosity, we change the relaxation time of the problem, which affects the efficiency of the control. For reference, the last two columns correspond to the Newton-Krylov method (see Table 2.3), where the number of cycles includes both non-linear cycles (typically 3-4) and Krylov iterations.

The corresponding periodicity error ℓ_2-norm evolutions are illustrated in logarithmic scale on Figure 3.10. Blue color corresponds to the standard non-controlled solution, red – to the controlled one.

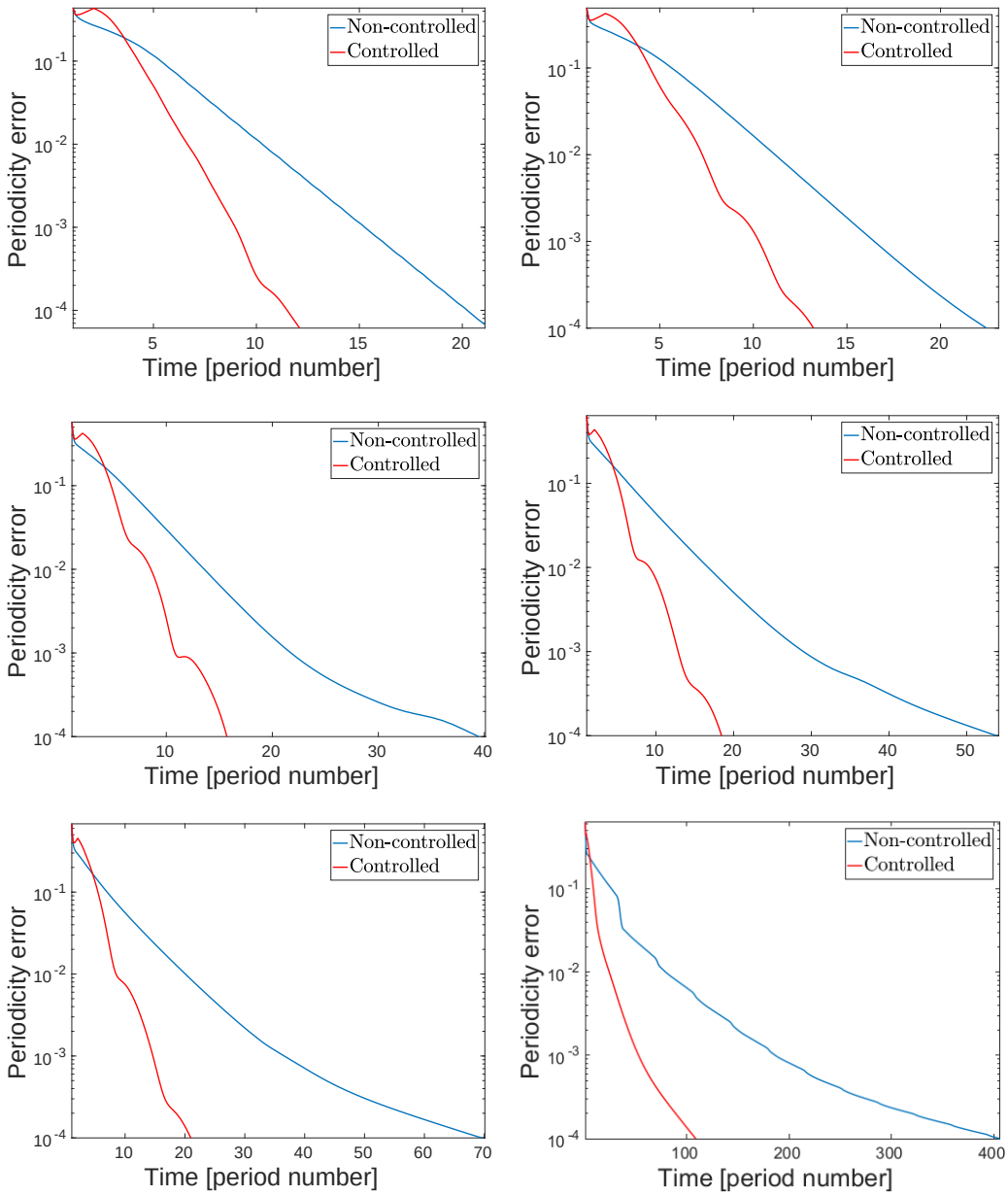

Figure 3.10: Rolling viscoelastic tyre. Sensitivity of the feedback control to relaxation time. Periodicity error ℓ_2-norm time-evolutions (logarithmic scale) using different values of viscosity coefficient $\eta_0 = 0.1,\ 0.25,\ 0.5,\ 0.75,\ 1$ and $10\ MPa \cdot s$ (left to right, top to bottom respectively). Varying viscosity, we change the relaxation time of the problem, which affects the efficiency of the control.

3.5.2 Industrial model

In this paragraph we present the results of implementation of the discussed feedback control technique in the Michelin industrial code. The non-linear mechanics of the steady rolling tyre is described in Section 1.1.1 with the mathematical definition of the problem given by (1.10):

$$F(t, \underline{\tilde{u}}, \dot{\underline{\tilde{u}}}) = 0,$$
$$\underline{\tilde{u}}(t) = S\underline{\tilde{u}}(t - T),$$

where F is defined by (1.11), T is the time period. The space shift operator S is defined through the rotation of the argument:

$$\forall \underline{v} \quad S : \underline{v}(\underline{X}) \mapsto \underline{v}(\underline{\underline{R}}_\theta \underline{X}),$$

where $\underline{\underline{R}}_\theta$ denotes rotation of the sculpture size θ. According to Section 3.3.1, the associated controlled problem, discretized in time with implicit Euler scheme, writes in the predictor-corrector form (3.32):

$$F\left(t_i,\ \underline{\tilde{u}}_i^{\#},\ \frac{\underline{\tilde{u}}_i^{\#} - \underline{\tilde{u}}_{i-1}}{\Delta t}\right) = 0,$$

$$\underline{\tilde{u}}_i = \underline{\tilde{u}}_i^{\#} + \hat{\mathcal{G}}\left(\underline{\tilde{u}}^{\#} - S\underline{\tilde{u}}_{i-m}\right),$$

where $\Delta t = T/m$, $m \in \mathbb{Z}$, is the time step, and the gain operator is in the form

$$\hat{\mathcal{G}} = a^{-1/m}\, \mathrm{D}\mathcal{W}_i \left(\frac{1}{m} \sum_{n=1}^{N_{terms}} c_{m,n}\, a^n S^{-n}\right)$$

with coefficients $c_{m,n}$ given by (3.29), and $N_{terms} = 60$. Gain parameter a is set to a_0, the norm of the tangent monodromy operator computed during the first cycle. Note that the control is not applied during the first cycle. The factor $a^{-1/m}\, \mathrm{D}\mathcal{W}_i$, where $\mathrm{D}\mathcal{W}_i$ stands for the Jacobian of the current forward operator, is supposed to preserve the "structure" of the solution vector, otherwise the local Newton resolution might fail. According to the numerical tests, omitting this factor leads to divergence of the local Newton loops.

We consider a simple geometric model (Figure 2.4), used in Section 2.9, with $M = 36$ periodic sculptures. It is a conforming (almost uniform) hexahedral mesh, periodic with respect to the angle $\theta = 2\pi/M = 10°$. In contrast to the previous academic model, here the periodicity of the model is given by the geometry. The mesh has 9830 nodes and 6624 "brick" Q_1-elements. Radius of the tyre is $270\, mm$, and the loaded radius (given constant distance from the tyre axle to the ground) is $r_{load} = 250\, mm$.

Along with the periodic tyre, we test a regular one, i.e. with no sculpture. In this case, the cyclic solution is simply the steady state. In absence of voids,

the contact zone is increased, thus the relaxation time becomes larger too. The corresponding mesh is presented on Figure (2.6) in Section 2.9. The number of sculpture motifs in this case is set to $M = 120$, which corresponds to the number of angular mesh steps.

The rolling configuration is defined by two parameters: the linear velocity of the wheel axle v_{ax} and the angular velocity of the rim ω. We consider a high speed regime with $v_{ax} = 22222.22\,mm/s$ $(= 80\,km/h)$ with $\omega = v_{ax}/r_{load} = 88.88888\ s^{-1}$.

The time period of one sculpture turn is $T = \theta/\omega = \frac{2\pi}{\omega M}$. We consider a time discretization with $m = 10$ time steps per period. That is, the time step is $\Delta t = T/m = 0.1 \cdot T$. Criterion of convergence to the periodic cycle is ℓ_∞-norm of the periodicity error $\underline{\varepsilon}_{per,i} = \underline{u}_i - S\underline{u}_{i-m}$. As the initial condition, we take the state, obtained after one standard time step, starting from the undeformed state.

All materials are incompressible (treated by penalty) and elastic, i.e. with no viscosity in the stress law. We do not take in account the inertia terms. So, all the memory effects come from the frictional contact (in the adherent regime), defined with the regularized Coulomb law (1.4).

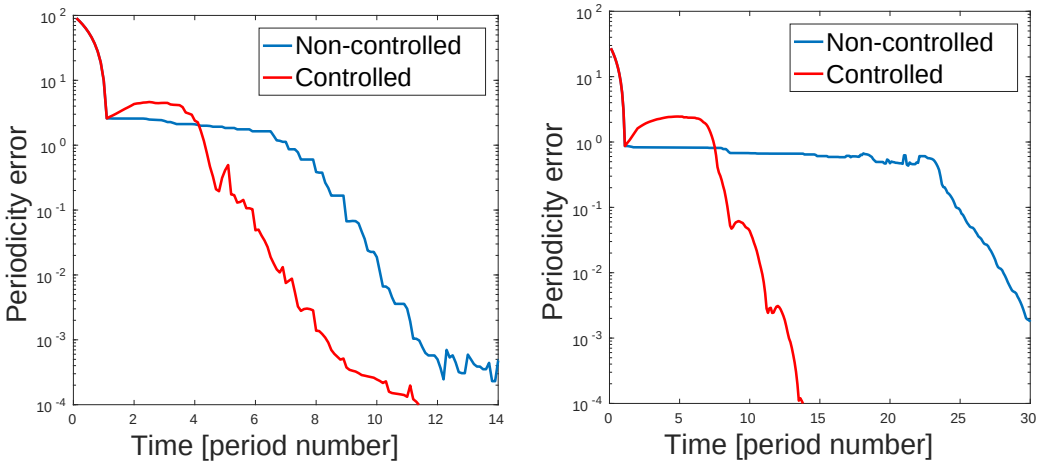

Figure 3.11: Rolling elastic tyre with friction (industrial simulations). Feedback control convergence results: time-evolutions of the periodicity error ℓ_∞-norm for the non-controlled and controlled problems. Left: tyre with periodic sculptures (Figure 2.4). Right: regular tyre with no sculptures (Figure 2.6). In absence of sculpture voids, the regular tyre has a larger contact area, which leads to stronger memory effects, hence slower convergence and better acceleration provided by the feedback control.

Convergence results are presented on Figure 3.11, while the simulation results are described on Figures 2.4 and 2.5 of Chapter 2. In absence of sculpture voids,

the regular tyre has a larger contact area, which leads to stronger memory effects. This is expressed in a slower convergence, which can be seen on the figure, as well as in the difference of the tangent monodromy operator's norm (which is actually associated to the relaxation time). In case of the periodic tyre, the monodromy norm is $a_0 = 0.9833$, while for the regular tyre it is $a_0 = 0.9884$. Therefore, the acceleration provided by the feedback control is greater in case of the regular tyre (see Figure 3.11, right).

In case of the periodic tyre (Figure 3.11, left), at periodicity error 10^{-3} the algorithm reaches the limit in accuracy of the stick-slip friction model, which becomes noisy when the mesh is not sufficiently refined next to sculpture edges.

3.6 Conclusion

In this chapter, we have studied the time-delayed feedback control [Pyragas 1992, Hövel and Schöll 2005] as a method for computing the space-time periodic states of evolution problems. In the industrial applications, in order to avoid the inversion of very large matrices, such cyclic states are often computed as the asymptotic limit solution of an initial value problem with arbitrarily chosen initial data. Calculating such initial value problems until the asymptotic limit may take a lot of time for "viscous" problems, when memory effects are very large. The feedback control method can be considered as an observer-controller type modification of this asymptotic method, where the lack of periodicity of the transient solution is an extra information (observation) on which one can apply control techniques to accelerate convergence. In other words, we can modify the initial value problem by introducing a closed loop feedback control term, based on this periodicity error and accelerating convergence to the limit cycle.

The time-delayed feedback control, first proposed in [Pyragas 1992], is a well-known and powerful tool widely used for stabilization of unstable periodic orbits and unstable steady states [Kittel et al. 1995, Pyragas 1995, 2002, Bleich and Socolar 1996, Hövel and Schöll 2005, Yanchuk et al. 2006]. In this work it is applied to an initially stable system in order to accelerate its convergence to the asymptotic limit solution. Moreover, given the space-time periodicity, along with the time-delay the feedback term includes also a shift in space, which must be carefully analyzed.

We have started from an analytical analysis of an abstract linear evolution problem in a very general form, modified by introducing a feedback control term. By performing a spectral decomposition of the controlled problem in space, we are able to reduce it to a time-delayed differential system [Bellman and Cooke 1963, Yi et al. 2010, Asl and Ulsoy 2003], whose explicit solution uses the Lambert W function [Corless et al. 1996, Shinozaki 2007, Valluri et al. 2000]. This calculation provides an existence and time convergence result for both the non-controlled and the controlled problems. Given this explicit solution, we have analyzed the

influence of the control term on the Floquet exponents of the controlled transient solution and have proposed then the optimal form of the gain operator optimizing the asymptotic convergence to the limit cycle.

The main result of this chapter is the explicit form of the optimal gain operator, which is given by a series combining shifted periodicity errors. Construction of the present theoretical control requires computing of matrix exponential, which provokes loss of sparsity and increases numerical cost. Then, a practical version of the optimal control has been proposed, where the matrix exponential is replaced by a scalar exponential, which is defined by the norm of the monodromy operator of the problem (that is by the relaxation time). In this form the control has much lower computational complexity, while preserving the acceleration rate.

In the same way we have also constructed the optimal control for an abstract time-discrete problem. This discrete form uses the series generalizing the Lambert W function and converges to the previously proposed continuous optimal control, when the time step size goes to zero.

Finally, a universal predictor-corrector scheme for the proposed practical control has been introduced. Simple in implementation, it can be easily added in the standard time evolution process at almost no computational cost. The correction step does not solve any linear system and only requires computing of a linear combination of shifted periodicity errors. This scheme has been also extended to non-linear cases.

The main difficulty is to choose the gain parameter associated to the relaxation time of the problem. In a non-linear framework, no explicit expression for its optimal value is available, and thus it should be approximated by a linear case equivalent or tuned with an adaptive tuning technique. For example, we have performed the gradient-descent adaptive tuning [Pyragas and Pyragas 2013], which has successfully led to the optimal gain value, but after a rather lengthy initialization time.

As for performance, we have studied the influence of the magnitude of the memory effects on the efficiency of the method. It was shown that the provided acceleration of the convergence rate increases with the relaxation time of the problem, what was justified in numerical tests. Thus, the method is more efficient for the "viscous" problems, when the memory effects are large.

The feedback control method has been applied to a couple of model problems and compared with the classic asymptotic method and the Newton-Krylov method [Govindjee et al. 2014]. To confirm the theoretical results obtained in the linear framework, we have first considered an academic linear 2D heat problem, where a planar disk is heated with a source periodically moving along a circular path. Then, we have tested the method on a non-linear academic model problem of steady rolling of a 3D viscoelastic tyre with periodic sculptures, in presence of stick-slip frictional contact with the soil. Finally, the present feedback control method in the predictor-corrector form has been successfully integrated into Michelin industrial code and tested on the above non-linear rolling tyre problem,

accelerating convergence to the limit cyclic state.

We conclude that the feedback control has a nice mathematical structure and can be successfully used for accelerating convergence to the limit cyclic steady state. The presented results help to better understand the structure of the optimal form of the delayed feedback control and its behavior. Its acceleration rate grows with the relaxation time of the problem. It is always more efficient than the classic asymptotic limit method, especially in case of large memory effects, but is usually more time consuming than the optimized Newton-Krylov shooting method, where the factorized Jacobians needed for the Krylov iterations are stored during the non-linear cycles. Nevertheless, this is also an advantage of the feedback control that in the contrast to the Newton-Krylov method it does not require the storage of large matrices. So, in cases when storage of factorized Jacobians is not available, or when Newton method is less robust than the fixed point method (ex., for "concave" problems), the delayed feedback control, being quite efficient for the problems with large diffusion effects, is of high practical use for computing the cyclic states.

CHAPTER 4

Delayed feedback control of dynamic systems

Summary

4.1 Delayed feedback control for linear dynamics

Let us consider an abstract linear second order differential equation on an unknown state vector $u(t) \in \mathbb{R}^d$, $d \in \mathbb{Z}$:

$$M\partial_{tt}u + C\partial_t u + Ku = f, \tag{4.1}$$

where matrices M, K and C are symmetric positive definite. We are looking for a time periodic solution to this equation with some time period $T > 0$. That is $u(t)$ must satisfy the periodicity condition

$$u(t) = u(t - T).$$

Positive definiteness of the matrices M, K and C introduces a natural damping in the evolution of $u(t)$. So, in practice, such a solution is sought as an asymptotic limit of the standard evolution from an arbitrary initial state. As in Chapter 3, we want to accelerate convergence to this limit cycle. In this chapter we want to extend the delayed feedback control technique, proposed in Chapter 3, to the second order differential problem. Note that periodicity in time is a particular case of periodicity in space-time. For this purpose, let us rewrite the second order differential equation (4.1) as a first order differential system. With notations

$$Y = \begin{bmatrix} u \\ \partial_t u \end{bmatrix}, \qquad A = \begin{bmatrix} & -K \\ K & C \end{bmatrix}, \qquad B = \begin{bmatrix} K & \\ & M \end{bmatrix}, \qquad F = \begin{bmatrix} \\ f \end{bmatrix},$$

the problem writes

$$\begin{aligned} B\,\partial_t Y + A\,Y &= F, \\ Y(t) &= Y(t - T). \end{aligned} \tag{4.2}$$

In this form it is reminiscent to the abstract problem (3.1) with the space shift S being the identity, for which the optimal delayed feedback control is already studied in Chapter 3. Though the "stiffness" operator A is not symmetric any more, we can still construct a spectral decomposition of problem (4.2), and thus the construction of the optimal gain of Section 3.2.3 can be reproduced in the current framework. However, the fact that the spectrum of the problem has now complex eigenvalues with non zero imaginary part makes it impossible to introduce the minimal eigenvalue version of the optimal gain operator (see Section 3.2.5). Therefore, in the present chapter, we want to develop an alternative strategy for the practical approximation of the optimal gain operator, which can be used in the case of non-symmetric operators.

The problem (4.2) is discretized in time, using Newmark scheme with time step $\Delta t = T/m$, $m \in \mathbb{Z}$:

$$\begin{gathered} B\,\frac{Y_i - Y_{i-1}}{\Delta t} + A\,\frac{Y_i + Y_{i-1}}{2} = F_{i-1/2}, \quad i \in \mathbb{N}, \\ Y_n = Y_{i-m}, \end{gathered}$$

where $F_{i-1/2}$ is the right hand side term computed in the middle point $t_{i-1/2} = (n - \frac{1}{2})\Delta t$. Then, we are looking the m-periodic solution as the asymptotic limit of the following sequence:

$$Y_i = (B + \tfrac{\Delta t}{2}A)^{-1}(B - \tfrac{\Delta t}{2}A)\, Y_{i-1} + \Delta t\, (B + \tfrac{\Delta t}{2}A)^{-1} F_{i-1/2}, \qquad i > 0,$$
$$Y_0 = \textit{"arbitrary initial data"}.$$

Applying the optimal delayed feedback control in the predictor-corrector form (3.27), the n-th time step becomes:

$$\begin{aligned} Y_i^{\#} &= (B + \tfrac{\Delta t}{2}A)^{-1}(B - \tfrac{\Delta t}{2}A)\, Y_{i-1} + (B + \tfrac{\Delta t}{2}A)^{-1}\Delta t\, F_{i-1/2}, \\ Y_i &= Y_i^{\#} + \hat{\mathcal{G}}\, (Y_i^{\#} - Y_{i-m}), \end{aligned}$$

where the gain operator is given by

$$\hat{\mathcal{G}} = \frac{1}{m} \sum_{n=1}^{N_{\text{terms}}} c_{m,n} \left((B + \tfrac{\Delta t}{2}A)^{-1}(B - \tfrac{\Delta t}{2}A) \right)^{mn} \tag{4.3}$$

with coefficients

$$c_{m,n} = \frac{1}{n!} \cdot \frac{(mn)!}{(mn - n + 1)! \cdot (m-1)^{n-1}} \cdot \left(1 - \frac{1}{m}\right)^{mn-1}.$$

The difference $Y_i^{\#} - Y_{i-m}$ defines the periodicity error.

4.2 Practical approach: control applied to principal modes

As it was mentioned above, the minimal eigenvalue strategy for construction of the practical control, previously used for symmetric problems (Section 3.2.5), does not work in the case of dynamic system, where the "stiffness" operator is not symmetric. The principal difficulty comes from its skew-symmetric part

$$A_{asym} = \frac{1}{2}(A - A^t) = \begin{bmatrix} & -K \\ K & \end{bmatrix}.$$

This skew-symmetric contribution introduces imaginary parts in the spectrum of A and causes the oscillations in time of the solution. It can not be replaced by a real scalar, as we did it for symmetric matrices (see Section 3.2.5). So, the theoretical control should be applied in its complete form. Since in practice it can be numerically expensive to apply the theoretical control to the whole solution, we propose to control only several principal modes, i.e. the modes converging with the slowest rate.

Indeed, the problem convergence rate is defined by the first principal mode. However, controlling only this mode will not control the second mode, which becomes in this case dominating. Thus, it is important to control all leading modes, such that the first one stays still the slowest

For this purpose, let us first separate the damping contribution (symmetric part) and the skew-symmetric part of A. Let α_0 be the minimal real part of the generalized eigenvalues of A and B:

$$\alpha_0 = \min\{\mathfrak{Re}(\alpha) > 0 \mid \exists \psi : \ A\psi = \alpha B\psi\}.$$

In the gain operator definition, we replace A by $\alpha_0 B + A_{asym}$. So the modified gain operator writes

$$\hat{\mathcal{G}} = \frac{1}{m} \sum_{n=1}^{N_{\text{terms}}} c_{m,n} \left((B + \tfrac{\Delta t}{2}(\alpha_0 B + A_{asym}))^{-1}(B - \tfrac{\Delta t}{2}(\alpha_0 B + A_{asym}))\right)^{mn}.$$

Let us consider the generalized eigenvalue problem for A_{asym} and B:

$$\begin{bmatrix} & -K \\ K & \end{bmatrix} \psi = \omega \begin{bmatrix} K & \\ & M \end{bmatrix} \psi.$$

Denoting by ψ_1 and ψ_2 the corresponding components of ψ, we have that

$$\begin{aligned} \psi_2 &= -\omega \psi_1 \\ K\psi_1 &= \omega M \psi_2. \end{aligned}$$

Hence, we obtain the generalized eigenvalue problem for K and M:

$$K\psi_1 = -\omega^2 M \psi_1.$$

Thus, ψ_1 is a generalized eigenvector of K and M corresponding to the eigenvalue λ, and $\omega = \pm \mathrm{i}\sqrt{\lambda}$. Then the diagonal matrix Ω, composed of the generalized eigenvalues of A_{asym} and B, and corresponding eigenbasis Ψ, such that

$$A_{asym}\Psi = B\Psi\Omega,$$

can be defined as

$$\Psi = \begin{bmatrix} \Phi & \Phi \\ -\mathrm{i}\Phi\sqrt{\Lambda} & \mathrm{i}\Phi\sqrt{\Lambda} \end{bmatrix}, \quad \Omega = \begin{bmatrix} \mathrm{i}\sqrt{\Lambda} & \\ & -\mathrm{i}\sqrt{\Lambda} \end{bmatrix}$$

where Λ is a diagonal matrix, composed of eigenvalues of K and M, and Φ is the associated eigenbasis:

$$K\Phi = M\Phi\Lambda.$$

If Φ is normalized with respect to the inner product defined by K, so that $\Phi^* K \Phi = \mathrm{Id}$, then $\Psi^* B \Psi = \mathrm{Id}$. In this case, we can write that

$$A_{asym} = B\Psi\Omega\Psi^* B,$$

which is used for the eigenvalue decomposition of the modified gain operator:

$$\begin{aligned}\hat{\mathcal{G}} &= \frac{1}{m}\sum_{n=1}^{N_{\text{terms}}} c_{m,n}\left((B+\tfrac{\Delta t}{2}(\alpha_0 B + A_{asym}))^{-1}(B-\tfrac{\Delta t}{2}(\alpha_0 B + A_{asym}))\right)^{mn} \\ &= \frac{1}{m}\Psi\left(\sum_{n=1}^{N_{\text{terms}}} c_{m,n}\left(((1+\tfrac{\Delta t}{2}\alpha_0)\,\mathrm{Id}+\tfrac{\Delta t}{2}\Omega)^{-1}((1-\tfrac{\Delta t}{2}\alpha_0)\,\mathrm{Id}-\tfrac{\Delta t}{2}\Omega)\right)^{mn}\right)\Psi^* B.\end{aligned}$$

If we introduce a diagonal matrix

$$D = \frac{1}{m}\sum_{n=1}^{N_{\text{terms}}} c_{m,n}\left(((1+\tfrac{\Delta t}{2}\alpha_0)\,\mathrm{Id}+\tfrac{\Delta t}{2}\mathrm{i}\sqrt{\Lambda})^{-1}((1-\tfrac{\Delta t}{2}\alpha_0)\,\mathrm{Id}-\tfrac{\Delta t}{2}\mathrm{i}\sqrt{\Lambda}\right)^{mn},$$

then $\hat{\mathcal{G}}$ can be written as

$$\begin{aligned}\hat{\mathcal{G}} &= \begin{bmatrix}\Phi \\ -\mathrm{i}\Phi\sqrt{\Lambda}\end{bmatrix} D \begin{bmatrix}\Phi^* & \mathrm{i}\sqrt{\Lambda}\Phi^*\end{bmatrix} B + \overline{\begin{bmatrix}\Phi \\ \mathrm{i}\Phi\sqrt{\Lambda}\end{bmatrix} D \begin{bmatrix}\Phi^* & -\mathrm{i}\sqrt{\Lambda}\Phi^*\end{bmatrix}} B \\ &= \begin{bmatrix}\Phi \\ -\mathrm{i}\Phi\sqrt{\Lambda}\end{bmatrix} D \begin{bmatrix}\Phi^* & \mathrm{i}\sqrt{\Lambda}\Phi^*\end{bmatrix} B + \overline{\begin{bmatrix}\Phi \\ -\mathrm{i}\Phi\sqrt{\Lambda}\end{bmatrix} D \begin{bmatrix}\Phi^* & \mathrm{i}\sqrt{\Lambda}\Phi^*\end{bmatrix}} B \\ &= 2\,\mathfrak{Re}\left\{\begin{bmatrix}\Phi \\ -\mathrm{i}\Phi\sqrt{\Lambda}\end{bmatrix} D \begin{bmatrix}\Phi^* & \mathrm{i}\sqrt{\Lambda}\Phi^*\end{bmatrix}\right\} B.\end{aligned}$$

So, we can define now the control, reduced to the first r principal modes:

$$\hat{\mathcal{G}}_r = 2\,\mathfrak{Re}\left\{\begin{bmatrix}\Phi_r \\ -\mathrm{i}\Phi_r\sqrt{\Lambda_r}\end{bmatrix} D_r \begin{bmatrix}\Phi_r^* & \mathrm{i}\sqrt{\Lambda_r}\Phi_r^*\end{bmatrix}\right\} B \tag{4.4}$$

with

$$D_r = \frac{1}{m}\sum_{n=1}^{N_{\text{terms}}} c_{m,n}\left(\left((1+\tfrac{\Delta t}{2}\alpha_0)\mathrm{Id}_r + \tfrac{\Delta t}{2}\mathrm{i}\sqrt{\Lambda_r}\right)^{-1}\left((1-\tfrac{\Delta t}{2}\alpha_0)\mathrm{Id}_r - \tfrac{\Delta t}{2}\mathrm{i}\sqrt{\Lambda_r}\right)\right)^{mn},$$

where Λ_r is a diagonal matrix composed of the r smallest eigenvalues of K and M, Φ_r is a reduced basis composed of the associated eigenvectors, and Id_r stands for the $r \times r$ identity matrix. The choice of r is still open. In practice, we use r between three and five.

4.3 Application. Linear 3D beating heart model

Let us now apply the control strategy proposed in the previous section to a simple academic linear problem. As an example of a second order in time system with time-periodicity condition, let us consider a beating heart model. We use the linear 3D heart model presented in [Moireau et al. 2008, 2009, Moireau 2009]. The numerical model implemented in MatLab and C was kindly provided by Philippe Moireau [M3disim team Inria n.d.].

As seen in Section 1.3.2, the corresponding variational form is given by system (1.30):

$$\int_\Omega \rho \ddot{\underline{u}} \cdot \underline{v} \, \mathrm{d}\Omega + \int_\Omega \underline{\underline{\underline{\underline{K}}}} \, (\eta \nabla_s \dot{\underline{u}} + \nabla_s \underline{u}) : \nabla \underline{v} \, \mathrm{d}\Omega = \mathcal{P}^{ext},$$
$$\underline{u}(t) = \underline{u}(t - T),$$

where $\underline{\underline{\underline{\underline{K}}}} \, \underline{\underline{t}} = \lambda \, \mathrm{tr}(\underline{\underline{t}}) \, \mathrm{Id} + 2\mu \, \underline{\underline{t}}$ for any $\underline{\underline{t}}$. Lamé coefficients λ and μ are defined by (1.15) through the Young's modulus $E = 12.4 \cdot 10^3 \, Pa$ and the Poisson ratio $\nu = 0.39$. Viscosity coefficient is $\eta = 1.6 \cdot 10^{-4} s$. Volumic mass is set to $\rho = 10^3 \, kg/m^3$. And the time period is $T = 1 \, s$.

The geometrical model is presented on Figure 4.1. We pose the homogeneous Dirichlet boundary condition at the base. The contractions are produced by a pre-stress (electrical activation), resulting to an external virtual work

$$\mathcal{P}^{ext} = \int_\Omega \sigma_0 w(|\underline{X} - \underline{X}_C| - ct) \, \nabla \cdot \underline{v} \, \mathrm{d}\Omega,$$

with the magnitude $\sigma_0 = 4.5 \cdot 10^4 \, Pa$ and the function w defined as in [Moireau et al. 2009] and representing a spherical wave with initiation center $\underline{X}_C$ (see Figure 4.1) and wave speed $c = 0.5 \, m/s$.

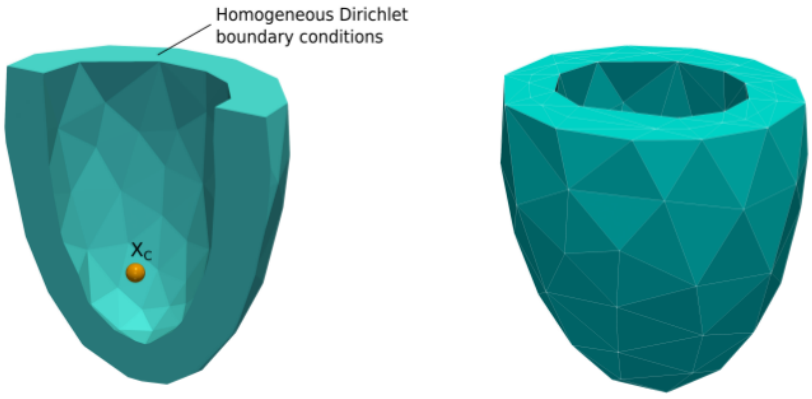

Figure 4.1: Academic heart ventricle model.

Problem (1.29) is discretized in space with the finite elements method using Lagrangian P_1-elements on a conforming tetrahedral mesh with 158 nodes and 463 tetrahedra. Denoting by u_h the finite element solution vector associated to the displacement field, we write the discretized system

$$M\ddot{u}_h + C\dot{u}_h + Ku_h = f,$$

where M, C and K are the finite element matrices associated respectively to the mass, viscosity and stiffness terms, and the vector f stands for the activation force. Introducing the notation

$$Y = \begin{bmatrix} u_h \\ \dot{u}_h \end{bmatrix}, \qquad A = \begin{bmatrix} & -K \\ K & C \end{bmatrix}, \qquad B = \begin{bmatrix} K & \\ & M \end{bmatrix}, \qquad F = \begin{bmatrix} \\ f \end{bmatrix},$$

we obtain the second-order system (4.2)

$$\begin{aligned} B\,\partial_t Y + A\,Y &= F, \\ Y(t) &= Y(t-T). \end{aligned}$$

Further, proceeding as in Section 4.1, we discretize the system in time with the Newmark scheme and apply then the delayed feedback control in the predictor-corrector form (3.27). Thus, the i-th time step writes

$$\begin{aligned} Y_i^{\#} &= (B + \tfrac{\Delta t}{2}A)^{-1}(B - \tfrac{\Delta t}{2}A)\,Y_{i-1} + (B + \tfrac{\Delta t}{2}A)^{-1}\Delta t\,F_{i-1/2}, \\ Y_i &= Y_i^{\#} + \mathcal{G}\,(Y_i^{\#} - Y_{i-m}), \end{aligned}$$

where $m = 500$ is the number of time steps per period, the time step is $\Delta t = T/m$, and $T = 1\,s$ is the time period.

Here we test and compare the optimal gain operator (4.3) and its reduced form (4.4) applied to $r = 3$, 5 and 10 principal modes, where the minimal eigenvalue α_0 of $B^{-1}A$ and the r smallest eigenvalues Λ_r of $M^{-1}K$ with the associated eigenvectors Φ_r are calculated with Krylov subspace method using the inverse matrix (provided by MatLab). Efficiency of the method is defined by the rate of decrease in time of the ℓ_2-norm of the periodicity error $\varepsilon_{per} = Y_i - Y_{i-m}$. Periodicity error evolutions for different numbers of controlled modes are depicted on Figure 4.2. We observe that controlling of the five principal modes is enough to obtain the fastest convergence until accuracy 10^{-3}, while the ten-modes control provides the same convergence rate as the theoretical optimal gain. Note that $r = 10$ is far away from the system's size, since the dimension of the system is of order $158 \times 3 \times 2$ (minus Dirichlet boundary conditions). Let us also notice a great acceleration about 10 times, provided by the optimal and the ten-modes controls.

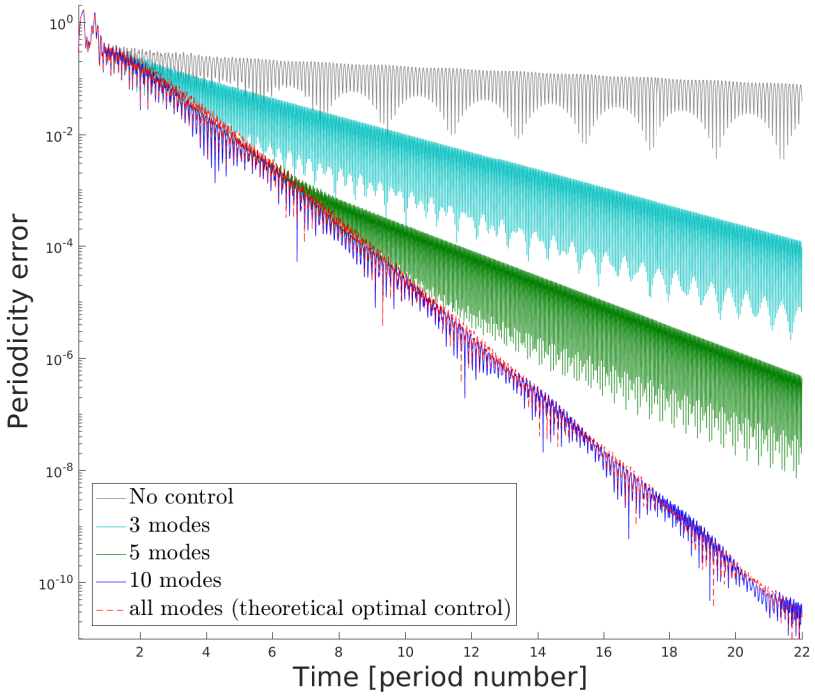

Figure 4.2: Linear 3D beating heart model. Time evolution of periodicity error, controlling first several modes. Comparison of performance using the optimal gain (4.3) and the reduced gain (4.4) applied to the 3, 5 and 10 principal modes. Controlling of the five principal modes is enough to obtain the fastest convergence until accuracy 10^{-3}, while the ten principal modes control provides the same convergence rate as the theoretical optimal gain.

General conclusion and perspectives

In this work, we have studied two alternative methods for the efficient calculation of a cyclic solution of non-linear evolution problems, satisfying space-time periodic conditions. For large problems, direct methods are not very convenient, since they require the inversion of very large matrices. In practice, such a cyclic solution is computed as an asymptotic limit of the associated initial value problem with arbitrary initial data. However, when the relaxation time is large, convergence to the limit cycle can be very slow. So alternative techniques providing fast access to the limit cycle are of current interest. Here, we have advocated the following two techniques:

- Solve the problem on the unknown initial state using a Newton non-linear solver, combined with a Krylov linear solver [Chan and Jackson 1984, Telichevesky et al. 1995, Knoll and Keyes 2004].
- Accelerate the standard asymptotic convergence by introducing a feedback control term in the problem [Pyragas 1992, Hövel and Schöll 2005].

Thus, the first one is the Newton-Krylov method (Chapter 2) computing the "correct" initial state that provides the cyclic solution, using a matrix-free Krylov iterative linear solver. This method can be found for example in [Govindjee et al. 2014, Brandstetter and Govindjee 2017]. In our approach, we optimize this method by reformulating the problem with respect to a time-advanced state and by using in the linear Krylov solver the information stored during the last cycle, so that the computation time of the Krylov part becomes negligible with respect to a non-linear cycle (global Newton iteration).

In more details, the method consist in considering the periodicity condition as an equation for the unknown "true" initial state, which provides the cyclic solution. Once the "correct" initial data is found, the desired space-time periodic state is provided by the solution of the initial value problem during one time

period. The equation on the unknown initial state includes a non-linear evolution function, requiring to solve an initial value problem during one time period. Applying Newton-Raphson technique, we obtain a linear system, where the residual is defined by the periodicity error, and the Jacobian includes the gradient of the evolution function (called tangent monodromy operator or global Jacobian). The construction of this operator, which can not be expressed explicitly, is quite challenging.

One Newton iteration corresponds to one time period and, after time discretization, includes several time steps. Each time step solves a local non-linear problem, using an internal Newton loop. Successive solutions of the linear systems, arising at the end of each such loop, are the constitutive parts of the global Jacobian. Thus, local Jacobians, stored during one cycle, can be used to construct the corresponding tangent monodromy matrix. However, in practice, for efficiency, this matrix is never assembled, but defined implicitly by the multiplication operation, using the stored operators. Then, one of the matrix-free Krylov iterative methods (GMRES, for example) can be used to solve the linear system that appears at each global Newton iteration.

During GMRES, each Krylov iteration is equivalent to the integration of one linearized cycle. That is, one Krylov iteration requires to apply the global Jacobian, which means to solve a sequence of linear systems, associated to the local Jacobians. However, each of these systems has been already solved during a corresponding time step. So, if its factorization (LU or Cholesky) is already performed, it has to be stored instead of the matrix itself. Using once-performed factorizations reduces considerably the numerical cost of local Jacobians inversion during Krylov iterations. In our simulations, it allowed to accelerate one Krylov iteration in about 30 times. In this way, the computation time needed to apply the global Jacobian (tangent monodromy operator) becomes negligible with respect to the time to compute the residual (periodicity error), which is the time to compute one time period (cycle).

To summarize, on each global Newton step, given an initial state (starting with an arbitrary guess), the method solves the non-linear initial value problem during the first period, in order to estimate the periodicity error and to store the tangent matrices. If the periodicity error is sufficiently small, the current initial state is accepted. Otherwise, a correction step is performed, where the increment (correction) is found from the periodicity error and the monodromy matrix, and the initial state is then updated for the next step.

The method can be considered as a kind of shooting method. Indeed, starting with an arbitrary left boundary value, we go through one period evolution to obtain the right boundary value and use it for correction of the left boundary value and so on.

In the proposed algorithm, each Newton step approximates the global initial state at time $t = 0$. However, it is more convenient to approximate the initial state of the current time period, i.e. at time $t = nT$, where n is the number of the

current cycle, which corresponds to a Newton step. This can be achieved by change of variable in the Newton algorithm, and leads to modification of a standard time evolution by introducing a correction of the current transient solution after each cycle. The correcting step involves the current periodicity error and the tangent monodromy matrix, defined implicitly, using operators stored during the cycle (along with the corresponding factorizations).

Both implementations are equivalent and present just two points of view to the same algorithm. The advantage of the last formulation is that it does not require any preconditioner in the Krylov solution of the associated linear system and that it can be easily added to the standard time evolution. Besides, it may be considered as an observer-controller process, where correction, performed in the end of each cycle, is based on the observation during this cycle.

On the other side, the present Newton-Krylov algorithm is memory greedy, because one needs to store a number of matrices, proportional to the number of time steps per cycle. That is, a fine time discretization of a large data problem (with a lot of degrees of freedom) implies a large number of large matrices to be stored (even along with their factorizations). Thus, the method favors problems either with few time steps per cycle, or with few degrees of freedom in space domain, which ensures a reasonable memory usage.

In contrast, the second method discussed in this work (Chapter 3) – the time-delayed feedback control [Pyragas 1992, Hövel and Schöll 2005] – does not require the storage of large matrices. It can be considered as an observer-controller type modification of the standard time-evolution, where the lack of periodicity of the transient solution is an extra information (observation) on which one can apply control techniques to accelerate convergence. In other words, we modify the initial value problem by introducing a closed loop feedback control term, based on this periodicity error and accelerating convergence to the limit cycle.

First proposed in [Pyragas 1992], the time-delayed feedback control is a well-known and powerful tool widely used for stabilization of unstable periodic orbits and unstable steady states [Kittel et al. 1995, Pyragas 1995, 2002, Bleich and Socolar 1996, Hövel and Schöll 2005, Yanchuk et al. 2006]. In our framework it is applied to an initially stable system in order to accelerate its convergence to the asymptotic limit solution. Moreover, given the space-time periodicity, along with the time-delay the feedback term includes also a shift in space.

We have presented an analytical analysis of an abstract linear evolution problem in a very general form, modified by introducing a feedback control term. By performing a spectral decomposition of the controlled problem in space, we are able to reduce it to a time-delayed differential system [Bellman and Cooke 1963, Yi et al. 2010, Asl and Ulsoy 2003], whose explicit solution uses the Lambert W function [Corless et al. 1996, Shinozaki 2007, Valluri et al. 2000]. This calculation provides an existence and time convergence result for both the non-controlled and the controlled problems. Given this explicit solution, we have analyzed the influence of the control term on the Floquet exponents of the controlled transient

solution and have proposed then the optimal form of the gain operator optimizing the asymptotic convergence to the limit cycle.

One of our main results is the explicit form of the optimal gain operator, which is given by a series combining shifted periodicity errors. Construction of the present theoretical control requires computing of matrix exponential, which provokes loss of sparsity and increases numerical cost. Then, a practical version of the optimal control in case of symmetric operators has been proposed, where the matrix exponential is replaced by a scalar exponential, which is defined by the norm of the monodromy operator of the problem (that is by the relaxation time). In this form the control has much lower computational complexity, while preserving the acceleration rate.

In the same way we have also constructed the optimal control for an abstract time-discrete problem. This discrete form uses the series generalizing the Lambert W function and converges to the previously proposed continuous optimal control, when the time step size goes to zero.

Finally, a universal predictor-corrector scheme for the proposed practical control has been introduced. Simple in implementation, it can be easily added to the standard time evolution process at almost no computational cost. The correction step does not solve any linear system and only requires computing of a linear combination of shifted periodicity errors. This scheme has been also extended to non-linear cases.

The main difficulty is to choose the gain parameter associated to the relaxation time of the problem. In a non-linear framework, no explicit expression for its optimal value is available, and thus it should be approximated by a linear case equivalent or tuned with an adaptive tuning technique. We have used both techniques. For example, we have performed the gradient-descent adaptive tuning [Pyragas and Pyragas 2013], which has successfully led to the optimal gain value, but after a rather lengthy initialization step.

As for performance, we have studied the influence of the magnitude of the memory effects on the efficiency of the method. It was shown that the provided acceleration of the convergence rate increases with the relaxation time of the problem, what was justified in numerical tests. Thus, the method is more efficient for the "viscous" problems, when the memory effects are large.

The indicated practical control, where the entries of the monodromy operator are replaced by its norm, provides the optimal efficiency only in the case of symmetric operators. Otherwise, the construction of a simplified version of the theoretical optimal gain is more sophisticated. In Chapter 4 we have proposed such a construction in the case of a linear differential system of second order in time, where the feedback control is applied only to the several principal modes in the spectral decomposition of the solution. This approach has been applied to a linear 3D beating heart model [Moireau et al. 2009], which is a particular example of space-time periodicity with the space shift given by the identity. Simulation results have shown that controlling only the three-five principal modes allows to

speed up the convergence three to five times, while ten controlled modes have provided the optimal acceleration of about ten times.

The feedback control and the Newton-Krylov methods have been applied to model problems and compared with the classic asymptotic approach. We started with a linear problem. As expected, Newton algorithm gives the solution after the first iteration (cycle). However, one Newton iteration solves a linear problem using GMRES, where each Krylov iteration is of the same complexity as the calculation of one cycle evolution. So, we have compared performance of the Newton-Krylov algorithm on this linear example to the asymptotic method and have observed that Newton-Krylov method requires less iterations with better accuracy. Besides, Newton-Krylov was less sensitive to the relaxation time growth. On the other hand, the feedback control has accelerated convergence to the limit cycle, requiring also less cycles to converge than the non-controlled asymptotic evolution, but still greater than Newton-Krylov.

Further, both methods have been applied to our main model problem: a rolling 3D tyre in presence of stick-slip frictional contact with the soil (Section 1.1.1). This problem is three dimensional and non-linear. First, we have studied the method on a simplified academic model (Section 1.1.4) using MatLab R2016b. Newton-Krylov method has converged with quadratic rate and has reached better accuracy four times faster than the asymptotic method. Storing LU factorizations of local Jacobians during the cycle and reusing them during the GMRES allowed to reduce computing time of one Krylov iteration in about 30 times.

Finally, the feedback control and the Newton-Krylov methods have been integrated into the Michelin industrial code. There, Newton-Krylov has not demonstrated quadratic convergence rate, because of using non-exact local Jacobians for the local Newton resolutions on each time step. In case of small rim couple, Newton-Krylov has been twice more efficient than the asymptotic method. But for a greater couple, efficiency of both methods was almost the same (asymptotic method converges even a little faster). In the case of a regular tyre (with no sculpture), when the cyclic solution is simply the steady state, Newton-Krylov has been more than five times faster.

While convergence time of the asymptotic evolution as well as of the feedback control method depends on the size of memory effects of the problem, Newton-Krylov method always converged within the same number of iterations/cycles. Instead, the variation of the relaxation time affected only the number of Krylov iterations on each cycle. Given that one Krylov iteration (equivalent to a linearized cycle, but with known factorization) is more than 100 times faster than one non-linear cycle, such a trade is quite advantageous. Thus, Newton-Krylov convergence time should be of the same order independently of the problem's relaxation time.

We conclude that the feedback control has a nice mathematical structure and can be successfully used for accelerating convergence to the limit cyclic steady state. The presented results help to better understand the structure of the optimal form of the delayed feedback control and its behavior. Its acceleration rate grows

with the relaxation time of the problem. It is always more efficient than the classic asymptotic limit method, especially in case of large memory effects, but is usually more time consuming than the Newton-Krylov method. Nevertheless, in cases when storage of factorized Jacobians is not available, or when Newton method is less robust than the fixed point method (ex., for "concave" problems), the delayed feedback control, being quite efficient for the problems with large diffusion effects, is of high practical use for computing the cyclic states.

Appendices

Appendix A. Introduction to Lambert W function

Let us take a brief overview on the Lambert W function. For more details see [Corless et al. 1996, 1997, Shinozaki 2007, Shinozaki and Mori 2006, Yi et al. 2010, 2006, Yi and Ulsoy 2006, Valluri et al. 2000].

- The Lambert W function is a solution of $W[z]e^{W[z]} = z$ and has an infinite number of branches W_k, $k \in \mathbb{Z}$. The branch cuts are depicted on the Figure A.1, taken from [Corless et al. 1996].

- The first derivative for any branch $k \in \mathbb{Z}$ is given by

$$\tfrac{d}{dz} W_k[z] = \frac{W_k[z]}{z(W_k[z]+1)}, \qquad k \in \mathbb{Z}. \tag{A.1}$$

- The principal branch W_0 is always the rightmost [Shinozaki 2007, Shinozaki and Mori 2006], i.e.

$$\max_{k\in\mathbb{Z}} \mathfrak{Re} W_k[z] = \mathfrak{Re} W_0[z], \quad \forall z \in \mathbb{C}. \tag{A.2}$$

  The real part of the principal branch $W_0[z]$, $z \in \mathbb{C}$, is plotted on Figure A.2.

- The real part of the principal branch is bounded from below by -1 and reaches the minimum at $z = -\frac{1}{e}$, that is

$$\begin{aligned} &\mathfrak{Re} W_0[z] \geq -1, \quad \forall z \in \mathbb{C}, \\ &W_0\left[-\tfrac{1}{e}\right] = -1. \end{aligned}$$

- Inside the circle $|z| < \frac{1}{e}$, the principal branch can be decomposed in power series [Corless et al. 1997]:

$$W_0[z] = \sum_{n=1}^{\infty} \frac{(-n)^{n-1}}{n!} z^n, \qquad \forall |z| < \frac{1}{e}. \tag{A.3}$$

- For the principal branch W_0 in the vicinity of zero it holds

$$\forall x \in [-e^{-1}, 0] \ : \quad W_0[x] = \min_{\phi\in(-\pi,\pi)} \mathfrak{Re} W_0\left[xe^{i\phi}\right]. \tag{A.4}$$

Appendix B. Maximum of the acceleration term

Given $T > 0$, $\beta \geq 0$, $\sigma \in \mathbb{C}$, $|\sigma| = 1$, we want to solve the following optimization problem on $\gamma \in \mathbb{C}$

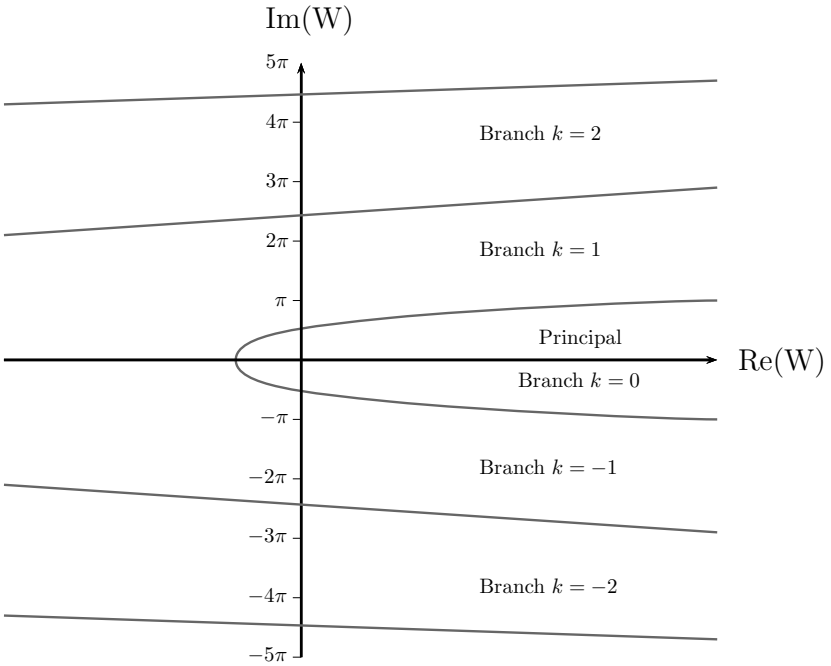

Figure A.1: Branch cuts of Lambert W function [Corless et al. 1996]. Each zone corresponds to the image of $\mathbb{C}$ by a specific branch of W.

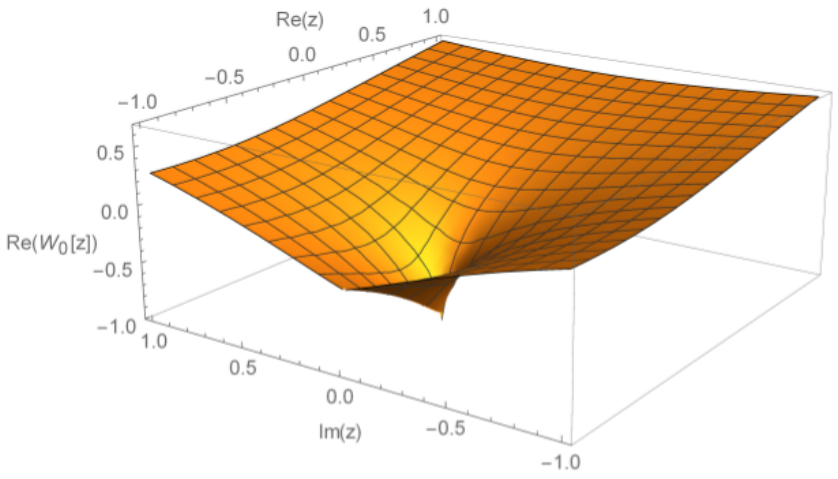

Figure A.2: Real part of the principal branch of Lambert W function (draw in Wolfram Mathematica 10.0).

$$\gamma_{opt} = \arg\max_{\gamma\in\mathbb{C}} J(\gamma),$$
$$J(\gamma) = \mathfrak{Re}\left(\gamma - \frac{1}{T} W_0\left[T\sigma\gamma\, e^{T(\gamma+\frac{1}{\beta})}\right]\right).$$

Let us denote $z := T\gamma\, e^{T\gamma}$ and $a := \sigma e^{T/\beta}$. Note that $|a| > 1$, since $\beta \geq 0$ and $|\sigma| = 1$. Thus we are looking for $z = z_{opt}$ maximizing

$$J(z) = \frac{1}{T}\,\mathfrak{Re}\left(W_0\left[z\right] - W_0\left[az\right]\right).$$

The function $W_0\left[z\right]$ being holomorphic in $\mathbb{C}\setminus(-\infty, -e^{-1}]$, the maximum of $J(z)$ can be reached either at the points where its derivative explodes or at infinity. At infinity, we estimate first the following auxiliary limit, using the L'Hôpital's rule:

$$\begin{aligned}\lim_{z\to\infty}\frac{W_0\left[az\right]}{W_0\left[z\right]} &= \lim_{z\to\infty}\frac{W_0'\left[az\right]}{W_0'\left[z\right]}\\ &= \lim_{z\to\infty}\frac{1+\frac{1}{W_0[z]}}{1+\frac{1}{W_0[az]}}\\ &= 1.\end{aligned}$$

Then, recalling that $W_0\left[z\right] = \log z - \log W_0\left[z\right]$, we have

$$\begin{aligned}\lim_{z\to\infty} T\,J(z) &= \lim_{z\to\infty}\mathfrak{Re}\left(W_0\left[z\right] - W_0\left[az\right]\right)\\ &= \lim_{z\to\infty}\mathfrak{Re}\left(\log z - \log W_0\left[z\right] - \log(az) + \log W_0\left[az\right]\right)\\ &= -\log|a| + \lim_{z\to\infty}\log\left|\frac{W_0\left[az\right]}{W_0\left[z\right]}\right|\\ &= -\log|a| \;< 0, \quad \text{since } |a| > 1.\end{aligned}$$

The value is negative and can not be a maximum, so let us now check the values of J where the derivative blows up. According to (A.1), $J'(z)$ gets unbounded when $W_0\left[z\right] = -1$ or $W_0\left[az\right] = -1$, that is at $z = -e^{-1}$ or $z = -(ae)^{-1}$ respectively:

$$\begin{aligned}J\left(-\tfrac{1}{e}\right) &= -\left(1 + \mathfrak{Re}W_0\left[-\tfrac{a}{e}\right]\right) &\leq 0,\\ J\left(-\tfrac{1}{ae}\right) &= \mathfrak{Re}W_0\left[-\tfrac{1}{ae}\right] + 1 &\geq 0,\end{aligned}$$

where the signs are defined by (A.2). Thus the maximum of $J(z)$ is reached at $z_{opt} = -(ae)^{-1} = -\sigma^{-1}e^{-T/\beta-1}$ and we have then

$$\gamma_{opt} = \frac{1}{T}W_0\left[z_{opt}\right] = \frac{1}{T}W_0\left[-\tfrac{1}{e}\,\sigma^{-1}e^{-T/\beta}\right].$$

Bibliography

Alart, P. and Curnier, A. [1991], 'A mixed formulation for frictional contact problems prone to newton like solution methods', *Computer methods in applied mechanics and engineering* **92**(3), 353–375.

Ambrose, D. M. and Wilkening, J. [2010], 'Computation of time-periodic solutions of the benjamin–ono equation', *Journal of nonlinear science* **20**(3), 277–308.

Asl, F. M. and Ulsoy, A. G. [2003], 'Analysis of a system of linear delay differential equations', *Journal of Dynamic Systems, Measurement, and Control* **125**(2), 215–223.

Balay, S., Abhyankar, S., Adams, M. F., Brown, J., Brune, P., Buschelman, K., Dalcin, L., Eijkhout, V., Gropp, W. D., Kaushik, D., Knepley, M. G., McInnes, L. C., Rupp, K., Smith, B. F., Zampini, S., Zhang, H. and Zhang, H. [2016], PETSc users manual, Technical Report ANL-95/11 - Revision 3.7, Argonne National Laboratory.
URL: *http://www.mcs.anl.gov/petsc*

Bellman, R. E. and Cooke, K. L. [1963], 'Differential-difference equations'.

Bleich, M. E. and Socolar, J. E. [1996], 'Stability of periodic orbits controlled by time-delay feedback', *Physics Letters A* **210**(1-2), 87–94.

Brandstetter, G. and Govindjee, S. [2017], 'Cyclic steady states of nonlinear electro-mechanical devices excited at resonance', *International Journal for Numerical Methods in Engineering* **110**(13), 1227–1246.

Bristeau, M., Glowinski, R. and Périaux, J. [1998], 'Controllability methods for the computation of time-periodic solutions; application to scattering', *Journal of Computational Physics* **147**(2), 265–292.

Caruel, M., Chabiniok, R., Moireau, P., Lecarpentier, Y. and Chapelle, D. [2014], 'Dimensional reductions of a cardiac model for effective validation and calibration', *Biomechanics and modeling in mechanobiology* **13**(4), 897–914.

Chan, T. F. and Jackson, K. R. [1984], 'Nonlinearly preconditioned krylov subspace methods for discrete newton algorithms', *SIAM Journal on scientific and statistical computing* **5**(3), 533–542.

Chapelle, D., Le Tallec, P., Moireau, P. and Sorine, M. [2012], 'Energy-preserving muscle tissue model: formulation and compatible discretizations', *International Journal for Multiscale Computational Engineering* **10**(2).

Chawla, K. K. and Meyers, M. [1999], *Mechanical behavior of materials*, Prentice Hall.

Christensen, R. [2012], *Theory of viscoelasticity: an introduction*, Elsevier.

Ciarlet, P. G. [1988], 'Mathematical elasticity. vol. i, volume 20 of studies in mathematics and its applications'.

Ciarlet, P. G. and Geymonat, G. [1982], 'Sur les lois de comportement en élasticité non linéaire compressible', *CR Acad. Sci. Paris Sér. II* **295**, 423–426.

Corless, R. M., Gonnet, G. H., Hare, D. E., Jeffrey, D. J. and Knuth, D. E. [1996], 'On the lambertw function', *Advances in Computational mathematics* **5**(1), 329–359.

Corless, R. M., Jeffrey, D. J. and Knuth, D. E. [1997], A sequence of series for the lambert w function, *in* 'Proceedings of the 1997 international symposium on Symbolic and algebraic computation', ACM, pp. 197–204.

de Dormale, B. M. and Gautrin, H.-F. [1975], 'Spectral representation and decomposition of self-adjoint operators', *Journal of Mathematical Physics* **16**(11), 2328–2332.

Govindjee, S., Potter, T. and Wilkening, J. [2014], 'Cyclic steady states of treaded rolling bodies', *International Journal for Numerical Methods in Engineering* **99**(3), 203–220.

Guzenko, P. Y., Hövel, P., Flunkert, V., Fradkov, A. and Schöll, E. [2008], Adaptive tuning of feedback gain in time-delayed feedback control, *in* 'Proceedings of 6th EUROMECH nonlinear dynamics conference (ENOC-2008).'.

Hövel, P. [2010], *Control of complex nonlinear systems with delay*, Springer Science & Business Media.

Hövel, P. and Schöll, E. [2005], 'Control of unstable steady states by time-delayed feedback methods', *Physical Review E* **72**(4), 046203.

Hüeber, S., Matei, A. and Wohlmuth, B. I. [2007], 'Efficient algorithms for problems with friction', *SIAM Journal on Scientific Computing* **29**(1), 70–92.

Imperiale, A. [2013], Image-based data assimilation methods for the personalization of mechanical models-Application to cardiac mechanics and tagged-MRI, PhD thesis, Université Pierre et Marie Curie-Paris VI.

Jazar, M. [2004], Spectral theory, PhD thesis, Theoretical and applied aspects of some PDEs coming from geometry or physics.

Kalman, R. E. and Bucy, R. S. [1961], 'New results in linear filtering and prediction theory'.

Kittel, A., Parisi, J. and Pyragas, K. [1995], 'Delayed feedback control of chaos by self-adapted delay time', *Physics letters A* **198**(5), 433–436.

Knoll, D. A. and Keyes, D. E. [2004], 'Jacobian-free newton–krylov methods: a survey of approaches and applications', *Journal of Computational Physics* **193**(2), 357–397.

Kowalski, E. [2009], 'Spectral theory in hilbert spaces', *ETH Zürich* .

Laursen, T. [2003], *Computational Contact and Impact Mechanics: Fundamentals of Modeling Interfacial Phenomena in Nonlinear Finite Element Analysis*, Springer Berlin Heidelberg.

Le Tallec, P. [2009], *Modélisation et calcul des milieux continus*, Editions Ecole Polytechnique.

Le Tallec, P., Ciarlet, P. and Lions, J. [1994], 'Handbook of numerical analysis', *Ciarlet, PG, Lions, JL,(Eds.)* **3**, 465–622.

Le Tallec, P. and Rahier, C. [1994], 'Numerical models of steady rolling for nonlinear viscoelastic structures in finite deformations', *International Journal for Numerical Methods in Engineering* **37**(7), 1159–1186.

M3disim team Inria [n.d.], 'Heartlab code', `https://raweb.inria.fr/rapportsactivite/RA2013/m3disim/uid14.html`.

Moireau, P. [2009], Assimilation de données par filtrage pour les systèmes hyperboliques du second ordre. Applications à la mécanique cardiaque., PhD thesis, Citeseer.

Moireau, P., Chapelle, D. and Le Tallec, P. [2008], 'Joint state and parameter estimation for distributed mechanical systems', *Computer methods in applied mechanics and engineering* **197**(6), 659–677.

Moireau, P., Chapelle, D. and Le Tallec, P. [2009], 'Filtering for distributed mechanical systems using position measurements: perspectives in medical imaging', *Inverse problems* **25**(3), 035010.

Pyragas, K. [1992], 'Continuous control of chaos by self-controlling feedback', *Physics letters A* **170**(6), 421–428.

Pyragas, K. [1995], 'Control of chaos via extended delay feedback', *Physics Letters A* **206**(5-6), 323–330.

Pyragas, K. [2002], 'Analytical properties and optimization of time-delayed feedback control', *Physical Review E* **66**(2), 026207.

Pyragas, K. [2012], A twenty-year review of time-delay feedback control and recent developments, *in* 'International Symposium on Nonlinear Theory and its Applications', Vol. 1, pp. 683–686.

Pyragas, V. and Pyragas, K. [2011], 'Adaptive modification of the delayed feedback control algorithm with a continuously varying time delay', *Physics Letters A* **375**(44), 3866–3871.

Pyragas, V. and Pyragas, K. [2013], 'Adaptive search for the optimal feedback gain of time-delayed feedback controlled systems in the presence of noise.', *European Physical Journal B–Condensed Matter* **86**(7).

Quarteroni, A., Sacco, R. and Saleri, F. [2010], *Numerical mathematics*, Vol. 37, Springer Science & Business Media.

Reese, S. and Govindjee, S. [1997], 'A presentation and comparison of two large deformation viscoelasticity models', *Journal of engineering materials and technology* **119**(3), 251–255.

Saad, Y. [2003], *Iterative methods for sparse linear systems*, SIAM.

Saad, Y. and Schultz, M. H. [1986], 'Gmres: A generalized minimal residual algorithm for solving nonsymmetric linear systems', *SIAM Journal on scientific and statistical computing* **7**(3), 856–869.

Sainte-Marie, J., Chapelle, D., Cimrman, R. and Sorine, M. [2006], 'Modeling and estimation of the cardiac electromechanical activity', *Computers & structures* **84**(28), 1743–1759.

Shinozaki, H. [2007], 'Lambert w function approach to stability and stabilization problems for linear time-delay systems', *Kyoto Institute of Technology, Thesis* .

Shinozaki, H. and Mori, T. [2006], 'Robust stability analysis of linear time-delay systems by lambert w function: Some extreme point results', *Automatica* **42**(10), 1791–1799.

Socolar, J. E., Sukow, D. W. and Gauthier, D. J. [1994], 'Stabilizing unstable periodic orbits in fast dynamical systems', *Physical Review E* **50**(4), 3245.

Telichevesky, R., Kundert, K. S. and White, J. K. [1995], Efficient steady-state analysis based on matrix-free krylov-subspace methods, *in* 'Proceedings of the 32nd annual ACM/IEEE Design Automation Conference', ACM, pp. 480–484.

Valluri, S. R., Jeffrey, D. J. and Corless, R. M. [2000], 'Some applications of the lambert w function to physics', *Canadian Journal of Physics* **78**(9), 823–831.

Weidmann, J. [2012], *Linear operators in Hilbert spaces*, Vol. 68, Springer Science & Business Media.

Westerhof, N., Lankhaar, J.-W. and Westerhof, B. E. [2009], 'The arterial windkessel', *Medical & biological engineering & computing* **47**(2), 131–141.

Wriggers, P. [2006], *Computational contact mechanics*, Springer Science & Business Media.

Yanchuk, S., Wolfrum, M., Hövel, P. and Schöll, E. [2006], 'Control of unstable steady states by long delay feedback', *Physical Review E* **74**(2), 026201.

Yi, S., Nelson, P. W. and Ulsoy, A. G. [2010], *Time-delay systems: analysis and control using the Lambert W function*, World Scientific.

Yi, S. and Ulsoy, A. G. [2006], Solution of a system of linear delay differential equations using the matrix lambert function, *in* '2006 American Control Conference', IEEE, pp. 6–pp.

Yi, S., Ulsoy, A. G. and Nelson, P. W. [2006], Solution of systems of linear delay differential equations via laplace transformation, *in* 'Decision and Control, 2006 45th IEEE Conference on', IEEE, pp. 2535–2540.

ÉCOLE DOCTORALE
Sciences mécaniques et énergétiques, matériaux et géosciences (SMEMAG)

Titre : Méthodes mathématiques et numériques pour la modélisation et le calcul des états établis cycliques en mécanique non-linéaire.

Mots clés : Périodicité en espace-temps, Etat établi cyclique, Roulage du pneu, Méthode de Newton-Krylov, Contrôle rétroactif retardé.

Résumé : Ce travail a pour objet l'étude des techniques rapides pour calculer l'état cyclique établi des problèmes d'évolution en mécanique non-linéaire avec des conditions de périodicité en espace-temps. Un exemple typique est le roulage stationnaire d'un pneu présentant des sculptures périodiques, où l'état en chaque point est le même que l'état observé au point correspondant de la sculpture suivante une période en temps auparavant.

L'application de solveurs directs pour la solution de tels problèmes est impossible car ils exigent l'inversion des matrices gigantesques. Pour résoudre ce genre de problèmes, les logiciels de calcul utilisés dans l'industrie recherchent une telle solution cyclique comme la limite asymptotique d'un problème à valeur initiale avec des données initiales arbitraires. Cependant, quand le temps de relaxation du problème physique est élevé, la vitesse de convergence vers le cycle limite peut devenir trop lente. Comme on ne s'intéresse pas à la solution transitoire et que seul importe d'avoir un accès rapide au cycle limite, le développement des méthodes qui accélèrent la convergence vers le cycle limite sont d'un grand intérêt. Ce travail développe, étudie et compare deux techniques d'analyse et de calcul rapide de la solution périodique en espace-temps.

La première est la méthode de Newton-Krylov, qui considère l'état initial comme l'inconnue du problème à calculer à partir de la condition de périodicité. Le problème résultant est résolu par l'algorithme de Newton-Raphson. Comme le Jacobien associé ne s'exprime pas explicitement mais uniquement implicitement à travers son action par multiplication, il est nécessaire d'introduire des solveurs itératifs de type Krylov. Par réutilisation optimale de l'information obtenue sur le Jacobien pendant le calcul du résidu, la résolution du système linéaire par algorithme de Krylov devient très rapide et de faible coût par rapport au calcul de l'erreur de périodicité. Cette technique de calcul peut être vue comme une méthode de tir. Mais nous l'écrivons ici par changement de variables sous la forme d'une méthode de type observateur-contrôleur, qui corrige la solution transitoire après chaque cycle et accélère ainsi la convergence vers la limite cyclique.

La deuxième méthode de calcul et d'analyse proposée dans ce travail met en œuvre une modification du problème d'évolution initial en y introduisant un terme de contrôle rétroactif, basé sur l'erreur de périodicité. Le contrôle rétroactif est un outil bien connu et puissant dans le cadre de la stabilisation des orbites périodiques instables des processus chaotiques. Dans le cadre de ce travail, il est appliqué à un système initialement stable pour accélérer la convergence vers la limite cyclique. De plus, le terme de contrôle inclut les décalages en temps ainsi qu'en espace, ce qui complique son analyse. L'enjeu est ici de construire l'opérateur de gain à appliquer à l'erreur de périodicité dans le terme de contrôle. Dans un cadre linéaire très général, après décomposition spectrale et introduction des fonctions de Lambert, nous pouvons analyser explicitement l'existence et la convergence de solutions en temps, et construire la forme optimale du gain qui assure la convergence la plus rapide vers la solution cyclique.

L'efficacité de la méthode proposée croit avec le temps de relaxation du problème. L'algorithme est présenté sous la forme d'un schéma prédicteur-correcteur en temps, où l'étape de correction est explicite et de très faible coût numérique. Sous cette forme, le contrôle proposé a été adapté et testé sur des problèmes non-linéaires.

Les deux méthodes ont été appliquées sur diverses applications académiques et comparées à la méthode asymptotique classique. Enfin, elles ont été intégrées et mises en œuvre dans le code industriel de Michelin pour application au roulage stationnaire d'un pneu complet avec sculptures périodiques en présence de forces de contact au sol en régime de frottement adhérant-glissant.

Title : Mathematical and numerical methods for modeling and computing the cyclic steady states in non-linear mechanics.

Keywords : Space-time periodicity, Cyclic steady state, Rolling tyre, Newton-Krylov method, Delayed feedback control.

Abstract : This work is focused on fast techniques for computing the steady cyclic states of evolution problems in non-linear mechanics with space and time periodicity conditions. This kind of problems can be faced, for instance, in the beating heart modeling. Another example concerns the rolling of a tyre with periodic sculptures, where the cyclic state satisfies "rolling" periodicity condition, including shifts both in time and space. More precisely, the state at any point is the same that at the corresponding point observed at the next sculpture one time period ago.

Direct solvers for such problems are not very convenient, since they require inversion of very large matrices. In industrial applications, in order to avoid this, such a cyclic solution is usually computed as an asymptotic limit of the associated initial value problem with arbitrary initial data. However, when the relaxation time is high, convergence to the limit cycle can be very slow. In such cases nonetheless, one is not interested in the transient solution, but only in a fast access to the limit cycle. Thus, developing methods accelerating convergence to this limit is of high interest. This work is devoted to study and comparison of two techniques for fast calculation of the space-time periodic solution.

The first is the well-known Newton-Krylov shooting method, looking for the initial state, which provides the space-time periodic solution. It considers the space-time periodicity condition as a non-linear equation on the unknown initial state, which is solved using Newton-Raphson technique. Since the associated Jacobian can not be expressed explicitly, the method uses one of the matrix-free Krylov iterative solvers. Using information stored while computing the residual to solve the linear system makes its calculation time negligible with respect to the residual calculation time. On the one hand, the algorithm is a shooting method, on the other side, it can be considered as an observer-controller method, correcting the transient solution after each cycle and accelerating convergence to the space-time periodic state.

The second method, considered in this work, is an observer-controller type modification of the standard evolution to the limit cycle by introducing a feedback control term, based on the periodicity error. The time-delayed feedback control is a well-known powerful tool widely used for stabilization of unstable periodic orbits in deterministic chaotic systems. In this work the time-delayed feedback technique is applied to an a priori stable system in order to accelerate its convergence to the limit cycle. Moreover, given the space-time periodicity, along with the time-delay, the feedback term includes also a shift in space. One must then construct the gain operator, applied to the periodicity error in the control term. Our main result is to propose and to construct the optimal form of the gain operator for a very general class of linear evolution problems, providing the fastest convergence to the cyclic solution. The associated control term can be mechanically interpreted.

Efficiency of the method increases with the problem's relaxation time. The method is presented in a simple predictor-corrector form, where correction is explicit and numerically cheap. In this later form, the feedback control has been also adapted and tested for a nonlinear problem.

The discussed methods have been studied using academic applications and they also have been implemented into the Michelin industrial code, applied to a full 3D tyre model with periodic sculpture in presence of slip-stick frictional contact with the soil, and then compared to the standard asymptotic convergence.

Université Paris-Saclay
Espace Technologique / Immeuble Discovery
Route de l'Orme aux Merisiers RD 128 / 91190 Saint-Aubin, France